Non-linear dynamics and power systems

Wilson, Jonathan P.

Award date:
2000

Awarding institution:
University of Bath

UNIVERSITY OF BATH

DEPARTMENT OF MATHEMATICAL SCIENCES

NON-LINEAR DYNAMICS AND POWER SYSTEMS

Submitted by

Jonathan P. Wilson

for the degree of Ph.D.
of the

University of Bath

2000

ProQuest LLC
789 East Eisenhower Parkway
P.O. Box 1346
Ann Arbor, MI 48106-1346

NON-LINEAR DYNAMICS AND POWER SYSTEMS

Submitted by

Jonathan P. Wilson

for the degree of Ph.D.
of the

University of Bath

2000

To my parents

"I am never forget the day my first book is published. This book was sensational! Pravda? Huh, well Pravda said ... 'It stinks!'. But Isvestia, Isvestia said ... 'It stinks!'. Metro-Goldwyn-Moscva buys the movie rights for 6 million roubles, changing title to 'The Eternal Triangle', with Ingrid Bergman playing part of hypotenuse." – T.L.

Abstract

In this thesis we investigate the dynamical behaviour of non-linear power system models. Particular attention is paid to giving a dynamical explanation of the phenomenon known as voltage collapse. We give a thorough presentation of the basic power system concepts and modelling details.

The bifurcation structure of a simple power system model (the 3-Bus model) is investigated, with respect to changes to both the real and reactive loads. Numerical methods for this bifurcation analysis are presented and discussed. The model is shown to have a Bogdanov-Takens bifurcation point and hence homoclinic orbits; these orbits can be of Šil'nikov type with many coexisting periodic and chaotic solutions. We may use the bifurcation calculations to divide the 2 parameter plane into a number of regions, for which there are qualitatively different dynamics. We classify and further investigate the dynamical behaviour in each of these regions, using a Monte Carlo method to investigate basins of attraction of various stable states. We then show how this classification can be used to denote each regions as either safe or unsafe with respect to the likelihood of voltage collapse.

A larger and more complex class of models is presented and a particular example, the M4B6 model, is investigated by the same methods. This is shown to have broadly similar behaviour to the reduced model, also governed by a BT-point.

Acknowledgements

Firstly I would like to thank all the staff and students of the Department of Mathematical Sciences. To all those who have had the questionable pleasure of sharing an office with me – thank you for putting up with the noise, the clutter and the constant interruptions, and for providing continual interest, entertainment and good advice. Thanks to Steve L., Mark P., Chris S., Aaron, Rob S., Bill Bill and all the other research students for many interesting conversations and shared pints. On the practical side I would like to thank Mark Willis, Jill Parker, Nada Harvey and colleagues, without whom the department would quickly come to a grinding halt.

I would like to thank members and staff of the University of Bath Students' Union and Bath Area Rag; far, far too numerous to be mentioned individually – you know who you are. You have helped make my time at Bath a rounded and complete experience. Thanks also to friends at various other universities, for many good times especially at BAMC99. Two of these deserve special mention; Rob Beardmore has been a source of inspiration, information, and motivation; Helen Tucker – thank you for fun and friendship.

Special thanks are due to the EPSRC and the National Grid Company for sponsoring this project. The NGC have been invaluable in providing advice, technical information and general direction when needed. I would particularly like to thank Fan Li and John McQueen for their genuine interest in the project and for many practical suggestions.

Thanks to all at Winchester Road for providing many, many interesting distractions – but also for providing much motivation for me to finish this thing!

My family have been a continual source of support and inspiration. I have much to thank them for, especially for inspiring in me by their actions a desire to always do something new and find out more about the world.

Finally I would like to thank Chris Budd for being an excellent supervisor. Thank you for providing an interesting project, giving excellent advice throughout and for keeping the research on track. Thanks in particular for all your patience and for supporting my extra-curricular activities.

Contents

List of Figures

Chapter 1

Introduction

1.1 The problem

Electrical power systems form some of the largest interconnected systems ever created. A typical network will span the whole of a medium sized country, with hundreds of major generators, thousands of supply lines, tens of thousands of components in the distribution network, millions of customers and many millions of devices drawing power from the mains supply. The end users expect a reliable supply of AC current, with voltage magnitude and phase angle within tight tolerances. For the distribution companies, maintaining such a supply is not an easy task, requiring constant attention in both the short and long term.

As a discipline within electrical engineering, power systems analysis can be traced back to the 1880's when Westinghouse, Edison, Tesla and others installed the first supply networks in the USA and Europe. In comparison to other fields with clear engineering applications, such as mechanics and fluid dynamics, power systems have received relatively little attention from the applied mathematics community. The standard power system models are not well known outside the field; perhaps as a consequence these models are sometimes represented in the engineering literature in a form which could be described as mathematically naive. In any case, there is much that power systems engineers and applied mathematicians can learn from each other.

A major problem facing the power systems community worldwide is that of avoiding voltage collapse in the network. The voltage collapse phenomenon will be discussed in more detail in Chapter 3. As we shall see, the concept of voltage collapse is not simple to describe. It is characterised by a rapid drop in the voltage supplied to users, followed by catastrophic failure of the system over a wide area. This is often preceded by high load on the system and/or localised

faults; however no complete explanation exists of exactly which factors or failures may precipitate voltage collapse.

We will discuss in detail efforts made over the last ten years to gain a better mathematical understanding of voltage collapse. Several explanations of voltage collapse have been posited, not all of them mutually exclusive. These variously consider both the origin of voltage collapse and the subsequent behaviour of the system. A particularly successful line of enquiry has been to consider the power system as a dynamical system and to apply non-linear techniques to analyse this system and it is this that we will pursue in this thesis.

1.2 Aims of the thesis

The main aims of this thesis are two fold. Firstly to present a class of models of power systems as examples of dynamical systems which can then be analysed using the theory and computational methods applied to other dynamical systems. Secondly, to use a combination of dynamical systems and related numerical methods to analyse some examples of power system models of increasing complexity. Having determined their dynamical behaviour we then aim to relate this to the observed behaviour of real power systems. By this process we can analyse the suitability of the dynamical tools for use in an engineering context.

In order to analyse power systems as a general class of dynamical systems, we need a clear mathematical exposition of power systems concepts and models. It is not possible to simply reference a single source for a clear and in-depth mathematical explanation and derivation of power system models suitable for analysis as a dynamical system. Many existing textbooks are, at best, targeted at an engineering readership, and at worst lacking in mathematical rigour.

It is common for different models to be used for analysis of different parts of power system behaviour, with the relationships between these not always clear. These models undoubtedly produce the results needed by power engineers – the safe and reliable daily operation of power networks worldwide is a testament to this. Indeed the UK network has yet to experience a voltage collapse incident. But this approach does not allow us to analyse the whole network as an interconnected dynamical system. While there are several papers discussing power systems as dynamical systems, it is out of the scope of the majority of them to produce a full description of the modelling process. We will review these in Chapter 3.

Once we have derived models we apply some analytical methods, both theoret-

ical and computational. This allows us to gain understanding of the mathematical behaviour of the system under analysis. It also allows for better understanding of the methods used. Many of the computational methods we shall discuss claim to be applicable to extremely wide classes of models (such as "all sufficiently smooth ODE models"). Only through careful implementation will we see if this is indeed true – there may be practical issues which mean the methods do not actually give the required results. Furthermore we may discover ways of implementing the methods more efficiently which may also apply to a larger class of models than just power systems.

Results gained about an abstract dynamical system must then be interpreted in the context of what that system is actual modelling. This will allow us to understand both the behaviour of the underlying physical system and at what point the model ceases to be an accurate description of that system. In particular we hope to gain better understanding of what factors and events might precipitate voltage collapse and how the system behaves whilst undergoing collapse. This may allow development of the mathematical methods used as practical tools for engineering analysis. This requires a good understanding of what modes of behaviour are "generic" in power system models. It also means that close attention must be paid to the efficiency and practicality of the tools used, especially computational methods.

This research has been funded by a CASE award from the EPSRC and the National Grid Company plc; this thesis forms the primary deliverable to the industrial sponsors. Two placements within the Modelling, Analysis and Forward Development research section of NGC have been invaluable in putting the results of this research in context. In particular it was possible to use a typical power systems analysis package, and compare its models, methods and algorithms with those presented here.

We have tried to keep a balance in the level and style of presentation in this thesis. The aim is to present a consistent and reasonably self-contained exposition of both the mathematical and the engineering concepts, accessible to readers with either a mathematical or an engineering background. We hope that this has been achieved without too much explanation of concepts that might appear trivial to those already familiar with them, whilst remaining intelligible to those who are not.

1.3 The main achievements of the thesis

The main achievements of this research can be summarised as follows.

- Numerical path following methods are developed and shown to be computationally feasible for use with power system models of the type we have studied. They can be used for the calculation and continuation of fixed points, bifurcation points and periodic orbits.
- A Bogdanov-Takens point has been found in both simple and more complicated power system models. Analysis of this bifurcation point appears to indicate that it acts as an organising centre for their dynamical structure.
- Local analysis of the BT-point and the resulting continuation of paths of bifurcations allows the computation of the full 2-parameter bifurcation structure of the models
- This bifurcation structure has been shown to include Šil'nikov homoclinic orbits, implying the existence of a wealth of dynamical behaviour in the system
- Knowledge of the bifurcation structure helps us investigate the basins of attraction of the model, and to associate the basins of attraction to the voltage collapse phenomenon.

1.4 The structure of the thesis

The layout of this thesis is as follows.

In Chapter 2 we present a review of power systems modelling. We will introduce the basic concepts of generation, distribution and load. For each of these parts of the system we will derive and discuss the models used later in the thesis, and ways in which they may be extended. The use of these models by power systems engineers is then discussed. We refer to the context and methodology in which the models are used, and to the algorithms commonly used to provide practical solutions.

Chapter 3 discusses the use of dynamical systems theory in the study of electrical circuits. We present a review of the mathematical theory needed for the remainder of the thesis and a summary of the computational methods that will be used. This is followed by a substantial review of the dynamics observed in power systems and related models.

In Chapters 4 and 5 we present and investigate a simple ODE power system model, the "3-Bus" model of two generators and one dynamic load. Chapter 4 presents a full derivation of this model. We present an asymptotic analysis of this model when undergoing collapse. We then concentrate on a 1-parameter bifurcation analysis of the model, presenting both the theory needed to carry out this analysis and the computational methods used. The results reveal a rich dynamical structure, including steady-state, periodic, chaotic and homoclinic behaviour, and saddle-node and Hopf bifurcations.

Chapter 5 concentrates on the 2-parameter investigation of the 3-Bus model. Again we present the theory and methods needed for this analysis. Two-parameter continuation of the bifurcation points found in the previous chapter reveals a Bogdanov-Takens point which acts as an organising centre for the system. This allows us to determine a full understanding of the two-parameter behaviour of the system. Armed with this knowledge we can then investigate systematically the effect of the parameters on the basins of attraction of the operating points, and relate this back to the problem of voltage collapse.

In Chapter 6 we introduce and analyse a larger power system model with 4 generators and two loads. In general, power system models take the form of a Differential Algebraic Equation (DAE), but we clearly identify the circumstances when they may be reduced to an Ordinary Differential Equation (ODE) model, and do so for this particular model. We apply the same investigatory methods to this new model as for the 3-Bus model, and present some results and conclusions. In particular we highlight the role played by a BT-point in this model.

In the final chapter, Chapter 7 we draw some more general conclusions from this work. This includes commentary on the study of power systems as mathematical objects; on the success of the application of the methods of analysis and the possibility of using these models as stimuli for further theoretical development. Consideration is also given to the practicality of developing some of the work in this thesis, and other associated research, into practical tools for engineering analysis. This discussion addresses both issues of computational efficiency and of the usefulness of dynamical results in an engineering context.

Chapter 2

Review of Power Systems Modelling

2.1 Introduction

Practical analysis of the design and operation of power systems forms a major discipline within electrical engineering. There is a substantial body of research into the modelling of individual components, and of the entire network as a single system.

In this chapter we discuss the basic concepts behind power system models, the models used by us and elsewhere, and how these models are implemented in a typical power system modelling package. We give reference where relevant to the problem of voltage collapse.

2.2 Basic concepts

2.2.1 The system

Power systems can be divided conceptually into three parts – generation, distribution and load. Each of these will be discussed in more detail below; here we present the basic common concepts.

With some notable exceptions[1] power systems worldwide operate using a sinusoidal three phase alternating current supply at a frequency of 50 or 60 Hz. This means that generators have a single rotor, driven by a mechanical power source and surrounded by a number of equally spaced stators. These generate

[1]For instance the high voltage DC interconnection between the French network and the England & Wales network, and the proposed North Sea DC link to Norway

three sinusoidal voltage waveforms (with respect to a common neutral) at phase differences of $\frac{2\pi}{3}$. The distribution network carries each phase separately, along with the common neutral. Large industrial users may have equipment (e.g. motors, electric arc furnaces) that uses all three phases; local supply companies typically split the phases and give smaller industrial and domestic users a single phase supply.

Design and operation of power systems is complicated by the fact that there is often no single organisation in total control of the entire system. For instance, in the highly deregulated England & Wales network, the division of the commercial operation is analogous to the conceptual division into generation, network and load. A variety of large and small generating companies (National Power, PowerGen, nuclear and other generators) supply power to the National Grid Company. NGC then distribute this power directly to large industrial users and to local supply companies. The local power companies distribute and sell power to smaller commercial and domestic users. From the point of view of modelling, this means that despite various obligations between the various companies to share long and short term information about the systems' states and parameters, there is a degree of uncertainty about the state and behaviour of the system. In the case of loads, even in countries with highly regulated and centralised power systems, it is impossible to know the properties of every single load connected to the system and we are forced to use empirical and stochastic methods to some extent.

2.2.2 Real and reactive Power

Let the instantaneous current flowing through an inductive component (for example a wire of negligible resistance) be

$$i_l(t) = I_m \sin(\omega_0 t) \tag{2.1}$$

where I_m is the peak current. (Here $i_l(0) = 0$, arbitrarily). The instantaneous induced e.m.f. across an inductance is proportional to the rate of change of current,

so

$$\begin{aligned} v_l(t) &= L\frac{d}{dt}i_l(t) && (2.2)\\ &= \omega_0 L I_m \cos(\omega_0 t) && (2.3)\\ &= \omega_0 L I_m \sin(\omega_0 t + \tfrac{\pi}{2}) && (2.4)\\ &= \omega_0 L i_l(t') && (2.5)\\ &= X_L\, i_l(t') && (2.6) \end{aligned}$$

where $t' = (t + \frac{\pi}{2\omega_0})$. So in an purely inductive component the voltage curve is a quarter of a cycle ahead of the current curve. The quantity $X_L = \omega_0 L$ is referred to as the inductive reactance.

In a circuit with perfect capacitance C, let the voltage across the capacitor be given by $v_c(t) = V_m \sin(\omega_0 t)$. The instantaneous current in a capacitor is proportional to the rate of change of voltage, so

$$\begin{aligned} i_c(t) &= C\frac{dv}{dt} && (2.7)\\ &= \omega_0 C V_m \cos(\omega_0 t) && (2.8)\\ &= \omega_0 C V_m \sin(\omega_0 t + \tfrac{\pi}{2}) && (2.9) \end{aligned}$$

which gives

$$\begin{aligned} v_c(t') &= V_m \sin(\omega_0 t + \tfrac{\pi}{2}) && (2.10)\\ &= \frac{1}{\omega_0 C} i_c(t) && (2.11)\\ &= X_C\, i_c(t). && (2.12) \end{aligned}$$

Hence in a purely capacitive component, the voltage curve is a quarter of a cycle behind the current curve. The quantity $X_C = 1/(\omega_0 C)$ is called the capacitive reactance.

We are often interested in *average* quantities over one AC cycle; that is the r.m.s. values

$$\begin{aligned} V &= \left(\frac{\omega_0}{2\pi}\int_0^{\frac{2\pi}{\omega_0}} v(t)^2 dt\right)^{\frac{1}{2}} && (2.13)\\ &= \frac{1}{\sqrt{2}} V_m && (2.14) \end{aligned}$$

and similarly $I = \frac{1}{\sqrt{2}} I_m$.

Now consider AC flow through a component consisting of a resistance R, a reactance X_L and a capacitance X_C in series, often referred to as an RLC circuit (Figure 2.1).

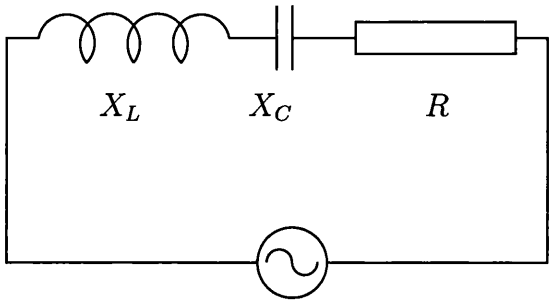

Figure 2.1: RLC circuit diagram

Let the instantaneous current through the components in this circuit be

$$i(t) = I_m \cos(\omega t) = \sqrt{2} I \cos(\omega t). \tag{2.15}$$

By Kirchoff's voltage law, the instantaneous voltage across the whole RLC component is given by

$$\begin{aligned} v(t) &= v_r(t) + v_l(t) + v_c(t) && (2.16)\\ &= I_m \left(R\cos(\omega t) - (X_L - X_C)\sin(\omega t)\right) && (2.17)\\ &= I_m Z \cos(\omega t + \phi) && (2.18) \end{aligned}$$

where

$$Z = \sqrt{R^2 + (X_L - X_C)^2} \tag{2.19}$$

and

$$\phi = \tan^{-1}\left(\frac{X_L - X_C}{R}\right). \tag{2.20}$$

Hence the maximum voltage is $V_m = I_m Z$, and the r.m.s voltage is

$$V = \frac{1}{\sqrt{2}} V_m = IZ \tag{2.21}$$

Then the instantaneous power is given by

$$\begin{aligned} p(t) &= p_r(t) + p_l(t) + p_c(t) && (2.22)\\ &= i(t)\left(v_r(t) + v_l(t) + v_c(t)\right) && (2.23)\\ &= \sqrt{2}I\cos(\omega t)\left(\sqrt{2}IR\cos(\omega t)\right. \\ &\qquad \left. -\sqrt{2}X_L I\sin(\omega t) + \sqrt{2}X_C I\sin(\omega t)\right) && (2.24)\\ &= I^2R(1+\cos(2\omega t)) - I^2(X_L - X_C)\sin(2\omega t) && (2.25)\\ &= I^2R + I^2\left(Z\cos(2\omega t + \phi)\right). && (2.26) \end{aligned}$$

Integrating (2.26) over one cycle, and noting that ϕ is constant and $\cos(2\omega t + \phi)$ has zero integral over a cycle, gives average power consumed by the circuit

$$P = I^2R = I^2Z\cos(\phi) = VI\cos(\phi). \tag{2.27}$$

This is the average rate of energy transfer, often called the *active* or *real* power.

The reactive components contribute to the instantaneous power, but their net energy transfer over one cycle is zero. A useful quantity is the maximum rate of energy flow through these components, that is

$$Q = I^2(X_L - X_C) = I^2Z\sin(\phi) = VI\sin(\phi). \tag{2.28}$$

This is referred to as the *reactive* power of the circuit.

Clearly it is in the interests of energy distributors to have as large a *power factor* $\cos(\phi)$ as possible (by making $\phi \approx 0$) in order to supply the maximum active power to consumers.

Note that if $X_C = X_L = 0$ we have $\phi = 0$ and so $P = IV$ as we expect for a resistance. If $R = 0$ and not both $X_L = 0$ or $X_C = 0$, then there is no net energy transfer and $P = 0$, $Q = IV$.

Also note that we would have reached the same definitions of P and Q had we replaced X_C by $-X_C$ and X_L by $-X_L$. This is because the charge flowing into and out of the reactive components is equal in magnitude as the current alternates. It is conventional to represent, in (2.17), the inductive reactance as $-X_L$ and the capacitive reactance as $+X_C$.

2.2.3 Phasor notation

The use of "phasor" notation is common in the electrical engineering literature. Quantities which are considered to be orthogonal in some sense, such as active and

reactive power, or resistance and reactance, may be represented in the (complex) plane as a modulus and an angle. For example, an impedance consisting of a reactance X and a resistance R can be represented as

$$\mathbf{Z} = R + \mathbf{i}X = Ze^{\mathbf{i}\phi} \tag{2.29}$$

where $\mathbf{i} = \sqrt{-1}$, $\phi = \arctan(\frac{X}{R})$ and $Z = \sqrt{R^2 + X^2}$, or even as

$$\mathbf{Z} = Z\angle\phi. \tag{2.30}$$

This interpretation of certain electrical quantities as being complex valued allows for efficient formulations of theorems and equations relating two such quantities, such as network theorems (see below), and also for graphical representation (Figure 2.2).

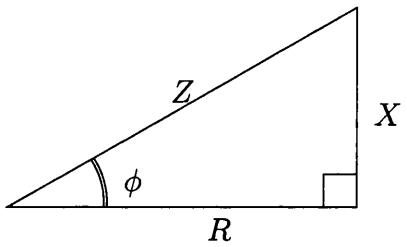

Figure 2.2: Typical "phasor" representation

In phasor notation we can refer to the complex power $\mathbf{S} = P + \mathbf{i}Q$. With respect some reference angle, let $\mathbf{V} = Ve^{\mathbf{i}\alpha}$ and $\mathbf{I} = Ie^{\mathbf{i}\beta}$. Generalising (2.27,2.28) we have $P = VI\cos(\alpha - \beta)$ and $Q = VI\sin(\alpha - \beta)$. Then

$$\begin{aligned}
\mathbf{S} &= P + \mathbf{i}Q && (2.31)\\
&= VI\left(\cos(\alpha - \beta) + \mathbf{i}\sin(\alpha - \beta)\right) && (2.32)\\
&= V\left(\cos(\alpha) + \mathbf{i}\sin(\alpha)\right)\ I\left(\cos(\beta) - \mathbf{i}\sin(\beta)\right) && (2.33)\\
&= \mathbf{V}\mathbf{I}^*. && (2.34)
\end{aligned}$$

In an RLC circuit with impedance $\mathbf{Z} = Ze^{\mathbf{i}\phi} = R + \mathbf{i}(X_L - X_C)$,

$$\begin{aligned}
\mathbf{V} &= V\left(\cos(\alpha) + \mathbf{i}\sin(\alpha)\right) && (2.35)\\
&= IZe^{\mathbf{i}\alpha} && (2.36)\\
&= Ie^{\mathbf{i}\beta}\ Ze^{\mathbf{i}(\alpha-\beta)} && (2.37)\\
&= \mathbf{I}\mathbf{Z}. && (2.38)
\end{aligned}$$

If we define the complex *admittance*

$$\begin{aligned} \mathbf{Y} &= G + \mathbf{i}B && (2.39) \\ &= \frac{1}{\mathbf{Z}} && (2.40) \\ &= \frac{R}{Z^2} + \mathbf{i}\frac{(X_L - X_C)}{Z^2} && (2.41) \end{aligned}$$

then

$$\mathbf{I} = \mathbf{VY} \quad (2.42)$$

We can refer to G as the *conductance* and B as the *susceptance.*

Thevenin's theorem states that *any* two terminal AC network can be represented by an equivalent circuit consisting of a voltage source and a series impedance [1], and we shall use this later to make some simplifications to certain circuits.

2.3 Generation

Large scale power generation is provided by a mechanical force driving a turbine, which in turn drives the generator. The varying magnetic field produced by electro-magnets in a rotor attached directly to the turbine induces an alternating current in coils surrounding the rotor (the stator).

In this section we show the derivation of an equation, the *swing* equation, which models the dynamics of the generator as it responds to varying load.

The coils in the stator are arranged in pairs on opposite sides of the rotor, each pair generating one phase of the multi-phase supply (Figure 2.3).

The driving mechanical force may come from a steam turbine (such as in coal fired or nuclear power plants), a gas turbine, wind or water power. Variation in the production of this mechanical force provides a governing mechanism, by which the generator may be controlled. Although there are differences in the speed and size of the turbines used with different mechanical power sources, the basic model described below remains the same. In our model we assume that the mechanical power produced is constant.

The electro-magnetic behaviour of the rotor and stator is complex and can be modelled in using the so-called Park equations [2]. However, the model described below is sufficient to describe generator behaviour in the context of the whole power network, and so for reasons of simplicity we do not consider the Park

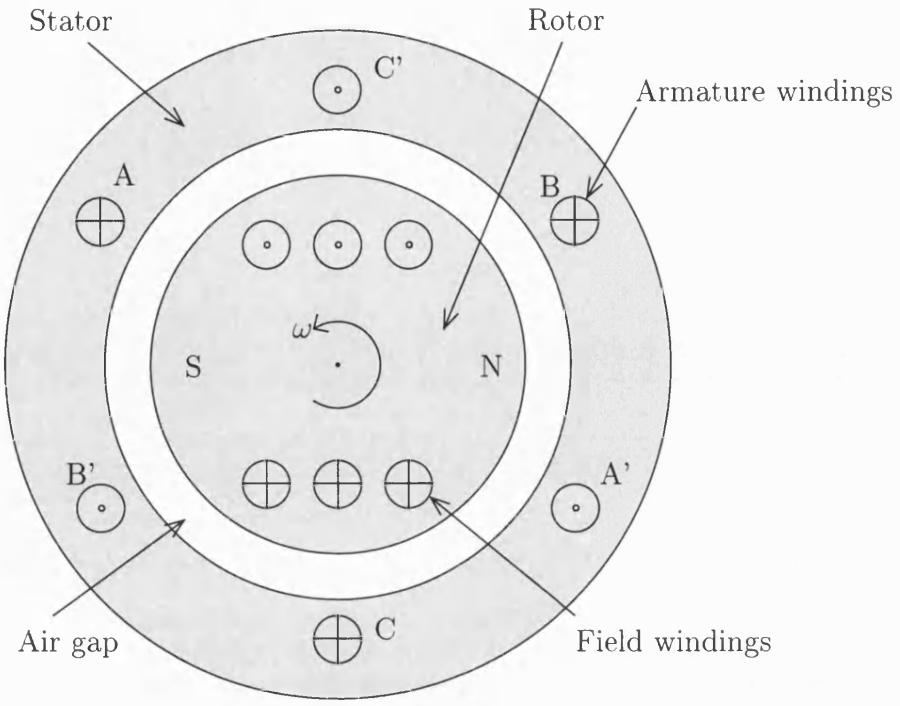

Figure 2.3: Generator cross-section schematic

equations here.

In our model below, we assume that the mechanical power produced is constant; this corresponds to assuming the above mechanical control and governing systems are working perfectly. We model frictional and electro-magnetical effects by assuming that damping is proportional to the rate of change of relative phase angle. Non-uniform damping models can also be used [3].

The magnetic field induced in the rotor windings does not have to remain constant. Changes in this field will induce changes in the output voltage from the stator windings. This may be used as a control mechanism (voltage regulation). In this model we assume that such a system is in place without modelling it explicitly, so that the generator provides a constant voltage output V_m. It is worth noting that in a real system, extraordinary parameter values and states could cause such a control system to break down and thus our model would become invalid. We should also note that if the voltage output from generators can be controlled successfully, then voltage collapse is likely to be a load dominated phenomenon.

Starting a generator is a non-trivial exercise. The mechanical start-up process itself requires a substantial electrical supply in order to power the electromagnetic parts of the generators and other equipment. Once turning, the generator must be

synchronised with the network before connection. The problem is compounded if several generators are required to be started at the same time. This is one of the major reasons why network operators are very keen indeed to avoid the wide-scale shutdowns typical in voltage collapse incidents.

Derivation of "swing equation" generator model

First we must introduce the concept of a synchronously rotating reference. This is a perfect sinusoidal signal at a fixed angular velocity ω_0. We can measure the frequencies and angular displacements of our electrical supplies with respect to this reference. In the case of examining only part of a power system this reference can be thought of conceptually as "the rest of the network", acting as a simple model of a much larger system we are feeding into. If we are examining the network as a whole, the reference might be a weighted average of all the phase angles at the different generators and loads.

The value of ω_0 is given by

$$\omega_0 = 2\pi f \tag{2.43}$$

where f is the frequency of the network, usually 50 or 60 Hz.

We shall show below (Section 2.4) that the AC power transfer between two points in a circuit (2.27,2.28) is dependent on the difference between the two phase angles, so measuring these angles with respect to a reference will make no difference to our later calculation of power transfers.

We can now derive an equation linking the mechanical power input and electrical power output. We consider the torque (rotating force) on the generator rotor. Let the turbine and generator rotor have combined moment of inertia J $(kg\,m^2)$ and angular velocity ω_m $(rad\,s^{-1})$. If T_a $(N\,m)$ is an accelerating torque, then Newton's 2nd law for a rotating body is

$$J\frac{d\omega_m}{dt} = T_a \qquad\qquad (kg\,m^2\,s^{-2}\,rad) \tag{2.44}$$

Now let ω_0 $(rad\,s^{-1})$ be the rated angular velocity of the system as above, and let VA_{base} (W) be a characteristic power value (usually 100MW, sometimes called the "base" power). We can then define an inertia constant $H = \frac{J\omega_0^2}{2VA_{base}}$ $(rad^2\,s)$. Analysis of actual generators show this inertia constant to be fairly independent of the speed and power of the machine, but is defined more by the type of generator (large/small, gas/coal/hydro, etc.).

Then equation (2.44) becomes

$$\frac{2H}{\omega_0^2} VA_{base} \frac{d\omega_m}{dt} = T_a \qquad (kg\, m^2\, s^{-2}\, rad) \tag{2.45}$$

and so

$$\frac{2H}{\omega_0} \frac{d\omega_m}{dt} = \frac{T_a \omega_0}{VA_{base}} \qquad \text{(dimensionless)} \tag{2.46}$$

which we can write as

$$2H \frac{d\omega_r}{dt} = P_a \tag{2.47}$$

where P_a is the dimensionless accelerating power and $\omega_r = \omega_m/\omega_0$ is the relative angular velocity.

We will actually use the angular velocity of the rotor with respect to the synchronously rotating reference,

$$\omega = \omega_m - \omega_0 \tag{2.48}$$

$$= \omega_0(\omega_r - 1) \tag{2.49}$$

Now let $\delta_m(t)$ be the angular position of our generator rotor with respect to the synchronously rotating reference; let ω_m be the angular velocity as above. Then at time t the rotor has relative angular position

$$\delta_m(t) = \delta_m(0) + \int_0^t \omega_m(\tau) d\tau \ - \omega_0 t \tag{2.50}$$

and so

$$\frac{d\delta_m}{dt} = \omega_m - \omega_0 \tag{2.51}$$

$$= \omega \tag{2.52}$$

and

$$\frac{d^2\delta_m}{dt^2} = \frac{d\omega}{dt} \tag{2.53}$$

$$= \omega_0 \frac{d\omega_r}{dt} \tag{2.54}$$

Then (2.47) can be written

$$\frac{2H}{\omega_0}\frac{d^2\delta_m}{dt^2} = P_a \tag{2.55}$$

Now consider the non-dimensionalised accelerating power P_a. It consists of mechanical power input P_m, electrical power generated P_e and a damping term. We shall model the damping torque as proportional to the change in angular velocity (2.52), giving

$$\frac{2H}{\omega_0}\frac{d^2\delta_m}{dt^2} = P_m - P_e - \frac{K_D}{\omega_0}(\omega_m - \omega_0) \tag{2.56}$$

$$= P_m - P_e - \frac{d_m}{\omega_0}\frac{d\delta_m}{dt} \tag{2.57}$$

In summary,

$$\frac{d\delta_m}{dt} = \omega \tag{2.58}$$

$$M\frac{d\omega}{dt} = P_m - P_e - d_m\frac{d\delta_m}{dt} \tag{2.59}$$

where $M = 2H/\omega_0$ and $d_m = K_D/\omega_0$. This equation is now non-dimensionalised with respect to all quantities except time (measured in seconds).

2.4 Distribution

Power is transmitted from generators to loads through a network of supply lines. These may be overhead lines supported on pylons or underground cables. Both types of line are typically made of low resistance copper. The two types of line have different inductive and capacitive behaviour; this can be represented by different parameter values in the model below.

The distribution network consists of many other components, relays and switch gear, protection devices, and reactive power compensation devices. In the following model these are not modelled explicitly, but are either assumed to be in constant states or are subsumed into the parameters describing the lines. The diagram shows the theoretical placement of a transformer, but we assume the ratio N to be 1.

The term *bus* or bus-bar is used to refer to an idealised point of connection between two or more points in a power systems circuit.

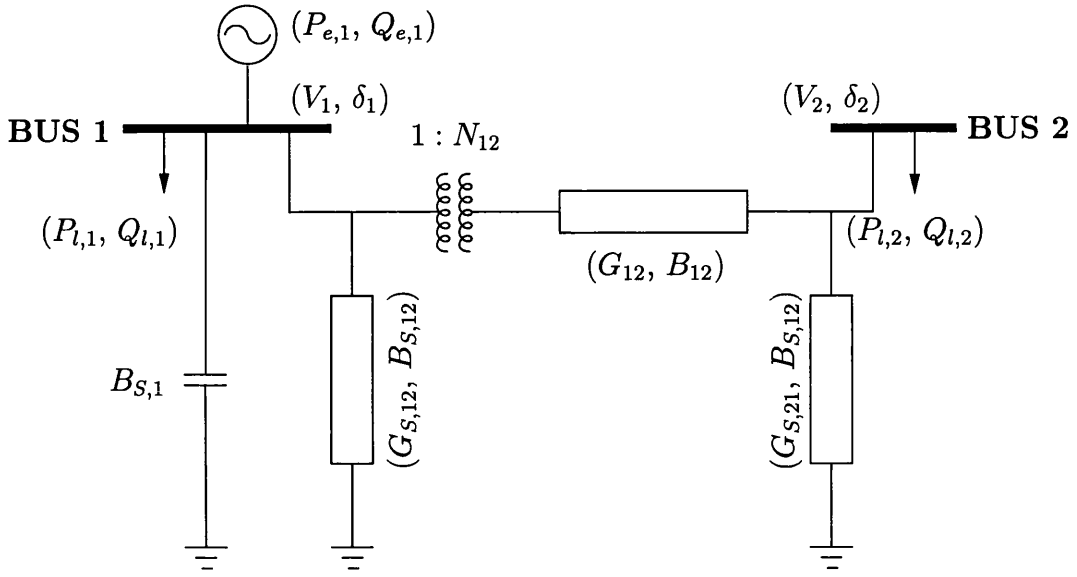

Figure 2.4: π network formulation

2.4.1 Power transfer between 2 buses

We can represent a single line connecting two bus-bars by the circuit known as the π-section representation, Figure 2.4.

The complex power injected into the network at Bus 1 is

$$\begin{aligned}
\mathbf{S}_1 &= \mathbf{V}_1\mathbf{I}_1^* \\
&= \mathbf{V}_1\Big(\mathbf{V}_1(\mathbf{i}B_{S,1} + G_{S,12} + \mathbf{i}B_{S,12}) + (\mathbf{V}_1 - \mathbf{V}_2)(G_{12} + \mathbf{i}B_{12})\Big)^* \\
&= V_1 e^{\mathbf{i}\delta_1}\big(V_1 e^{-\mathbf{i}\delta_1}(G_{S,12} - \mathbf{i}(B_{S,12} + B_{S,1})) \\
&\qquad +(V_1 e^{-\mathbf{i}\delta_1} - V_2 e^{-\mathbf{i}\delta_2})(G_{12} - \mathbf{i}B_{12})\big) \\
&= V_1^2(G_{S,12} + G_{12}) - V_1V_2\big(G_{12}\cos(\delta_1 - \delta_2) + B_{12}\sin(\delta_1 - \delta_2)\big) \\
&\quad + \mathbf{i}\Big(-V_1^2(B_{S,1} + B_{S,12} + B_{12}) \\
&\qquad -V_1V_2\big(G_{12}\sin(\delta_1 - \delta_2) - B_{12}\cos(\delta_1 - \delta_2)\big)\Big)
\end{aligned} \tag{2.60}$$

To find the active and reactive power injections into the network at Bus 1, we take the real and imaginary components of (2.60) respectively. By Kirchoff's current law, the active power injection at Bus 1 must balance the difference between the

active generation and load at Bus 1; likewise the reactive powers. This gives

$$\begin{aligned} P_{e,1} - P_{l,1} &= V_1^2(G_{S,12} + G_{12}) \\ &\quad -V_1V_2\big(G_{12}\cos(\delta_1 - \delta_2) + B_{12}\sin(\delta_1 - \delta_2)\big) \qquad (2.61) \\ Q_{e,1} - Q_{l,1} &= -V_1^2(B_{S,1} + B_{S,12} + B_{12}) \\ &\quad -V_1V_2\big(G_{12}\sin(\delta_1 - \delta_2) - B_{12}\cos(\delta_1 - \delta_2)\big) \qquad (2.62) \end{aligned}$$

2.4.2 Power transfer between n buses

Now let $j \in c(i)$ if Bus i is connected to Bus j with such a circuit. The network equations (2.61,2.62) generalise obviously to

$$\begin{aligned} P_{e,i} - P_{l,i} &= V_i^2 \sum_{j\in c(i)} (G_{S,ij} + G_{ij}) \\ &\quad -V_i \sum_{j\in c(i)} V_j\big(G_{ij}\cos(\delta_i - \delta_j) + B_{ij}\sin(\delta_i - \delta_j)\big) \qquad (2.63) \\ Q_{e,i} - Q_{l,i} &= -V_i^2\left(B_{S,i} + \sum_{j\in c(i)} (B_{S,ij} + B_{ij})\right) \\ &\quad -V_i \sum_{j\in c(i)} V_j\big(G_{ij}\sin(\delta_i - \delta_j) - B_{ij}\cos(\delta_i - \delta_j)\big) \qquad (2.64) \end{aligned}$$

We will typically have values or expressions for $P_{e,i}$,$P_{l,i}$ and $Q_{l,i}$. The problem of finding the V_i and δ_i that satisfy these power values is known as the *load flow* problem. We will discuss methods for this problem and how it relates to and can be combined with the process of calculating values for the generator and load powers.

Note that all occurrence of electrical phase angles δ_i are as differences, hence (2.63,2.64) will not be effected by a global change in phase angle. In order to solve the system there must be a fixed reference frequency. For instance we can fix the phase angle at one bus to be zero, or we may define a (weighted) average of the phase angles to be zero.

2.5 Load

Power system loads consist of the total real and reactive power demands of all electrical devices connected to the network. These devices will primarily be resistive (lighting, heating, etc.) but may also be reactive (for instance induction motors). Given the enormous number of loads connected to the system, it is not

practical to model them individually; except for perhaps the largest loads, such as electric arc-furnaces [4]. Network operators will attempt to model the aggregate load at each point where the main network supplies the local distribution systems and the largest individual customers. Both the real and reactive loads at each of these *load buses* will be of interest.

We must give some consideration to the time scale that we are interested in. In the very long term, load variation will depend on seasonal and economic factors. Models on this time scale can be used to make design decisions for the supply network and decide the viability of investing in new generating capacity.

On a daily time scale, there will be a large variation between the highest and lowest total loads, by a factor of about 2. The exact values will largely be dependent on the prevailing weather conditions, which effect load due to domestic heating, and the time of year, which will effect the use of street and domestic lighting. The estimated loads in each time period are used by the network operators to decide which generators will be connected to the network and (in countries with a competitive market for bulk electricity supply) the price of power. In the UK such load and pricing calculations take place for each half-hour interval of the day. Within each time interval, the network operators may have to take account of likely sudden surges in power, and hold reserves of power to cope with this in the form of generators that are running but not connected to the network. These surges can be caused by the end of televised events, followed by a large number of customers switching on domestic appliances such as kettles[2]. The sudden increase in demand can be over 5% of the total power supplied by the network; however these surges can be predicted and generally do not lead to system instabilities.

On a very short time scale (seconds and minutes) we can assume that the arrangement of the system stays constant; that no generators are being connected to or disconnected from the network, that network parameters remain constant and that loads are purely dependent on the characteristics of the supply and not on any external changes. We have described simple models for behaviour of generators and the flow of power through the transmission network. This will supply an AC voltage to the load buses at particular phase angles δ and magnitudes V. At each load bus there will be aggregate real and reactive loads P_l and Q_l. We want to model the dependency of these values on one another, and possibly on their time derivatives also. The dynamics of load devices such as induction motors will effect the system dynamics on these short time scales [5] so

[2]The record such surge in the UK was over 3000MW, occurring after the solar eclipse of August 11th 1999.

we must include these in our model. It is on this shorter time scale that voltage collapse occurs.

2.5.1 "Static" and "dynamic" load models.

There is a distinction in the power engineering literature between "static" and "dynamic" load models. This is probably historical and is somewhat artificial from a mathematical perspective – it is not always true that "static" load models are those without time derivatives.

The simplest load model is to take P_l and Q_l to be constants independent of V and δ. A general *static* model would be of the form

$$P_l = P(V, \delta), \tag{2.65}$$
$$Q_l = Q(V, \delta). \tag{2.66}$$

This could be an exponential model, for instance

$$P = P_0 (V)^{\alpha} \tag{2.67}$$

or perhaps a polynomial model

$$Q = q_2 V^2 + q_1 V + q_0. \tag{2.68}$$

Despite the name "static", this class of models would also include those combining an exponential or polynomial model with a representation of the frequency dependence of the load, for instance

$$P = P_0 (V)^{\alpha} \left(1 + K_{p\omega} \dot{\delta}\right), \tag{2.69}$$
$$Q = Q_0 (V)^{\beta} \left(1 + K_{q\omega} \dot{\delta}\right). \tag{2.70}$$

At least one author [6] has gone to great lengths to justify the use of a derivative in a "static" model. Load at a given time is proposed to be dependent on the overall change in frequency, then this change is *approximated* by a derivative, as follows

$$\Delta f = f - f_0 \tag{2.71}$$
$$\approx \dot{\delta}. \tag{2.72}$$

All these models may be combined if so desired. The constants α, P_0, q_i, etc.

might be found by empirical methods, using data sets from load measurements of actual power systems.

Such "static" models are typically used in investigation of the distribution network alone. One might wish to specify load and generating powers and then investigate the behaviour of the network by examining the existence and form of solutions to the "load flow" problem determined by (2.63,2.64).

A second class of load models are those referred to as "dynamic". In such models an attempt is made to explicitly model the short term behaviour of certain types of load. This might be the behaviour of relays and switches after they have been tripped, or automatic tap-changing transformers (if not included in the network model), or thermostatically controlled devices. These can generally be formulated as closed loop control systems and hence an equation could be written relating V, δ, ω, P, Q and their time derivatives. For further details of particular models, see a survey of load modelling formulations [7] or a standard textbook [6].

In [8] there is a discussion of the use of such models and their failure to prevent a major voltage collapse incident in Sweden. Laboratory experiments on the load response of induction motors suggested that a class of models could be improved by including a dependency on $\dot{V}$ (representing the inertia of such devices).

$$P_l = P_0 + P_1 + K_{p\omega}\dot{\delta} + K_{pv}(V + T\dot{V}) \tag{2.73}$$

$$Q_l = Q_0 + Q_1 + K_{q\omega}\dot{\delta} + K_{qv}V + K_{qv^2}V^2 \tag{2.74}$$

This model is further discussed in [7, 9] and in Chapter 3. The constants P_1, Q_1 represent a static domestic load, with the other terms including the constants P_0, Q_0 represent induction motor load.

2.6 Model formulation and solution

Now we have models for all three sections of the system; generation, distribution and load. We can combine these as described below. We must make a careful distinction between unknowns where we have an expression involving a time derivative of the variable and unknowns where we do not. These are typically referred to in general as x and y respectively.

At each generator bus we have differential unknowns – phase angle δ_m and relative angular velocity ω_m – with expressions for their derivatives (2.58,2.59). The constant machine input power P_m, damping coefficient d_m, output voltage

V and constant real and reactive loads at the generator P_l, Q_l, are all assumed to be known. Algebraic unknowns are the real and reactive outputs P_e and Q_e (although the latter is not needed in order to solve the system, but may be calculated once the solution is known).

At each load bus we have differential unknowns – supply voltage V and supply phase angle δ – with expressions for their derivatives (2.73,2.74) using a number of specified constants. Algebraic unknowns at the load buses are the real and reactive loads P_l and Q_l.

At every bus we must satisfy Kirchoff's current law, leading to the algebraic constraints (2.63,2.64). At each bus with dynamic variables (in our case load and generator buses) we may substitute the expression from Kirchoff's law into the differential equation. For example (2.63) with $P_l = 0$ can be subsituted into (2.59) to eliminate P_e. In general this leads to

$$\dot{x} = f(x, y, \lambda). \tag{2.75}$$

where x is a vector of all differential variables, y a vector of all algebraic variables (e.g. voltage magnitudes and phase angles at buses without a dynamic generator or load model) and λ a vector of all parameters and constants.

At buses where we do not have differential equations relating the unknowns, for instance simple junctions between supply lines, we will have algebraic unknowns voltage V and phase angle δ. We must again also apply the constraints (2.63,2.64), where the load and generation, and hence the net power, are zero. This gives an algebraic constraint on the system of the form

$$0 = g(x, y, \lambda). \tag{2.76}$$

We will also get a constraint of this type at load buses if we choose a load model containing no time derivatives, such as of type (2.65,2.66).

So if we have non-algebraic load models and no "junction" buses, we will have an ODE system (2.75) to solve with no algebraic variables y. If we choose algebraic load models and/or have junctions in the system then we will get algebraic constraints (2.76) on the system and hence a more complicated DAE model. This will have implications on the numerical methods chosen for solution and analysis of the system (2.75,2.76). Much traditional power engineering analysis has focused on the generation and distribution part of the modelling problem (see next chapter). The implicit assumption has been that more complicated load models lead to more complicated mathematical and computational problems. Here we

have shown that this is not necessarily true.

2.7 Practical usage

Given the complexity of any "real-world" power system model, it is not surprising that tools have been developed to allow automated assembly and solution of the equations governing a given network configuration composed of specified components. Several systems exist to allow graphical assembly and solution of power system and other electrical models.

Notable amongst these are the EUROSTAG system, developed by Electricité de France, and the power system block-set, which is a set of modules for the Simulink control system that forms an add-on to Matlab. These both make use of block diagrams and a graphical user interface to specify system components, configuration and parameters. A block might specify a basic "swing" equation generator model; to this could be added blocks representing control devices for both the mechanical power input and the voltage output. In each block, relevant parameters and initial conditions can be specified. Similar blocks, or groups of blocks, can represent the network and loads. The package will automatically generate and solve the equations, calculating trajectories over time, and produce user output as required.

The advantages of this system are that the same graphical interface can be used to define the models and view their predicted behaviour. They are of great use to the engineer who may not be interested in the detail and theoretical behaviour of the underlying mathematical models of each component, but must find a way of replicating and predicting the behaviour of a real or proposed power system.

For the same reasons that such systems are useful to engineers dealing with practical problems, they may cause difficulties to mathematicians (or theoretically inclined engineers) who are interested in the underlying mathematical models and the numerical methods used to approximate their behaviour. A major disadvantage of systems relying on block-sets is that they only offer a finite number of blocks with which to represent system components and a finite number of methods with which to solve the system. For example it is not possible in the EUROSTAG system to specify a load model of the form $P = f(\dot{V})$. In the same package, a variety of numerical methods can be chosen to solve the differential equations defined by the blocks and produce trajectories of system states over time, however there is no simple way to implement a continuation method to

investigate the parameter dependence of the systems.

2.8 Non-linear models of specific power system components

A number of related problems in power systems modelling are currently attracting interest in the non-linear mathematical community.

2.8.1 The DC–DC buck converter

There exist several DC–DC links connecting national power networks, such as the cross–channel connection linking the French and English networks. It is desirable to use DC for such links, since this avoids any frequency or phase linkage between the two systems and can lead to more efficient power transfer. In an AC system, transformer devices can utilise the principle of self induction to step the voltage up or down to the desired level; this is not possible in a DC system. The DC–DC Buck converter uses a switch driven by a non-smooth signal and a circuit containing resistance, reactance, capacitance and a diode, in order to step down the DC voltage. The non-smooth signal leads to dynamical effects which are interesting both physically and mathematically, such as grazing and sliding [10].

2.8.2 Transformers

Ferro-resonance

Hysteresis is an important phenomenon in the study of large magnetic fields. In the operation of transformers it can lead to multiple stable states co-existing; the states other than the normal operating state are termed *ferro-resonant.*

Dynamical systems techniques are well suited to examination and understanding of such behaviour. Lamba et al. [11] show how experimental data can be used efficiently and accurately to determine parameter values needed to describe the magnetic response in a standard model of magnetic hysteresis. This allows the complete specification of a (non-smooth) dynamical system. At each parameter value, random initial points were chosen and the system iterated over time. Application of a Poincaré section allows the generation of bifurcation diagrams which clearly show the multiple stable states occurring during ferro-resonance and at which parameter values such behaviour occurs. These numerical results show good correlation with data obtained from laboratory experiments.

On-load tap changing transformers

The voltage increase or decrease at a transformer is dependent on the "tap ratio". Transformers in modern networks have the ability to have their tap ratio changed without being taken off-line, and so are known as On-Load Tap Changers (OLTCs'). This may be done remotely, either due to the direct intervention of an operator, or as the result of some control algorithm which aims to maintain a constant voltage supply to the end user while maximising efficiency in the distribution network. Since the tap-ratio may be set at one of a finite number of discrete settings, behaviour of an OLTC system can naturally be interpreted as a discrete dynamical system.

It has been suggested [12, 13] that OLTC's may contribute adversely to the stability of the system in a voltage collapse situation. Dynamical systems analysis of power system models incorporating OLTC's is theoretically problematic, since they consist of a discrete system (the OLTC), a continuous system (generation and load) and a control system (which may be non-smooth). Further study of OLTC's as individual dynamical components is needed before they can be meaningfully incorporated into a dynamical model of an entire power system.

2.8.3 Electric arc furnaces

As individual loads, electric arc furnaces each consume enormous amounts of power. This can sometimes be detected by domestic users as a flicker in lighting systems, which corresponds to an arc furnace being connected to the network. The large power use of these components suggests that the application of a nonlinear model is both necessary (since each individual load has a measurable effect on the entire system) and potentially tractable (since data collection is much easier from a single large load, and hence model validation and parameter selection more likely to be successful).

O'Neill-Carrillo et al. [4] attempt to use a chaotic system to reproduce some of the behaviour of an electric arc furnace. Measures are taken from time series data from actual furnaces and from the small chaotic system; one such measure is an estimate of the largest positive Lyapunov exponent calculated using an embedding method. The parameters in the chaotic system can be adjusted in order to most accurately reproduce the behaviour of the actual furnace.

Whilst this method cannot be used for direct prediction (i.e. accurate calculation of trajectories), this is often not what is wanted. This method can yield valuable information about the stability and other qualitative behaviour of arc

furnaces, which can be used for planning and performance assessment.

2.8.4 Use in this work

We have not taken specific account of DC-DC links, transformers or arc-furnaces in the power system models used in subsequent chapters.

One reason for this is to allow proper comparison of our results with previous research. A sensible methodology in an area of application where both models and techniques are being developed, is to make substantial change to either one or the other. In the following chapters we use a power system model which has been developed by a number of other researchers; we examine and extend a range of techniques to analyse this model and can directly compare our results to previous research. In Chapter 6 we apply the same techniques to a more complex extension of this model. Addition of further complexity (for instance incorporation of an arc-furnace load model) would be simple in the cases where such models can be written in the form of a smooth ODE or DAE. However, use of a model with non-smooth behaviour (e.g. excitation control with limits in generator models) or with non-continuous behaviour (e.g. on-load tap changing transformers) would first require the development application of further numerical and analytic techniques for power system models.

A second reason for limiting the complexity of our model is the consideration of evidence for particular components contributing to the problem of voltage collapse. When modelling any complex system, it is impractical to explicitly account for the behaviour of every single component; the behaviour of a class of components can be homogenised and treated as a single dynamic component, or represented by some constant value (either implicitly or explicitly). There is good evidence that reactive load level is an important factor in voltage collapse [14, 15], and that the dynamic response of induction motors has a large effect on this load [8] hence we include them in our model. This is not to say that a good case cannot be made for including further components in a model used to study voltage collapse, but this has not been the primary focus of this work.

Chapter 3

Dynamics of Electrical Circuits

3.1 Introduction

In this chapter, the basic mathematical definitions of a dynamical system and the necessary bifurcation theory are introduced, together with the outline of some related numerical tools. We motivate all of these theoretical concepts by relating them to the observed and desirable behaviour of the dynamics of systems such as the National Grid. We describe some circuits for which the use of a dynamical systems approach has been effective and discuss the dynamics observed both in experiments and in numerical simulations, looking at steady, periodic and chaotic behaviour. We discuss some particular voltage collapse incidents in this context, relating the observed time series behaviour and known physical information to possible dynamical explanations.

3.2 Review of dynamical systems theory

3.2.1 Dynamical systems

Background

Dynamical systems as a subject can can trace its origins back to the work of Poincaré, but with the advent of cheap computational power has undergone a massive expansion in the last thirty years, in terms of theory and application. Advances in computational and analytical techniques have often been made due to the study of one of a number of standard "test" systems. A number of these attempt to describe electrical phenomena. We present these briefly here, in order to illustrate the applicability of dynamical systems theory to electrical and electronic problems.

Examples

The Van der Pol oscillator (c.1920) describes a simple series circuit containing triode valve. The resistive properties of this valve are current dependent. The two-dimensional dynamical system

$$\ddot{x} + (x^2 - 1)\dot{x} + x = f(t) \tag{3.1}$$

describes the current flowing through this system, where the non-linear term $(x^2 - 1)$ describes the resistive properties of the valve. The system may be either forced (non-autonomous) or unforced (autonomous, $f(t) = 0$) and contains saddle-node and Hopf bifurcations leading to a wide variety of periodic, quasi-periodic and chaotic behaviour. A good presentation can be found in Guckenheimer and Holmes [16].

Chua's circuit, introduced in 1983, consists of a number of linear RLC components and a non-linear diode. This is described by the system

$$\dot{v}_{c1} = \frac{1}{C_1}\left(\frac{1}{R}(v_{c2} - v_{c1}) - g(v_{c1})\right) \tag{3.2}$$

$$\dot{v}_{c2} = \frac{1}{C_2}\left(\frac{1}{R}(v_{c1} - v_{c2}) + i_L\right) \tag{3.3}$$

$$\dot{i}_L = \frac{1}{L}\left(-v_{c2} - R_0 i_L\right). \tag{3.4}$$

The voltage-current relationship of the non-linear diode is usually modelled by the piecewise linear function

$$g(v_R) = G_b v_R + \frac{1}{2}\left(G_a - G_b\right)\left(|v_r + E| - |v_r - E|\right) \tag{3.5}$$

or possibly by some smooth function [17]. As a circuit parameter increases, the three-dimensional dynamical system undergoes a period doubling cascade to chaos; the chaotic attractor then collides with a second such attractor which exists due to symmetry in the system. This circuit is useful because it can easily be built [17, and references therein] and the complex dynamics then observed directly and compared with numerical simulations.

Both these circuits are motivated by the study of circuits that are in some sense small (i.e. can easily be built in a laboratory). Realistic power system models as described in Chapter 2 are in no sense "small", in terms of either physical length, power, voltage or Euclidean dimension. This is perhaps why dynamical systems theory has only been applied to power systems in the last few

years.

3.2.2 Definition of a dynamical system

A *dynamical system* consists of a *state space* χ (the set of all possible states $x \in \chi$ of the system), a set $\mathcal{T}$ of *times* at which we consider our system to have a state, and a set of *flow maps* $\phi_t : \chi \to \chi$ which define the evolution of states $x \in \chi$ through a time $t \in \mathcal{T}$. The set of maps ϕ_t must form a semi-group; that is that $\phi_0(x) = x, \forall x \in \chi$ and $\phi_{t_1}(\phi_{t_2}(x)) = \phi_{t_1+t_2}(x) = \phi_{t_2}(\phi_{t_1}(x)), \forall x \in \chi, \forall t_1, t_2 \in \mathcal{T}$.

In the following work we will use finite dimensional states spaces, $\chi \subseteq \mathbb{R}^n$ for some fixed n. We will consider systems with continuous time, $\mathcal{T} \subseteq \mathbb{R}$, and also systems with discrete time, $\mathcal{T} \subseteq \mathbb{N}$. The flow maps will typically be dependent on a number of parameters $\lambda \in \mathbb{R}^m$.

For the continuous time case, the flow mapping is typically defined by the solution to a differential equation; for electrical circuits this is normally an ODE or a DAE describing the rate of change of the state variables. The parameters $\lambda \in \mathbb{R}^m$ are normally considered to be constant with respect to changes in time or state. The rates of change of states may theoretically be dependent on t (non-autonomous) but the models we shall use to describe power systems are not. We are therefore primarily interested in the solutions to the problem

$$\begin{aligned} \tfrac{dx}{dt} &= f(x, \lambda) \\ x(t) &\in \chi \subseteq \mathbb{R}^n \\ \lambda &\in \mathbb{R}^m \\ t &\in \mathbb{R}. \end{aligned} \tag{3.6}$$

The dimension n may be in the thousands for a realistic power system model. The parameters λ will correspond to such system parameters as real and reactive load demands P, Q. We present here a short summary of the theory for such differential systems. Later in this chapter will consider modifications for the index one differential algebraic systems needed for large scale electrical modelling.

For the rest of this thesis we will assume that f is smooth. This means we are making various assumptions in the model (discussed in Chapter 2.) such as not including switches or automatic transformer tap-changers.

If $f : \mathbb{R}^{n+m} \to \mathbb{R}^n$ is a globally Lipschitz function, then for each starting value $x(0) = x_0 \in \chi$, a solution $x(t)$ exists $\forall t \in \mathbb{R}$, and the flow mapping can be defined as $\phi_t(x(t_0)) = x(t_0 + t)$. In contrast the power systems models are all *locally* Lipschitz functions and this guarantees local existence of solutions. The

case where solutions do not exist for all time is very relevant to voltage collapse; this special feature is discussed further in Section 4.3. Indeed, a voltage collapse incident might be said to occur precisely when the flow map becomes singular.

Discrete dynamical systems can arise directly from a mathematical model of some system. An example of this could be the spot price of UK bulk electricity supply, which is traded in "the Pool" at half-hourly intervals. Another example might be the behaviour of a transformer with an on-load tap changer, where the transformer (discrete) tap ratio can be changed at various times according to some specified control. However, in this work we only need to consider discrete mappings which arise as a consequence of the continuous problem (3.6).

3.2.3 Fixed points and stability

A *fixed point* of a dynamical system is a state that does not change over time; that is $x_0 \in \chi$ such that $\phi_t(x_0) = x_0$, $\forall t \in \mathcal{T}$. With reference to (3.6) a fixed point is defined by

$$\left.\frac{dx}{dt}\right|_{x=x_0} = f(x^0, \lambda) = 0. \tag{3.7}$$

Given a point $x_0 \in \chi$, the *trajectory* passing through that point is the set $\{x(t) = \phi_t(x_0) : t \in \mathcal{T}\}$. If we are interested only in $t \in [0, \infty)$ we might refer to the *forward* trajectory starting at x_0.

We say a fixed point x_0 is *asymptotically stable* if trajectories near the fixed point stay near it and evolve to it in forward time. Formally, $\forall \epsilon > 0\ \exists \delta > 0$ such that $||x(t_0) - x_0||_2 < \delta \Rightarrow ||x(t) - x_0||_2 < \epsilon$, $\forall t > t_0$, and $\lim_{t \to +\infty} x(t) = x_0$. There are other mathematical definitions of stability, but asymptotic stability is sufficient for this work. The word stability often has specific meanings in different engineering contexts, which we discuss below. The normal operating state of a large power system is at a fixed point of the system, which remains stable with slow variations of parameters λ.

Taking the Taylor series expansion of f about the fixed point it can be shown, by the Poincaré Linearisation Theorem [18], that under mild conditions on f, the stability of the fixed point depends on the eigenvalues of the Jacobian matrix $\frac{\partial f}{\partial x}$ at the fixed point x_0. If these are all in the left half of the complex plane then x_0 is stable; if one or more has a positive real part then x_0 is unstable.

In the case of an eigenvalue λ having $Re(\lambda) = 0$, we can determine the behaviour of the system at this point by performing a *centre manifold reduction.* If we have eigenvalues of f_x with positive real part then x_0 will be unstable. Let E^s, E^c be the eigenspaces corresponding to eigenvalues with negative and zero real

parts, respectively. Then there are invariant manifolds W^s, W^c tangent to these at the fixed point. We can re-write the system as differential equations in terms of co-ordinates (y, z) on E^s, E^c respectively. It can be shown [19, 20] that the solution of the system on the centre manifold is described by a function $y = h(z)$ and that this can be approximated by a power series in order to determine when points on the centre manifold will have trajectories leading towards or away from the fixed point, and so determine its stability and the local behaviour.

We can also demonstrate the stability of fixed points x_0 by the use of *Lyapunov functions* $V : cl(G) \to \mathbb{R}$ where G is some open neighbourhood of x_0. If V is continuously differentiable, and has the properties that $V(x_0) = 0$, $V(x) > 0$, $\forall x \in cl(G) \setminus x_0$ and $\dot{V} = \sum f_i(x) \frac{\partial V}{\partial x_i} < 0$, $\forall x \in G \setminus x_0$ then Lyapunov's Second Stability theorem (see for example [18]) gives that x_0 is asymptotically stable. This method is used widely in many different engineering contexts, particularly in control theory problems; we discuss some of these below. V is typically some measure of energy in the system, which is at a minimum at a stable fixed point. Fixed points and their stability can be found by looking for local minimums of the energy functions. Forming useful Lyapunov functions for an arbitrary power system can be difficult as they will be dependent on the particular model used and may not give good a good approximation to the basin of attraction (see below).

3.2.4 Attractors

A point x_∞ is a *limit point* of an orbit $\{x(t)\}$ if for every $\epsilon, \tau > 0$ there is a time $t_1 > \tau$ such that $|x(t_1) - x_\infty| < \epsilon$ [21]. In essence this is a point that our trajectory $x(t)$ goes arbitrarily close to, given enough time. The set of such limit points for a given orbit is called an *ω-limit set.* If all orbits in some neighbourhood tend to the same ω-limit set, we call it an *attractor.* The simplest example of an attractor in this sense is a stable fixed point.

A *periodic orbit* of period T is a trajectory such that $x(t+T) = x(t) : \forall t \in \mathcal{T}$. We can define a subset $\mathcal{P}$ of χ such that the periodic orbit intersects $\mathcal{P}$ once only for $t \in [0, T)$, Figure 3.1. The periodic orbit and trajectories close to it then induce a discrete dynamical system on a set of points lying on a hyper-plane transverse to the orbit. The map associated with the return map of the periodic orbit is known as a Poincaré map. We can define the stability of the periodic orbit in terms of the stability of this Poincaré map. We observe such periodic orbits in power systems models.

An orbit is *quasi-periodic* if it has fundamental frequencies which are not

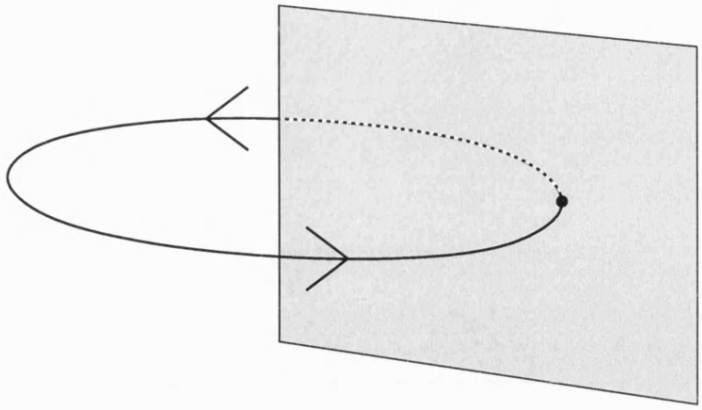

Figure 3.1: Schematic of a Poincaré section

rational multiples of each other; that is $x(t) = P(f_1 t, f_2 t, \ldots, f_n t)$ where $n \geq 2$, P is 2π periodic in each argument, and no frequency f_i is a rational multiple of another. The canonical example of such an orbit lies on the surface of a torus in phase space; if we have a Poincaré section cutting through one side of this torus, the intersections of the quasi-periodic orbit will lie densely on a circle on the Poincaré section.

A *strange attractor* is an example of an attracting ω-limit set that is not a fixed point, periodic orbit or quasi-periodic orbit. Strange attractors are usually associated with *chaotic* behaviour – trajectories on a strange attractor demonstrate a sensitivity to initial conditions associated with a folding and stretching of the associated phase-space. We will observe strange attractors in our models of power systems. As motion on the strange attractor is bounded, the trajectories do not exhibit collapse; however chaotic motion is still highly undesirable from the point of view of the performance of the grid.

If we cannot define a bounded set Ω such that $x(t) \in \Omega$, $\forall t \in [0, \infty)$, then we say the the orbit is *escaping*. We can also say that ∞ is the attractor for points on this orbit, or in the case of power system models, that *collapse* has occurred.

Given a stable fixed point x_0, we are interested in the set of points which have trajectories leading to x_0. The *basin of attraction* of x_0 is defined to be $\{x(0) \in \chi : lim_{t \to +\infty} x(t) = x_0\}$. A subset of the basin of attraction can be computed by the formation of Lyapunov functions and examining for which values $x \in cl(G)$ the inequality $\dot{V}(x) < 0$ holds; however there may be points outside G which have trajectories leading to x_0. If a power system receives a perturbation from some external source, then the system will return to a stable operating point if the perturbation lies inside the basin of attraction of the operating point.

3.2.5 Bifurcation

Bifurcation theory plays a central role in our investigation of the dynamics of power systems, as bifurcation points mark a transition from a "safe" operating point to one where voltage collapse occurs or is likely.

A *bifurcation point* is a point $(x_0, \lambda_0) \in \mathbb{R}^{n+m}$ at which the flow mapping ϕ undergoes a qualitative change [18]. Bifurcations can be classified as either global or local, static or dynamic; we define these terms properly below after giving some examples.

The *co-dimension* of a bifurcation is the minimum number of parameters λ that need to be changed in order for the bifurcation to be observed in a persistent way [16, p.123]. We are interested in certain co-dimension 1 bifurcations and a particular co-dimension 2 bifurcation, and their existence, computation and implications in power systems models.

For simplicity, in the following paragraphs we often define bifurcation as the transition between stable and unstable states. However, bifurcation can be defined less restrictively in terms of more general changes to the dimensions of the stable and unstable manifolds of the points in question.

Saddle-node bifurcations

The *saddle-node* or *fold* bifurcation occurs at λ_0 when the Jacobian $\frac{\partial f}{\partial x}$ at a stationary point x_0 has a simple zero eigenvalue, with left and right eigenvectors w and v respectively and

$$w f_{\lambda}^{0} \neq 0, \tag{3.8}$$

$$w f_{xx}^{0} v v \neq 0. \tag{3.9}$$

Then the following holds for (x, λ) in some neighbourhood of (x_0, λ_0) (where the inequalities can be reversed throughout). For $\lambda < \lambda_0$ there exist locally two fixed points of the system[1], the unstable manifiolds of which differ in dimension by 1; or $\lambda > \lambda_0$ there exist (locally) no fixed points of the system. [16]. Typically, although not necessarily, the saddle-node point occurs when a stable and an unstable fixed point coalesce.

This bifurcation is co-dimension 1, local and static. This structure of a pair of (stable and unstable) fixed points coalescing and disappearing has been observed

[1]Without loss of generality, we have presented the case where fixed points exist for $\lambda < \lambda_0$. However a similar analysis can be preformed for the mirror image case where fixed points only exist locally for $\lambda > \lambda_0$.

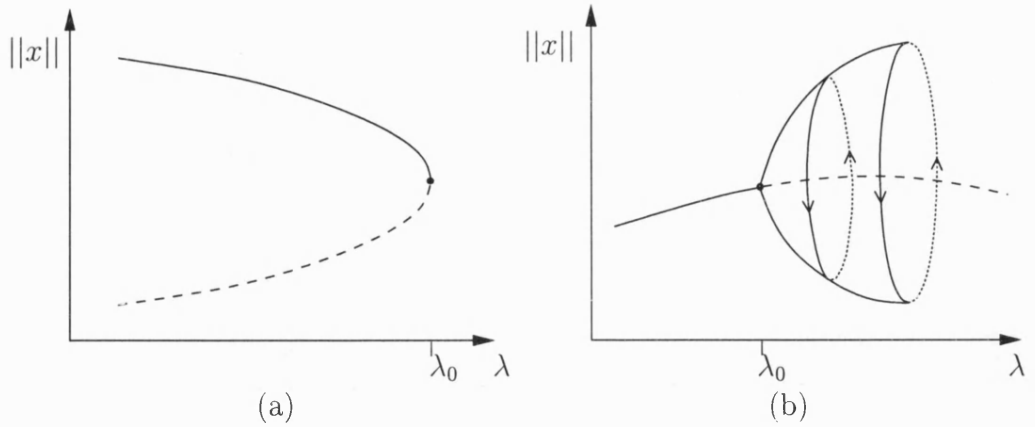

Figure 3.2: Example forms of system at bifurcation point λ_0. — denotes stable, -- unstable. (a) Saddle-node, (b) Hopf

in the calculation of the ability of a power distribution network (2.27,2.28) to supply increasing loads. In a power system $\lambda > \lambda_0$ will mean that there are no fixed points and thus voltage collapse is always observed. Calculating λ_0 has been used as part of the determination of safe operating regimes for power systems [22]; however we will show that there are significant areas of parameter space away from such points where voltage collapse is observed.

Hopf bifurcations

A *Hopf* bifurcation from a path of fixed points $x(\lambda)$ occurs at $\lambda = \lambda_0$ when the Jacobian f_x at a fixed point $x_0 = x(\lambda_0)$ has a pair of purely imaginary (but non-zero) eigenvalues $\mu(\lambda_0) = \pm i\beta$, with no other eigenvalues with zero real part and the along the path of fixed points these critical eigenvalues have the property

$$\frac{d}{d\lambda} Re(\mu(\lambda))\Big|_{\lambda=\lambda_0} = d \neq 0. \tag{3.10}$$

Then the behaviour of the system at this point is governed by its dynamics on a two-dimensional centre-manifold around x_0, upon which the system has the normal form

$$\dot{r} = (d\lambda + ar^2)r \tag{3.11}$$

$$\dot{\theta} = \beta + c\lambda + br^2 \tag{3.12}$$

in polar coordinates, with the coefficients[2] defined by performing a centre manifold reduction [18]. If $ad > 0$ ($ad < 0$ respectively) then there exists a path of periodic orbits emanating from (x_0, λ_0) for $\lambda < 0$ ($\lambda > 0$). If $d > 0$ ($d < 0$) then the fixed point is stable (unstable) for $\lambda < 0$ ($\lambda > 0$) and is unstable (stable) for $\lambda > 0$ ($\lambda < 0$). The periodic orbit takes the opposite stability to the fixed point it surrounds; if it is stable (unstable) we refer to the Hopf bifurcation as being supercritical (subcritical). [16].

This bifurcation is co-dimension 1, local and dynamic. We will show that Hopf bifurcations create periodic orbits in Power Systems models. Although such orbits may be stable and bounded in the mathematical sense, they do not represent desirable operating states from an engineering standpoint, because the end users of electricity require it to be delivered to them at a fairly constant voltage and frequency.

Bifurcations of periodic orbits

We have noted that the stability of a periodic orbit can be defined in terms of the stability of the associated Poincaré return map. However, this is not directly useful for determining the stability of a given orbit in practice.

If (3.6) has a periodic orbit $p(t)$ of period T, then the first order variations from this orbit must satisfy

$$v'(t) = f_x\left(p(t), \lambda\right) v(t) \tag{3.13}$$

$$v(0) = v_0 \tag{3.14}$$

This system is linear, and so we can write its solution in terms of a fundamental matrix Y:

$$v(t) = \mathbf{Y}(t)\, v_0. \tag{3.15}$$

The matrix $\mathbf{Y}(T)$ is called the *monodromy matrix* and its eigenvalues are usually referred to as the *Floquet multipliers* for the system. One multiplier will always lie on the unit circle; the periodic orbit can be shown [16] to be stable if all the remaining Floquet multipliers μ satisfy $|\mu| < 1$. The calculation of the Floquet multipliers can be achieved efficiently, as part of algorithms to approximate periodic orbits [23].

Subject to transversality and non-degeneracy conditions, the bifurcations of periodic orbits can be classified in terms of how Floquet multipliers leave the

[2] An expression for the coefficients d can be found in a standard textbook, e.g. [16]

unit circle as a parameter is varied. A *period doubling* bifurcation occurs if one multiplier crosses the unit circle at -1. This leads to the creation of a new stable orbit with twice the period. Repeated period doublings can occur in a *cascade* leading finally to chaotic behaviour; this has been observed in a wide variety of different systems and we show below that it is a feature of power systems models.

A turning point on the parameter dependent branch of periodic orbits occurs when a Floquet multiplier crosses the unit circle with value $+1$, also called a *cyclic fold* bifurcation. This allows for the existence of both stable and unstable periodic orbits at the same parameter value.

A *Homoclinic orbit* is a periodic orbit of infinite period, such that $\lim_{t\to\pm\infty} x(t) = x_0$. If such an orbit exists for some λ_0, but does not for λ in an ϵ-neighbourhood of λ_0 then we have a *Homoclinic bifurcation.* This bifurcation is co-dimension 1, global and dynamic. We will see such a bifurcation occurring at a Šil'nikov bifurcation point in our power system, leading to highly complex dynamics.

Bogdanov-Takens bifurcations

A *Bogdanov-Takens* bifurcation point (BT-point) is a co-dimension 2 bifurcation point where the Jacobian at a fixed point has a zero eigenvalue of geometric multiplicity 1 and algebraic multiplicity 2 [24, 16]. This is equivalent to the linearisation at the fixed point having a Jordan-Normal form with a block of the form $\begin{pmatrix} 0 & 1 \\ 0 & 0 \end{pmatrix}$ and no other blocks associated with the zero eigenvalue. This point is of great interest as it can be shown ([16] and also Section 5.2.2) that emanating tangentially from the path of saddle-node bifurcations in $(x, \lambda_1, \lambda_2)$ space, are paths of Hopf and homoclinic bifurcations. It can be thought of as being the point at which the Hopf and saddle-node points both become degenerate and meet; information about the path of homoclinic orbits is then gained "for free". We shall show that this is of great importance both theoretically and computationally, as it acts as an organising centre for many of the features associated with power systems models.

Other co-dimension 2 bifurcations exist which also describe interactions between paths of saddle-node, Hopf and homoclinic bifurcations. These are characterised by different Jordan blocks. Further details can be found in a suitable advanced textbook [16].

Further definitions

Having given examples of various bifurcations, we can now define *local* bifurcations as those which can be detected merely by observation of eigenvalues of the Jacobian at a fixed point, and *global* bifurcations as those which cannot. *Static* bifurcations can be seen to involve only fixed points, whereas *dynamic* bifurcations involve non-trivial trajectories such as periodic orbits. It is important to note that here *dynamic* does not necessarily mean that the bifurcation is observed as the system is studied over time, even though evidence for co-dimension one bifurcations might be found as a parameter is change slowly over time (normally much slower than the time scale of a typical event in the system such as a periodic orbit). Bifurcations may occur with respect to parameters which will not normally change over time; these might be design parameters such as the mass of generator rotors, or the length of a particular power line.

Normal forms

The above local bifurcations have *normal forms* which are canonical systems of minimal dimension to which the system at the bifurcation points can be reduced by an appropriate change of co-ordinates. These simple and well-understood normal forms can then be used to make important predictions, for instance regarding the location of periodic orbits in the neighbourhood of a Hopf bifurcation, or the location of paths of co-dimension 1 bifurcations in the neighbourhood of a BT-point. The change of co-ordinates can be then be reversed in order to show the location of this behaviour in the original system. Normal forms are very useful for our studies of power systems as they allow us to reduce, locally, the very complicated equations to much better understood smaller systems.

3.3 A summary of computational methods for bifurcation problems

Before we consider the application of the theoretical concepts of dynamical systems to the problem of power system stability, we must consider some of the numerical methods we will use in our investigation. We present a very short account here – further details of the specific use of the methods to investigate power systems models will be described in further chapters. Dynamical systems and bifurcation theory is applicable to systems of arbitrary dimension. Due to the non-linearity and high dimension of systems of any reasonable complexity, for

example such as those needed to accurately model power systems, we are forced to use numerical methods to detect and analyse the phenomena discussed in the previous section. We use three basic tools.

Numerical integration methods, such as Runge-Kutta and BDF schemes, are used to calculate the trajectories passing through specified points in state space, for a fixed parameter value (or set of parameter values).

Root finding algorithms (such as Newton's method, Broyden's method) can be used to find fixed points of the dynamical system. If applied to a suitably defined extended system, they can also be used to accurately locate bifurcation points. For the calculation of periodic and homoclinic orbits, a suitable Boundary Value Problem can be defined, and the numerical solution of this, for example by a collocation method [25], will typically be implicit and so require a numerical root finding technique to be applied.

We will be interested in parameter dependent loci of fixed points in (x, λ) space, obtained by changing one parameter λ only (and considering any other parameters to be fixed). The Implicit Function Theorem [26, for example] tells us that such a locus exists uniquely in some neighbourhood of a fixed point (x_0, λ_0), and passes through the fixed point, as long as f is differentiable and its Jacobian at the fixed point is non-singular.

We can approximate sections of these paths using *continuation methods* to calculate a finite number of points $\{(x_i, \lambda_i) \in \mathbb{R}^{(n+1)} : f(x_i, \lambda_i) = 0,\ i = 1, \ldots, N\}$. If we know a fixed point x_1 at a parameter value λ_1, we wish to find a fixed point x_2 at a nearby parameter value λ_2. We could just take a step $\lambda_2 = \lambda_1 + \Delta\lambda$ in parameter space, and apply a root finding algorithm using x_1 as our starting guess and with λ_2 fixed. However this *parameter continuation* algorithm will break down at a saddle-node bifurcation $\lambda_2 > \lambda_1$ (with reference to Figure 3.2a). Keller's *pseudo-arc length* continuation method [27] avoids this problem by stepping and root finding, not in parameter space $\mathbb{R}$ only, but in state and parameter space $\mathbb{R}^{(n+1)}$ together. The initial guess for the root finding algorithm is given by stepping along the tangent to the locus at the last step, and then the root is found in the hyper-plane perpendicular to this tangent.

This method is also applicable to those systems of non-linear equations which define periodic and homoclinic orbits. If we have extended systems which define bifurcation points, we may also apply a continuation method to find loci of bifurcation points with respect to changes in further parameters [28].

All these methods will be discussed at greater length as they are applied in later chapters.

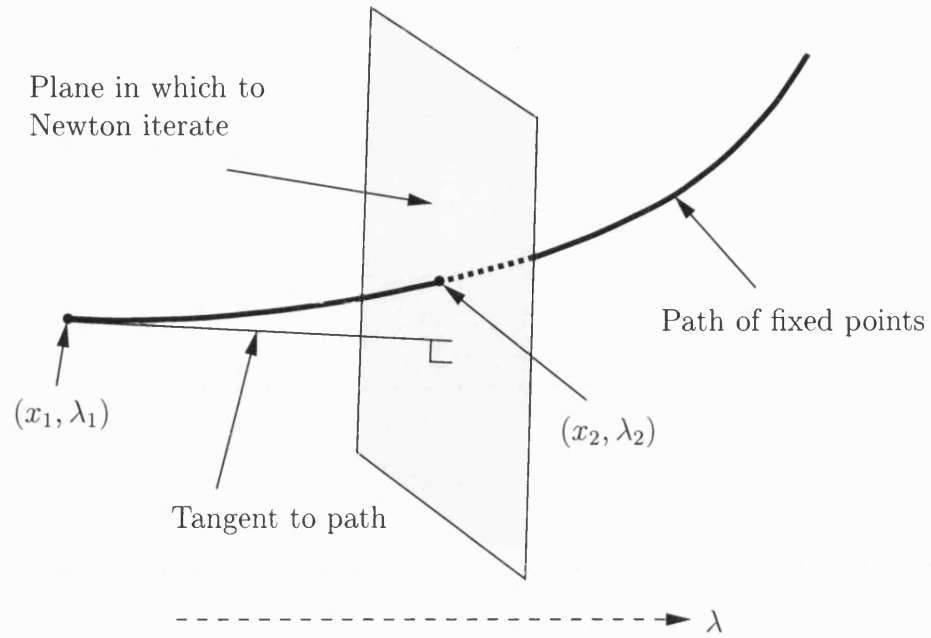

Figure 3.3: Schematic of pseudo-arc continuation method

3.4 Review of the dynamics observed in power systems and power systems models

It has been recognised recently that the grid can be considered as a dynamical system. The dynamics of a number power systems models have been considered by various authors. In this section we consider the current state of the literature relating to voltage collapse and the application of dynamical systems theory to power systems. With a few exceptions, these papers are all recent and have appeared in engineering journals, such as the publications of the IEEE, over the last ten years.

3.4.1 What is voltage collapse?

The most dramatic form of dynamics observed in power supply networks is voltage collapse. This is behaviour which occurs when [22]

> "the system is heavily loaded ... characterised by a slow decline in voltage magnitude at [load] buses over a period of minutes and hours, followed by a sharp decrease in voltage magnitude".

This final sharp decrease occurs on a time-scale of seconds or less. In the engineering literature voltage collapse is considered to be quite different from the

"transient stability" problem, i.e. the ability of the system to return to a sensible operating state after a perturbation. We should make a distinction between undesirable states of the whole system (such as slowly declining load voltages) and the actual local processes which trigger blackouts, such as individual protection devices reaching their limits, thus triggering local shutdown and possibly cascading behaviour leading to wider blackouts. In all of our models voltage collapse is just the start of a widespread and often catastrophic behaviour of the control systems of the whole grid.

Dynamically this behaviour has been related to saddle-node bifurcation [29], Hopf bifurcation [30], chaos [31], global bifurcations [32], and shrinking stability regions [12]. There is clearly an on-going debate about the exact nature of voltage collapse, and the best means to describe and hence predict it. A comprehensive bibliography (of over 300 entries) on voltage stability and collapse, including descriptions of specific incidents and of non-linear analysis techniques can be found in Ajjarapu and Lee [33].

Of course voltage collapse is complex and its initiation (for example by a tree falling on a line) cannot be built into any simple model. However, a reasonable way of considering the initiation of voltage collapse by a fault, is that a dynamical system in a stable state has either (i) a sudden change in the parameters governing the system, or (ii) a sudden change in the system state but with the same parameter values.

Dynamics of actual voltage collapse incidents

Fortunately such events are rare and have not occurred in the U.K. However over the last 20 years a catalogue of such incidents has been observed around the world. We now describe some of these with reference to the actual dynamics of the networks.

A voltage collapse incident occurred in Sweden [8]. This was initially caused by a fault at a switching station during a period of high load. This fault caused some oscillations in the system, which subsided. The supply to south-eastern Sweden was subsequently left in a low voltage, high load state; this overloaded a critical line which tripped[3], subsequently leading to further voltage decay, overloading and tripping of much of the rest of the system. A time plot of the voltage is shown in Figure 3.4.

The voltage profile shows a clear drop between 8-11 seconds, followed some

[3]Removed from the circuit, typically by the action of automatic protection and switching equipment

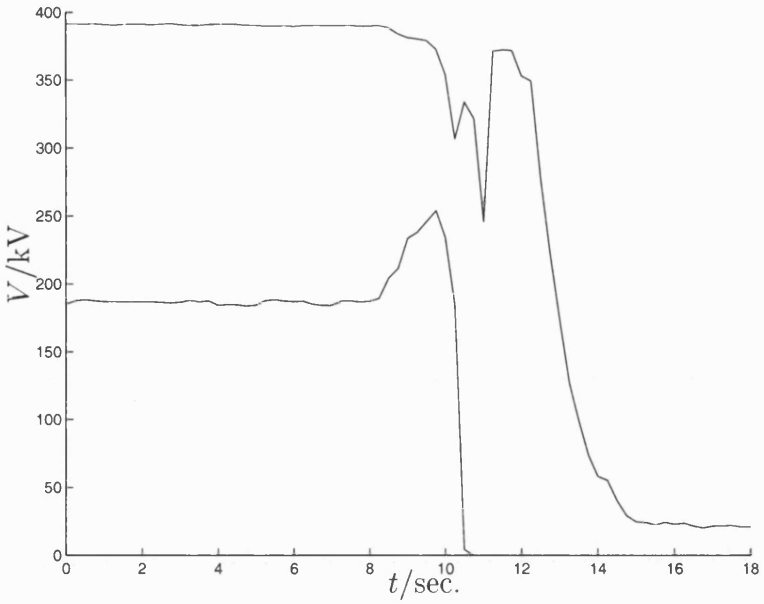

Figure 3.4: Voltage profiles at different buses during Swedish collapse incident, from [8]

oscillatory behaviour, followed by final collapse.

A voltage collapse incident occurred in western France in 1987 [14], Figure 3.5. Cold weather conditions meant that loads levels were high, but the system was running well within its perceived safety margins. Complete generator failure at one site led to decreasing voltages over the next few minutes and the disconnection of several other generators. In this case blackout occurred in only part of the network, and the system was eventually restored to a stable state.

This picture also shows collapse occurring over a period of less than 10 seconds. The recovery of the system to a normal operating state was successful in this case.

In July 1996 a voltage collapse incident occurred in the North-West USA [15], leading to power cuts for over 2 million customers for periods of up to six hours. Kosterev et al. [34] attempt to simulate this incident. This event was initiated by a line sagging and touching a tree; the subsequent short circuit led to the line being isolated and created further effects in other parts of the network. For more than 40 seconds there were voltage and power oscillations in the system; this eventually led to the tripping of protection devices and a cascading collapse of the system. In trying to replicate this behaviour computationally, the authors of [34] found that changes needed to be made to the standard models, and in particular that "dynamic load representation" was required. They recommend further analysis of load representation to better understand and avoid such events.

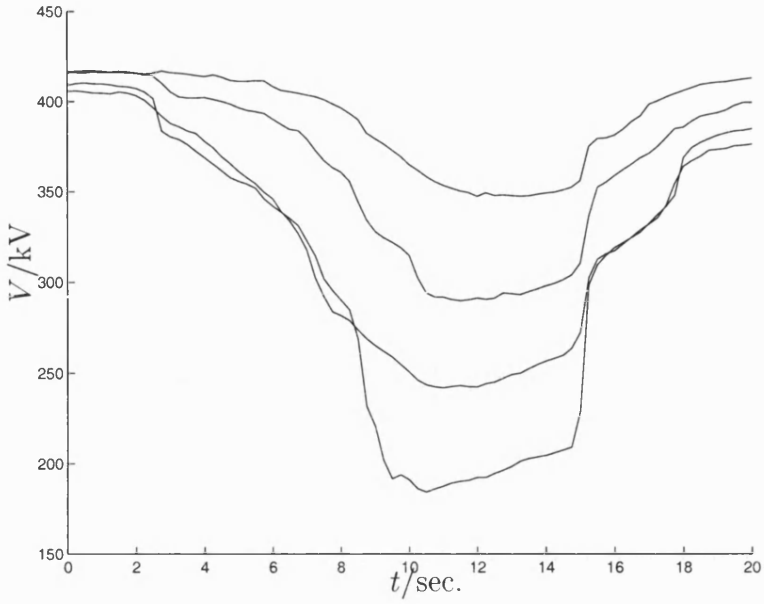

Figure 3.5: Voltage profiles at different buses during French collapse incident, from [14]

Another incident occurred in Chile in 1997 [35]. A major line was tripped, overloading other lines and showing a decline in system voltages. Sample time series from this incident can be seen in Figure 3.6.

This figure is similar to Figure 3.5; the voltage time series is not identical at all buses but collapse occurs over a time-scale of the order of seconds. Recovery was not successful in this incident and blackout could not be avoided.

References to other discussions of voltage collapse incidents can be found in Ajjarapu and Lee [33].

Relating the voltage collapse incidents to the mathematical theory

The incidents described above share various common points. Each incident was precipitated by some kind of fault causing a discontinuous change to the operating state of the system. This typically removes a line or generator, therefore if we consider this fault to be instantaneous we can distinguish between the pre-fault and the post-fault systems, which will be two different dynamical systems. The fault then gave rise not to immediate blackout, but to a transitional phase where voltage declined ever more rapidly.

We might think of the fault as pushing the (post-fault) dynamical system outside the basin of attraction of some stable operating state, hence directly leading to collapse. Or we can can think of the post-fault system as having

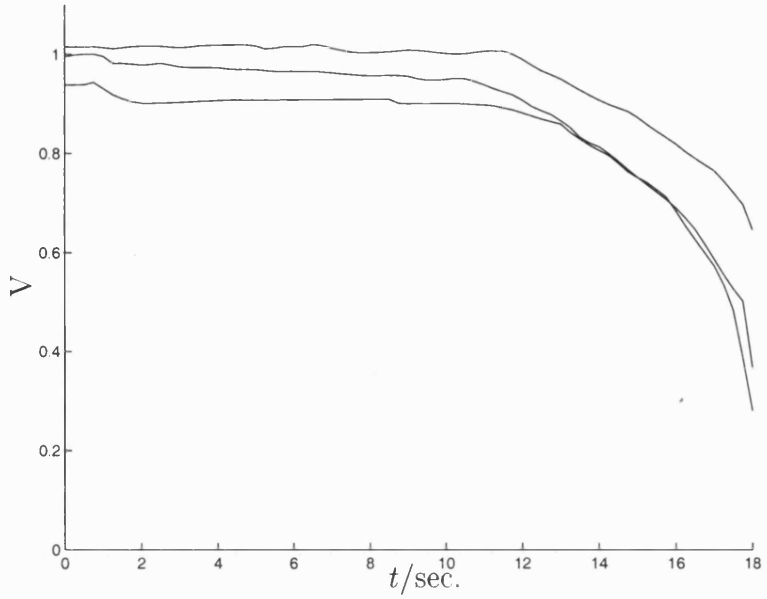

Figure 3.6: Voltage profiles at different buses during Chilean collapse incident, from [35]

parameters (derived from the pre-fault system) which make loss of stability due to bifurcation the more likely. The oscillatory behaviour seen in Figure 3.4 is highly reminiscent of the periodic behaviour, or a periodic transient, which would follow a Hopf bifurcation. It may also be due to the co-existence of a periodic solution some distance in parameter space from the Hopf bifurcation point – we will show evidence for this in the next chapter. It is also likely that the slower changes in state (voltage decrease) followed by much more rapid loss of system stability seen in Figures 3.6 is related to a saddle-node bifurcation and a slowly time-changing parameter. These explanations have been presented by some authors (see below) but are perhaps rather naive; we show below how a number of different bifurcations could lead to collapsing behaviour, and how proximity to these bifurcations effects the basin of attraction of the operating point.

The final wide scale blackouts which follow voltage collapse seem to occur on a cascading basis, as subsequent protection devices are triggered and lines, generators and loads are removed from the system. The consideration of this process is beyond the scope of this thesis – the models described in Chapter 2 do not include such protection devices and the formulation of the entire network in cascading collapse as a single dynamical system would not be easy, since it would involve the theory of discontinuous dynamical systems. However further study of

this cascading process is likely to be mathematically interesting and could even lead to practical ways to halt or limit the collapse.

From these incidents it can be concluded that both the existence of saddle-node and Hopf bifurcations may be contributory factors to a voltage collapse incident.

3.4.2 Modelling and dynamics

The modelling of power systems as a system of DAEs has been discussed in the previous chapter, and further details can be found in textbooks such as [6, 36, 2]. However there are a small number of papers which discuss the importance and methodology of modelling of power systems with reference to voltage collapse and dynamical systems, with particular emphasis on the importance to the dynamics of the load models used.

Hill [37] discusses the possibility of loads depending on the time derivative of voltage. In particular, non-linear dynamic models for induction motors, transformer tap-changers, and heating load are examined. It is noted that parameter estimation can be difficult in non-linear models.

Karlsson and Hill [38] specify a general active load model of the form

$$f(\dot{P}, P, \dot{V}, V) = 0 \tag{3.16}$$

and a similar general model for reactive load Q. Experimental result are given in order to find parameters in examples of this type of model.

In a very thorough paper, Lesieutre et al. [7] present a summary of a variety of load models and discuss how they can be adapted most usefully into a dynamical model of the whole network. Also considered are the transformations needed to represent these models in terms of the "bus variables" P, Q, V, θ. A clear derivation of a 5th order induction motor model is given and then this is reduced to 3rd order. This model is linearised and reduced to each of the previously stated models, so making clear the assumptions present in each of them. The model presented originally in [8] and used in the 3-Bus model is shown to be useful for representing small induction motors. A general form for dynamical representation of power system load is given, which simplify the calculation of aggregate loads by allowing easy combination of several different load models.

It is clear from these papers that the load model (2.73,2.74) is reasonable. Dynamic load models should be used for investigations of the type we carry out below but the exact form of these models will depend on some further analysis

and experimentation.

The 3-Bus model

A large number of papers have discussed the so-called *3-Bus* power system model; this model is stated in full in Chapter 4. It is remarkable for the richness of dynamics observed including voltage collapse. There is a clear chronological progression in the complexity of the behaviour found in and the methods used to investigate this model.

Dobson et al. [29] first introduce the 3-Bus power system, consisting of a swing equation generator model (2.58,2.59) along with an infinite bus to represent further generation, a dynamic load model (2.73,2.74) and a standard network model (2.63,2.64). Sample trajectories for this system are presented, and an approximate calculation of saddle-node bifurcation point is given. In a seminal paper Dobson and Chiang [22] develop the usage of this model. System breakdowns are said to be related to dynamic responses to disturbances. The useful definition of voltage collapse used at the start of this section is given here. The 3-Bus model is investigated by using the reactive load as a slowly increasing, time varying parameter, and the voltage collapse point is identified as being synonymous with the saddle-node bifurcation. However the value at which a saddle-node bifurcation occurs is determined by direct calculation of the system Jacobian and subsequent approximation of explicit conditions for a zero eigenvalue. The paper also contains a good introduction to dynamical systems defined by ODEs, but excludes *a priori* the possibility of Hopf bifurcations in such a model. Chiang et al. [9] also consider the 3-bus model. The position of the saddle-node bifurcation is noted to depend on other parameters, but this is only approximated, not found via continuation.

In a short conference paper, Abed et al. [30] observe Hopf bifurcation in the 3-Bus model, and also in other unspecified models. Wang et al. [39, 32] also detect a Hopf bifurcation in the 3-Bus system (using different parameters to Chiang & Dobson). Periodic and chaotic orbits emanate from this point, and are shown to hit the path of unstable fixed points to give global ("blue sky") bifurcation. Trajectory plots show that the transient behaviour of the system prior to collapse may last for a considerable time.

Ajjarapu and Lee [40] and Lee and Ajjarapu [41] also consider periodic behaviour in the 3-Bus model, and a period doubling cascade is shown to exist, using continuation methods. The bifurcation parameter Q_1 is considered to be one which varies slowly in time. This period doubling cascade to chaos is also

mentioned by Chiang et al. [31] and by Tan et al. [42]. In both these papers apparently periodic orbits are plotted. The ratios of successive positions of these period doubling bifurcation points are shown by Lo and Qi [43] to correspond to the well-known Feigenbaum number, to the extent of being able to use this number to predict the parameter value of the next such bifurcation.

The papers of Tan et al. [42, 44] make two important points while considering steady state and periodic behaviour in the 3-Bus model. Firstly that some form of bifurcation is likely to always exist in power system models, because of the well known existence of multiple solutions to the "power flow" problem (2.63,2.64) [6]. Secondly, that bifurcation affects regions of stability, and hence changes both the nature and multiplicity of fixed points (operating points) and also their "transient" stability (i.e. their basins of attraction).

In a long and interesting paper Chiang et al. [45] examine the 3-Bus model using AUTO. Continuation of bifurcation points is performed with respect to increased values of a second parameter, generator damping constant d_m. However the relevance of using this parameter is not fully discussed. A Poincaré map is formed to further investigate the chaotic attractor. The paper also contains a good survey of continuation methods in power systems, and the authors' own code CPFLOW is discussed. This code performs pseudo-arc length continuation in 1 parameter dimension for power system ODEs. The application to a larger system is discussed, but the exact model is not specified. This paper recognises that "the recent availability of inexpensive computing power and progress in dynamical systems theory allows one to simulate, understand and analyse several complicated behaviours in power systems", but that "existing numerical algorithms [...] are not effective for high-dimensional nonlinear systems".

Finally Nayfeh et al. [46] use their own code (the algorithms used are not stated) to perform two-parameter continuation (with respect to a control parameter) of Hopf and saddle-node points in a version of the 3-Bus model with nonlinear control. It is noted that the period doubling cascade is not present at different values of their second parameter.

The 3-Bus model is of importance, not because of the number of papers discussing it (although there are many), or their quality (mixed) or that it accurately describes a specific incident or situation (it doesn't), but because the users of the model accept that consideration of a dynamical power system model, treating load, generation and transmission in a holistic manner, is both valid and highly useful, and that the tools of dynamical systems theory are the correct ones to use to investigate this system. It would not be incorrect to say that power en-

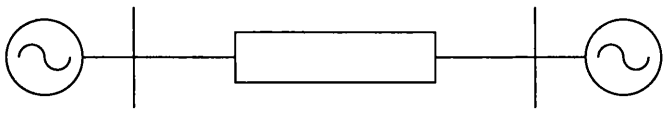

Generator modelled by swing equation

Infinite bus

Figure 3.7: Single Machine Infinite Bus model

gineers may sometimes be reluctant to adopt new techniques – both analytical and numerical. This cautiousness is certainly related to the fact that failure of the networks they are involved in operating is neither financially nor politically acceptable. The results discussed above could be said to be representative of paradigm shift in the type of mathematical techniques used by at least some engineers in the academic environment, and may lead to to new methods of analysis at the industrial level.

This model will be investigated at length in Chapters 4 and 5, where we will demonstrate a range of behaviour including a Bogdanov-Takens point which acts as an organising centre for the system.

Single machine – infinite bus

A model widely used in power systems stability analysis is the "Single Machine – Infinite Bus" (SMIB) model, consisting of one generator (modelled by (2.58,2.59), for instance) connected by a single transmission line to another bus of fixed voltage magnitude and phase angle (an "infinite bus"). This can be used to examine the dynamic behaviour of generator models, but it is not clear whether this behaviour can be said to be indicative of what might happen in a larger systems.

Abed and Varaiya [47] find a Hopf bifurcation point at "realistic parameter values" in a SMIB model, using a secant method. Their generator model can be extended from (2.58,2.59) to allow frequency dependent torque, and variable excitation. They encourage other researchers to apply bifurcation theory, and particularly Hopf bifurcation theory, to power system models. Nayfeh et al. [48] also consider a SMIB model, finding Hopf and torus bifurcations. They also investigate the effect of parameters on the boundaries of basins of attraction, and present plots of 2-parameter loci of Hopfs, but with no clear presentation of the methods used.

It is clear that the SMIB model is useful for developing generator models, and

possibly numerical methods, but the lack of representation of load and network dynamics mean that this model will probably not shed much light on the problem of voltage collapse.

DAE power system models

As we have said in the previous chapter, power systems models of realistic dimension will have a semi-explicit DAE representation (2.75,2.76). This defines a dynamical system, but there are non-trivial differences between the analysis of DAEs and ODEs, both theoretically and computationally. In particular it is easy to show that the stability of fixed points will not depend simply on the eigenvalues of the Jacobian matrix f_x. Let the system

$$\dot{x} = f(x, y, \lambda) \tag{3.17}$$

$$0 = g(x, y, \lambda) \tag{3.18}$$

have a fixed point (x^*, y^*, λ^*). Linearisation of the system around this fixed point gives

$$\begin{pmatrix} I & 0 \\ 0 & 0 \end{pmatrix} \begin{pmatrix} \dot{\delta x} \\ \dot{\delta y} \end{pmatrix} = \begin{pmatrix} f_x & f_y \\ g_x & g_y \end{pmatrix} \begin{pmatrix} \delta x \\ \delta y \end{pmatrix} + O(\delta x^2, \delta y^2, \delta x \delta y). \tag{3.19}$$

Hence the stability of the fixed point is dependent on the solutions to the generalized eigenvalue problem

$$\lambda \begin{pmatrix} I & 0 \\ 0 & 0 \end{pmatrix} \mathbf{v} = \begin{pmatrix} f_x & f_y \\ g_x & g_y \end{pmatrix} \mathbf{v} \tag{3.20}$$

for which the most well known numerical solution method is the QZ algorithm [49, pp375-390].

If the the matrix g_y is invertible, then (3.19) reduces to

$$\dot{\delta x} = \left(f_x - f_y g_y^{-1} g_x\right) \delta x + O(\delta x^2, \delta y^2, \delta x \delta y). \tag{3.21}$$

and so the eigenvalues of the *Schur complement* matrix

$$(f_x - f_y g_y^{-1} g_x) \tag{3.22}$$

determine the local stability of the system near the fixed point.

The methods used to calculate trajectories must also be carefully chosen,

to make sure that numerical approximations preserve the dynamical behaviour present in the system itself. This can generally be achieved by the use of implicit numerical schemes which solve for a solution (x, y) of (2.75) at a new time-step simultaneously with satisfying the constraint (2.76).

Kwatny et al. [50] examine such DAE power system models with constant load. The system is defined to be "causal" if the matrix g_y is invertible; that is if the network is capable of supplying the generated power to the loads – mathematically if it has index one. This paper is important in that it accepts that power system stability can be analysed in a bifurcation theory context with DAE models. In a later paper, Kwatny et al. [51], the same model is reconsidered. A thorough survey of mathematical techniques, including co-dimension two bifurcations is given. Numerical methods to find bifurcation points are discussed, including the use of the Schur complement for determining local stability and of the Recursive Projection method for root finding. The authors make a clear distinction between voltage stability (the inability of the system to maintain load bus voltage magnitudes) and dynamic stability (the ability of the system to return to a steady operating point after perturbations). They define the system to be "practically stable" if the equilibrium is Lyapunov stable and the system is structurally stable (i.e. not at a bifurcation point).

Chiang et al. [9] attempt to remove the problem of the singularity of g_y by making a singular perturbation to transform the DAE model to an ODE system, but note that the exact choice of ϵ in this perturbation process is difficult. Yorino et al. [52] also investigate this method.

Gou and Schlueter [53] attempt to classify all the possible bifurcation and stability behaviour of a DAE power system model.

In the analysis of the network part of power system models, it is common to consider the point at which g_y becomes singular to be the point at which the network breaks down. Mathematically this is a point where the index of the DAE increases. It is common to plot P-V curves, that is calculations of the different voltages supplied by the system for different values of the constant reactive load. These bear a superficial resemblance to saddle-node bifurcation diagrams. However, these plots are not true bifurcation diagrams as they only consider the behaviour of the network part of the model. Lee and Ajjarapu [54] present such calculations for a DAE model, along with some analysis of eigenvalues and eigenvectors of the network Jacobian g_y. They define the "nose-point" of the P-V curve to be the point of maximum power transfer. Vournas [55] dispute this method, noting that singularity of g_y is not a necessary condition

for voltage collapse. That singularity of g_y is not equivalent to a saddle-node bifurcation can easily be seen by examining the trivial system

$$\begin{array}{rcccl} \dot{x} & = & \lambda - x^2 & = & f(x,y) \\ 0 & = & x - y & = & g(x,y) \end{array} \tag{3.23}$$

Clearly $g_y = -1$ is never singular, but the dynamical system has a saddle-node bifurcation at $(x, y, \lambda) = (0, 0, 0)$. Thus we claim that the full richness of the dynamics involves studying the whole system (f and g) and not only the network (g).

Cañizares [56] investigates power systems as parameterised dynamical systems defined by semi-explicit DAEs, with parameters that are (slowly) time varying. However they incorrectly state that eigenvalues of the matrix

$$\begin{pmatrix} f_x & f_y \\ g_x & g_y \end{pmatrix} \tag{3.24}$$

will always determine stability at fixed points, and not (3.20) or (3.22). Hence they will fail to properly detect Hopf bifurcations.

Particular mention must be given to the work of Venkatasubramanian and co-authors [57, 58, 59, 60, 61]. In the first of these papers a DAE power systems model is presented. The "loss of causality" at $det(g_y^{-1}) = 0$ is noted, and that this can lead to a definition of a new form of bifurcation specific to DAEs, the Singularity Induced Bifurcation (SIB). All the analysis presented is done analytically, not numerically and the authors states that it "cannot be expected that a similar comprehensive analysis can be achieved for a large power system in general". The theory of the SIB is developed further [58], using the eigenvalues of the Schur complement matrix. This theory has since been simplified and extended Beardmore [62].

Venkatasubramanian et al. [59] make several points regarding the meaning of "stability" and "state". $y \in R^m$ are said to be "instantaneous" state variables, that is that they are assumed that they change so fast that the algebraic term $g(x, y, \lambda) = 0$ holds. This is not unreasonable as the speed at which changes in the current flows through the transmission lines will be orders of magnitude faster than load and generation effects. They also define the general concepts of "viability" when system states are within acceptable operating limits, "feasibility" when parameters permit a "continuously movable" (i.e. structurally stable) stable equilibrium, and "transient stability" when specified contingencies (per-

turbations) all give trajectories leading back to to the stable equilibrium. It is claimed [61] that global bifurcations have no effect on the feasibility region (practical operating parameter space). We will show that all these engineering concepts can be related to dynamic effects and bifurcations, and that they they can be connected in some sense.

In the following chapters we will make clear the conditions under which an *a priori* reduction of the DAE to an ODE can be made, which will greatly simplify the subsequent analysis.

3.4.3 Methods used to analyse power systems

Traditional analysis tools

A variety of methods are used by power engineers to assess the performance of existing and proposed power system networks and equipment.

We have already mentioned $P - V$ curves, which are plots of the voltage supplied by the network to a load against the real power demanded by that load. It is repeatedly stated within the electrical engineering community that the "load flow" equations (2.63,2.64) typically have two solutions – one stable, one unstable. For a single line, we can express the load P as a function of the input voltage magnitude V and plot curves resembling saddle-node bifurcation diagrams; similar diagrams can be plotted for the reactive load Q [6, sec. 6.1].

The stability of the whole power system with respect to various "contingencies" (perturbations or faults) is usually examined by making a calculation of the trajectories starting from the state of the post-perturbation or post-fault system and examining whether or not such trajectories lead to a stable operating point. The particular contingencies may be selected from knowledge of actual or likely scenarios, and/or by Monte Carlo type methods. The models used in such analysis usually focus on the representation of generator, control and protection devices, and the load models used are typically constant or simple algebraic models. The software designed for this procedure, such as EUROSTAG [63, 64, 65] or the Matlab/Simulink power system block-set, is very flexible regarding selection of the system and states to analyse, as long as only one of a number of "standard" models is used. However, the representation of different load models can be hard and the representation of the system ODE or DAE in the form (2.75,2.76) for analysis as a dynamical system is not easy.

Lyapunov functions

Lyapunov functions have been used by several authors to estimate boundaries of stability regions for power system models. They have two major drawbacks in that they can be hard to construct and they will typically underestimate stability regions. However once formulated they are easy to apply to give reliable results. Usually such functions are based on the energy contained in the system.

Davy and Hiskens [66] and Cao et al. [3] are typical papers in that the energy function derived is dependent on the particular generator and load model used and does not allow dynamic load models of the form (2.73,2.74).

Varghese et al. [67] describe a method to exactly characterise the boundary of stability regions by the use of "Maximal Lyapunov Level sets". This can be contrasted with the use of cell-mapping methods [68] to calculate stability boundaries of a swing equation generator model (2.58,2.59). This paper shows that traditional Lyapunov function based methods underestimate the size of the basin of attraction of operating points.

Another danger of of using Lyapunov functions is that it can falsely be assumed [69] that the local asymptotic stability proved by such a function implies the global absence of periodic behaviour. It is clear from the study of the 3-Bus model that stable fixed points and stable periodic orbits may co-exist at the same parameter value (see for example Section 4.5.1) but this stable periodic behaviour will not be detected by the local Lyapunov function at the fixed point.

It is quite possible to also use Lyapunov functions for DAE system. This is done by Hill et al. [70] who present a stability theory for DAE power systems models using Lyapunov functions. In this paper constraint manifolds $\{y : g(x, y) = 0\}$, impasse surfaces $\{y : g_y \text{ is singular}\}$ and stability regions are discussed.

Continuation

Continuation methods as described in Section 3.3 have been used by a number of power system researchers to find solutions to the algebraic "load flow" problem (2.63,2.64) with fixed generator inputs and load values as a parameter.

Many investigators of power system network models have viewed the "nose" of the "load flow" curve as a point which prohibits continuation solutions being found. More recently, methods have been proposed in the power literature [71, 72, 73, 74] to find all the solutions to (2.63,2.64) despite a point of singularity of the Jacobian of this system. These are based on extensions to the simplistic parameter continuation method. Ma and Thorp [72] use continuation methods

to find load flow solutions of parameterised power system model. They claim, based presumably on computational evidence, that the curve of solutions always forms a closed loop.

Other papers have applied the pseudo-arc method to the problem of solving the network equation, although not always described as such [75]. This method is also used by most of the papers investigating power systems as dynamical systems, such as those described above, several of which use the method as implemented in AUTO.

It would appear that the use of homotopy and continuation methods would be very useful in a power systems context and the relatively few uses of this either in the literature or in simulators used in practice is somewhat strange. This is possibly due to the view that it is a computationally "hard" problem, which is compounded by the wide use of direct methods based on LU factorisation as a solution method for the large linear systems involved. Flueck and Chiang [76] show that use of an iterative method (preconditioned GMRES) is practical and leads to much greater efficiency – this needs further study, both in the context of continuation methods and for traditional power engineering techniques. The use of other root finding techniques for solving the power system network equations, such as Recursive Projection [77] would also seem possible, and the exploitation of the underlying physical network structure in some way could also be further investigated.

Proximity measures

Following the introduction of non-linear methods such as in the 3-Bus papers described above, a number of authors have made suggestions as to how the bifurcations and dynamical behaviour could be exploited to provide an index or measure of how "close" the system is to voltage collapse. This could be used as both a design tool and an operating indicator. The main feature of these methods is to estimate the location of bifurcation points in terms of operating parameters.

Lee and Ajjarapu [78] examine a DAE power system model. The eigenvalues of the Schur complement matrix (3.22) of the DAE system are calculated. The sensitivity of the system to change in parameters p is measured by calculating the matrices $\frac{\partial x}{\partial p}$ and $\frac{\partial y}{\partial p}$, expressions for which are given. A projection is used to estimate the parameter sensitivity of the different eigenspaces of the Schur complement. The authors claim that the behaviour of the system is governed by the subspace related to the "critical eigenvalue". Their method would allow an investigation of how parameter change effects this "critical" subspace. With

saddle-node, Hopf and singularity induced bifurcations all possible, it is not clear how one would identify this critical eigenvalue, assuming an efficient method could be found for calculating *all* the eigenvalues of the Schur complement. No consideration is given to non-local phenomena. The method is applied to a 39-bus system with static loads.

Joshi and Srivastava [79] assume that a $(p-1)$-dimensional surface Σ of Hopf bifurcation points x^H exists in the p-dimensional parameter space of a DAE power system model. In order to estimate the "distance to Hopf bifurcation" a method is proposed to find $min_{x^H \in \Sigma} ||x^* - x^H||$, by minimisation of an objective function. This function assumes that the eigenvalue at x^* with the smallest real part is always the "critical" eigenvalue which will lead to Hopf bifurcation.

Alvarado et al. [80] also assume a $(p-1)$-dimensional surface, this time of saddle-node bifurcations. A likely direction of parameter change is chosen and the distance to saddle-node bifurcation calculated using an iterative method to find the bifurcation. A Monte Carlo method is used to select different parameter changes vectors. This method is both simple and practical, but does make the assumption that only saddle-node bifurcation will cause collapse.

Greene et al. [81] assume or predict a likely pattern of load increase. A saddle-node point ('nose') curve of a DAE or differential equation power system model is found by continuing the operating state in the parameter direction of this predicted load increase. The *loading margin* is defined to be the distance in parameter space from the current operating point to the bifurcation point. It is assumed that in the event of some contingency, the post-fault system will have a lower loading margin. A formula is proposed to provide linear or quadratic estimates of the load margin in the post-fault system, calculated from the Jacobian of the original system. This paper makes the assumption that the fixed points and bifurcation point of the post-fault system can be approximated in terms of the behaviour of the pre-fault system. As a consequence of this unjustified assumption, the derivations of the formulae given are somewhat unclear. A second assumption is that saddle-node bifurcation is the only cause of voltage collapse.

Despite these assumptions the concept of load margin is a useful one; we clearly show below that saddle-node bifurcation is a sufficient condition for collapse and so the parameter "distance" to such bifurcation points is an important quantity. However, to derive a useful methodology for contingency planning using bifurcation theory, much better account must be taken of the difference between the pre-fault and post-fault systems, which are distinct (albeit related) dynamical systems.

In following chapters we use a simple Monte Carlo method to investigate the behaviour of basins of attraction of power system models. We can make few assumptions about the dynamical behaviour of these systems as we can efficiently compute the bifurcation structure of the models prior to performing the Monte Carlo calculations.

3.4.4 Summary

An electrical circuit, such as a power system, can successfully be represented as a dynamical system. The problem of voltage collapse may be explained in terms of the dynamical behaviour of such a system. It is possible to use non-linear concepts such as bifurcation and basins of attraction to investigate this behaviour. In particular a dynamical systems approach may identify wider possible state and parameter conditions as well as new mechanisms which may lead to voltage collapse. This may yield performance and safety indices which could be used in power system planning or operation, but current research in this area needs to be given a firmer theoretical basis before such methods could be said to be mature.

In general, there is no complete agreement on exactly which components should be included in a a power system model to investigate voltage collapse, or how these should be modelled as part of a dynamical system. However, all such models can be represented as a dynamical system, so reasonable models can be chosen which give good qualitative representation of power system behaviour and can be used to test and develop numerical and other techniques to examine this.

Chapter 4

3-Bus Model – 1-Parameter Investigation

4.1 Introduction

In this chapter and the next we consider a reduced power system model, previously investigated by a number of researchers. This model comprises three buses modelling two generators supplying power to a load. The real and reactive power demands of the load then become parameters which we vary and the resulting dynamics of the system can be compared at different load values. Whilst highly simplified from a stand-point of electrical engineering, this model is still very rich dynamically and exhibits many of the features of voltage collapse that we are interested in. It also is likely that more complex systems can be effectively reduced to such simpler problems when we are concerned with the large scale dynamical effects where only a few components go unstable initially, with the rest following.

We show some important previously unobserved behaviour in this system and in particular demonstrate that the parameter regimes which might be considered stable by some authors [22, 9] may be overly optimistic.

The layout of the remainder of this chapter is as follows. In Section 4.2 we introduce the model used and briefly discuss some of the dynamics associated with voltage collapse. An asymptotic solution for escaping trajectories is given in Section 4.3. In Section 4.4 we present the numerical methods used to compute trajectories in the model and investigate it with respect to changes in 1-parameter. Finally, in Section 4.5 we present some results which clearly explain the dependence and sensitivity of the system with respect to two different load parameters.

4.2 Model description

We consider the 3-bus model introduced in [29, 22] and further investigated in [30, 40, 31, 32, 46, 44]. The model is intended to be the simplest possible system containing the basic elements of power system structure – load, generation and interconnection, and uses the component models introduced in Chapter 2. Whilst being simple it has the same basic dynamical structure of more realistic power system models. The model comprises two generator buses and a load bus. One generator bus is a "slack bus" acting as an infinite power source at fixed voltage magnitude $V_0 = 1$ and relative phase angle $\delta_0 = 0$. This models the response of the whole of the power system network, and is not affected by the load on the system. The other generator is considered to be influenced by the load. Its relative phase angle δ_m, frequency $\omega_m = \dot{\delta}_m$ and electrical power output P_e are modelled by a "swing" equation of type (2.58,2.59)

$$M\ddot{\delta}_m = P_m - P_e - d_m\omega_m \tag{4.1}$$

with machine moment of inertia M, damping coefficient d_m and mechanical power input P_m all constant.

The real and reactive loads at the third bus comprise fixed real and reactive loads P_1 and Q_1, in parallel with an empirical model of induction motor load suggested by [8]. For a voltage V with phase angle δ supplied to the load, the real and reactive power demands of the load are are given by

$$\begin{aligned} P_l &= P_0 + P_1 + K_{p\omega}\dot{\delta} + K_{pv}(V + T\dot{V}) \\ Q_l &= Q_0 + Q_1 + K_{q\omega}\dot{\delta} + K_{qv}V + K_{qv^2}V^2 \end{aligned} \tag{4.2}$$

Here P_1 and Q_1 are parameters which we will vary; the other parameters are considered to be fixed.

The generator and load buses are connected according to the circuit diagram in Figure 4.1.

The two transmission lines connecting the generator buses to the load bus are modelled as inductances $Y_m\angle(-\theta_m - \frac{\pi}{2}), Y_0\angle(-\theta_0 - \frac{\pi}{2})$ along with a capacitance C representing the shunt capacitance of the whole system. Kirchoff's current law applied at the generator bus tells us that the electrical power generated must be

$$P_e = -V_m V Y_m \sin(\delta - \delta_m - \theta_m) - V_m^2 Y_m \sin(\theta_m) \tag{4.3}$$

Using a Thevenin equivalent circuit, we can eliminate the capacitance C, changing

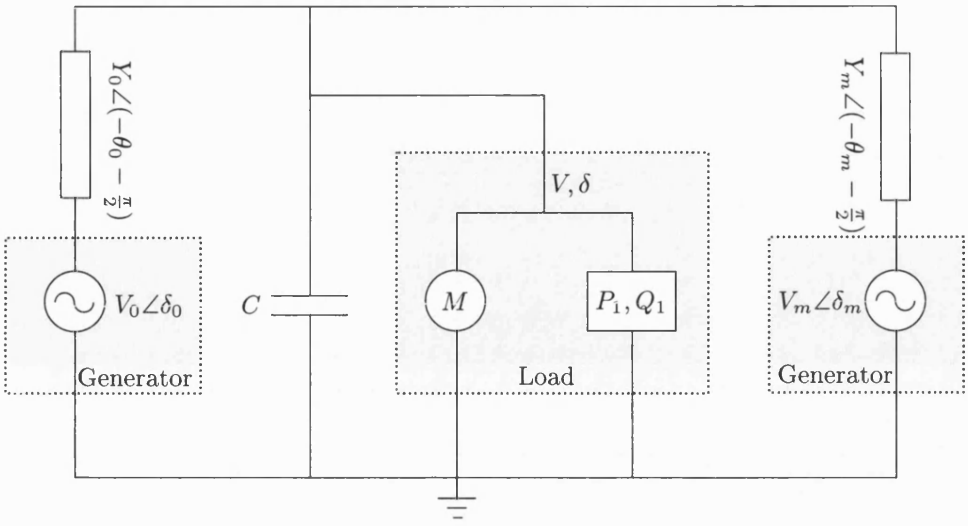

Figure 4.1: Circuit diagram for 3-Bus model

V_0, Y_0 and θ_0 to V_0', Y_0' and θ_0' respectively [1, 22]. Kirchoff's current law then tells us that the powers supplied by the network to the combined load are

$$\begin{aligned} P_l =& - V_0' V Y_0' \sin(\delta + \theta_0') - V_m V Y_m \sin(\delta - \delta_m + \theta_m) \\ & + (Y_0' \sin(\theta_0') + Y_m \sin(\theta_m))\, V^2 \\ Q_l =& V_0' V Y_0' \cos(\delta + \theta_0') + V_m V Y_m \cos(\delta - \delta_m + \theta_m) \\ & - (Y_0' \cos(\theta_0') + Y_m \cos(\theta_m))\, V^2 \end{aligned} \tag{4.4}$$

This is completely equivalent to the representation in equations (2.63,2.64), where $G_{S,12} = 0, G_{12} = -Y_m \sin(\theta_m), B_{12} = -Y_m \cos(\theta_m)$.

Normally the application of Kirchoff's laws to calculate the power flow through the network would give an algebraic constraint on the system leading to a differential–algebraic system. However, with this simple network we substitute P_e, P_l and Q_l into the dynamical part of the model and re-write the entire system as a

4-dimensional ordinary differential equation

$$\begin{aligned}
\dot{\delta}_m &= \omega_m, \\
\dot{\omega}_m &= \frac{1}{M}\left(-d_m\omega_m + P_m - P_e(V,\delta,\delta_m)\right), \\
\dot{\delta} &= \frac{1}{K_{q\omega}}\left(-K_{qv}V - K_{qv^2}V^2 - (Q_0 + Q_1 - Q_l(V,\delta))\right), \qquad (4.5) \\
\dot{V} &= \frac{1}{TK_{q\omega}K_{pv}}\Big(K_{p\omega}K_{qv^2}V^2 + (K_{p\omega}K_{qv} - K_{q\omega}K_{pv})V \\
&\qquad + K_{p\omega}(Q_0 + Q_1 - Q_l(V,\delta)) - K_{q\omega}(P_0 + P_1 - P_l(V,\delta))\Big).
\end{aligned}$$

where P_e, P_l and Q_l are given by (4.3) and (4.4).

We use the following system parameters, which are all dimensionless, apart from the angles which are in radians. Generator parameters: $M = 0.3$, $D = 0.05$, $P_m = 1.0$. Load parameters: $K_{p\omega} = 0.4$, $K_{pv} = 0.3$, $K_{q\omega} = -0.03$, $K_{qv} = -2.8$, $K_{qv^2} = 2.1$, $T = 8.5$, $P_0 = 0.6$, $Q_0 = 1.3$. Network parameters: $V_m = 1.0$, $Y_m = 5.0$, $\theta_m = -5\pi/180$, $V_0' = 2.5$, $Y_0' = 8.0$, $\theta_0' = -12\pi/180$. These have been chosen for two reasons. Firstly they are to those used by previous investigators of this model, and so we can compare our results directly with theirs. Secondly, discussions with researchers at the National Grid Company have shown that these figures are a reasonable approximation to the parameters occuring in real systems, and so the model has as much physical validity as can be expected for such a small and simple system.

In the load, the constant parts of the real and reactive power demands (P_1 and Q_1) are parameters which could in principle be varied in an experiment. (In principle we could also vary the system damping, or line inductance or other parameters, but we shall not consider doing this here.) By varying P_1 and Q_1 we identify certain types of dynamics of (4.5) and the transitions between them.

4.2.1 A brief description of the system dynamics

We show below that the long-time behaviour of 3-bus model trajectories fall into 4 sets: (1) attracted to fixed points, (2) attracted to periodic orbits, (3) attracted to a strange attractor and (4) escaping (unbounded, collapsing).

The system represented by the three bus model (4.5) ideally operates in a fixed, stable, steady state. If such a state is unique and globally attracting – or at least has a large basin of attraction – then we can consider the overall system

to be operating safely. Large deviations of initial conditions from the steady state (caused, for example, by a power line failure or some other fault) will not prevent the system from returning to its stable operating condition. For a wide class of parameter values it is known [6, chap. 14] that power systems with networks of this type will generally have two (or indeed several) fixed operating points where all time derivatives vanish. One of these points is a stable attractor whereas the other is an unstable saddle point.

As either P_1 or Q_1 are varied then the fixed points also vary, typically meeting at a saddle-node bifurcation point (a fold point); say when $P_1 = P_1^{SN}$. The value of P_1^{SN} depends upon Q_1 and other parameter values. This point gives the value of P_1 at which we have maximum real power transfer. If $P_1 << P_1^{SN}$ then the system operates safely overall. For $P_1 > P_1^{SN}$ there are no fixed operating points and typically the power system is unstable with an immediate collapse of the voltage. Such voltage collapse corresponds mathematically to an *unbounded* solution of (4.5).

Voltage collapse can occur either when there is no attracting bounded solution (such as $P_1 > P_1^{SN}$) or when an initial state (for instance caused by a transient due to a local power failure) lies outside the basin of attraction of such a bounded state. The computation of P_1^{SN} and other related saddle-node bifurcations is important, as it defines the maximum possible region of safe operation. Various attempts have been made to obtain estimates for these points in more general systems, however voltage collapse can easily occur for $P < P_1^{SN}$.

For $P_1 < P_1^{SN}$ but close to P_{SN} we may observe complex behaviour with coexisting periodic, steady and chaotic solutions. All of these states represent *bounded* behaviour of the system. In this region voltage collapse may easily occur as the basin of attraction of the stable fixed point is eroded. Thus although $P_1 < P_1^{SN}$ we cannot guarantee that the system will not go through collapse. We also note that periodic and chaotic motion, whilst bounded, may still not represent a desirable operating state of the power network and might reasonably also be considered to be unstable from the view point of power engineering. Typically the periodic orbits arise either through Hopf bifurcations or through more global effects such as the Šil'nikov homoclinic bifurcation. It is this region of parameter space that we will consider in this paper as it represents the transition point from a safe to an unsafe region. To fully reveal the overall structure of this region we consider variations of both Q_1 and P_1. This gives a picture for the dynamics as a series of Hopf and period doubling bifurcations organised around a Bogdanov-Takens point.

4.3 Asymptotic solutions

We now present an asymptotic solution for escaping (collapsing) trajectories in the 3-Bus model.

4.3.1 Derivation

Rewrite the 3-bus model (4.5) as

$$\begin{aligned}
\dot{\delta}_m =& \omega_m, && (4.6)\\
\dot{\omega}_m =& \gamma_1\omega_m + \gamma_2 + V\gamma_3 \sin(\delta - \delta_m - \theta_m) + \gamma_4, && (4.7)\\
\dot{\delta} =& \beta_1 V + \beta_3 + \beta_4 V\cos(\delta - \theta_0') + \beta_5 V\cos(\delta - \delta_m + \theta_m) + (\beta_2 + \beta_6)V^2, && (4.8)\\
\dot{V} =& \alpha_1 V + \alpha_2 V^2 + \alpha_3 + \alpha_4 V\sin(\delta + \theta_0') + \alpha_5 V\sin(\delta - \delta_m + \theta_m)\\
&+ \alpha_6 V^2 + \alpha_7 V\cos(\delta + \theta_0') + \alpha_8 V\cos(\delta - \delta_m + \theta_m). && (4.9)
\end{aligned}$$

where the constant parameters have been re-written for clarity as

$$\begin{aligned}
\gamma_1 &= \tfrac{-d_m}{M}, & \gamma_2 &= \tfrac{P_m}{M},\\
\gamma_3 &= \tfrac{V_m Y_m}{M}, & \gamma_4 &= \tfrac{V_m^2 Y_m \sin(\theta_m)}{M},\\
\beta_1 &= \tfrac{-K_{qv}}{K_{q\omega}}, & \beta_2 &= \tfrac{-K_{qv2}}{K_{q\omega}},\\
\beta_3 &= \tfrac{-Q_0-Q_1}{K_{q\omega}}, & \beta_4 &= \tfrac{V_0' Y_0'}{K_{q\omega}},\\
\beta_5 &= \tfrac{V_m Y_m}{K_{q\omega}}, & \beta_6 &= \tfrac{-(Y_0'\cos(\theta_o')+Y_m\cos(\theta_m))}{K_{q\omega}},\\
\alpha_1 &= \tfrac{K_{p\omega}K_{qv}-K_{q\omega}K_{pv}}{TK_{q\omega}K_{pv}}, & \alpha_2 &= \tfrac{K_{p\omega}K_{qv2}}{TK_{q\omega}K_{pv}},\\
\alpha_3 &= \tfrac{K_{p\omega}(Q_0+Q_1)-K_{q\omega}(P_0+P_1)}{TK_{q\omega}K_{pv}}, & \alpha_4 &= \tfrac{-K_{q\omega}V_0'Y_0'}{TK_{q\omega}K_{pv}},\\
\alpha_5 &= \tfrac{-K_{q\omega}V_m Y_m}{TK_{q\omega}K_{pv}},\\
\alpha_6 &= \tfrac{K_{p\omega}(Y_0'\cos(\theta_o')+Y_m\cos(\theta_m))+K_{q\omega}(Y_0'\sin(\theta_o')+Y_m\sin(\theta_m))}{TK_{q\omega}K_{pv}},\\
\alpha_7 &= \tfrac{-K_{p\omega}V_0'Y_0'}{TK_{q\omega}K_{pv}}, & \alpha_8 &= \tfrac{-K_{p\omega}V_m Y_m}{TK_{q\omega}K_{pv}}.
\end{aligned} \qquad (4.10)$$

Load bus

Observe that if V is large, (4.8,4.9) reduce to $\dot{\delta} = (\beta_2 + \beta_6)V^2, \dot{V} = (\alpha_2 + \alpha_6)V^2$. Accordingly we consider the following leading order ansatz for the behaviour of

the 3-bus model load variables at voltage collapse;

$$\bar{\delta} = \frac{\Delta}{T_0 - t}, \tag{4.11}$$

$$\bar{V} = \frac{C}{T_0 - t}. \tag{4.12}$$

Note that both expressions become infinite at $t = T_0$. Differentiation of these identities and substitution into (4.8,4.9) yields

$$\begin{aligned} 0 =& -\Delta + (\beta_2 + \beta_6)C^2 \\ &+ (T_0 - t)\left(\beta_1 C + +\beta_4 C\cos(\delta - \theta_0') + \beta_5\cos(\delta - \delta_m + \theta_m)\right) \\ &+ (T_0 - t)^2\beta_3, \end{aligned} \tag{4.13}$$

$$\begin{aligned} 0 =& (-C + \alpha_2 C^2 + \alpha_6 C^2) \\ &+ (T_0 - t)\left(\begin{array}{c} \alpha_1 + \alpha_4\sin(\delta + \theta_0') + \alpha_5\sin(\delta - \delta_m + \theta_m) \\ +\alpha_7\cos(\delta + \theta_0') + \alpha_8\cos(\delta - \delta_m + \theta_m) \end{array}\right) \\ &+ (T_0 - t)^2\alpha_3. \end{aligned} \tag{4.14}$$

Letting $t \to T_0$, these expressions imply that the asymptotic estimates are first order accurate if

$$\Delta = \frac{\beta_2 + \beta_6}{(\alpha_1 + \alpha_6)^2}, \tag{4.15}$$

$$C = \frac{1}{\alpha_1 + \alpha_6}. \tag{4.16}$$

These estimates, and hence the behaviour of the load as it approaches collapse, are independent of the generator variables δ_m, ω_m, parameters γ_i and initial conditions. So in the 3-Bus model, collapse can be said to depend only on the configuration and behaviour of the load and the network. We would expect this result to generalise to larger models of a similar nature.

Generator bus

The asymptotic behaviour of the generator can be derived as follows. Let

$$s = \frac{1}{T_0 - t} \tag{4.17}$$

so that $t \to T_0$ is equivalent to $s \to \infty$. This identity gives

$$\frac{ds}{dt} = \frac{1}{(T_0 - t)^2} = s^2 \tag{4.18}$$

and hence

$$\frac{d\omega}{ds} = \frac{1}{s^2}\frac{d\omega}{dt} \tag{4.19}$$

$$= \frac{\gamma_1 \omega_m}{s^2} + \frac{\gamma_1 + \gamma_2}{s^2} + V(t)\sin(\delta(t) - \delta_m(t) - \theta_m). \tag{4.20}$$

The *Sine Integral*

$$Si(t) = \int_0^t \frac{\sin(\tau)}{\tau}\, d\tau \tag{4.21}$$

is a special function with many well known properties [82] including

$$\lim_{t\to\infty} Si(t) = \frac{\pi}{2} \tag{4.22}$$

Now consider asymptotic estimates:

$$\bar{\omega}_m = \Omega Si\left(\frac{\Delta}{T_0 - t} + \phi\right) + k = \Omega Si\left(\Delta s + \phi\right) + k, \tag{4.23}$$

where Ω, ϕ, k are constants, and

$$\bar{\delta}_m = \int_0^t \bar{\omega}_m\, dt$$

$$= \int_0^{T_0} \bar{\omega}_m\, dt - \int_t^{T_0} \bar{\omega}_m\, dt. \tag{4.24}$$

But $\bar{\omega}_m(T_0) = \frac{\Omega\pi}{2}$, so in the limit $t \to T_0$

$$\bar{\delta}_m = c - \frac{\Omega\pi}{2}(T_0 - t) \tag{4.25}$$

where c is a constant.

Substituting the asymptotic estimates $(\bar{\delta}_m, \bar{\omega}_m, \bar{V}, \bar{\delta})$ for $(\delta_m, \omega_m, V, \delta)$ into

(4.20) gives

$$\frac{d\bar{\omega}_m}{ds} - \frac{d\omega_m}{ds} = \frac{\Omega}{s+\frac{\phi}{\Delta}}\sin(\Delta s+\phi) - \left(\frac{\gamma_1\omega_m}{s^2} + \frac{\gamma_1+\gamma_2}{s^2} + \frac{C\gamma_3}{s}\sin(\Delta s - c + \frac{\Omega\pi}{2s} - \theta_m)\right). \tag{4.26}$$

As $s \to \infty$, the leading order expression reduces to

$$\frac{d\bar{\omega}_m}{ds} - \frac{d\omega_m}{ds} = \frac{\Omega}{s}\sin(\Delta s+\phi) - \frac{C\gamma_3}{s}\sin(\Delta s - c - \theta_m) \tag{4.27}$$

Thus $\bar{\omega}_m \to \omega_m$ as $s \to \infty$, provided that

$$\Omega = C\gamma_3. \tag{4.28}$$

$$\phi = -(c+\theta_m) \tag{4.29}$$

Summary

In summary, an asymptotic description of voltage collapse in the 3-Bus model as $t \to T_0$ is given by

$$\bar{\delta} = \frac{\Delta}{T_0 - t} \tag{4.30}$$

$$\bar{V} = \frac{C}{T_0 - t} \tag{4.31}$$

$$\bar{\delta}_m = c - \frac{\Omega\pi}{2}(T_0 - t) \tag{4.32}$$

$$\bar{\omega}_m = \Omega Si\left(\frac{\Delta}{T_0 - t} - c - \theta_m\right) + k \tag{4.33}$$

with constants Δ, C, Ω given by (4.15,4.16,4.28) and with k, c and T_0 determined by the initial conditions.

4.3.2 Comparison with numerical results

These asymptotic estimates can be compared with numerically calculated voltage collapse trajectories. The numerical integration methods used to calculate the trajectories are described below. The evaluation of the function $Si(t)$ is performed using an algorithm presented in [83].

The problem arises of not being able to exactly determine the blow-up time T_0 and the constants k, c in the asymptotic description of the generator behaviour, nor what starting point $(\bar{\delta}_m, \bar{\omega}, \bar{\delta}, \bar{V})(0)$ to use for the asymptotic estimate. In

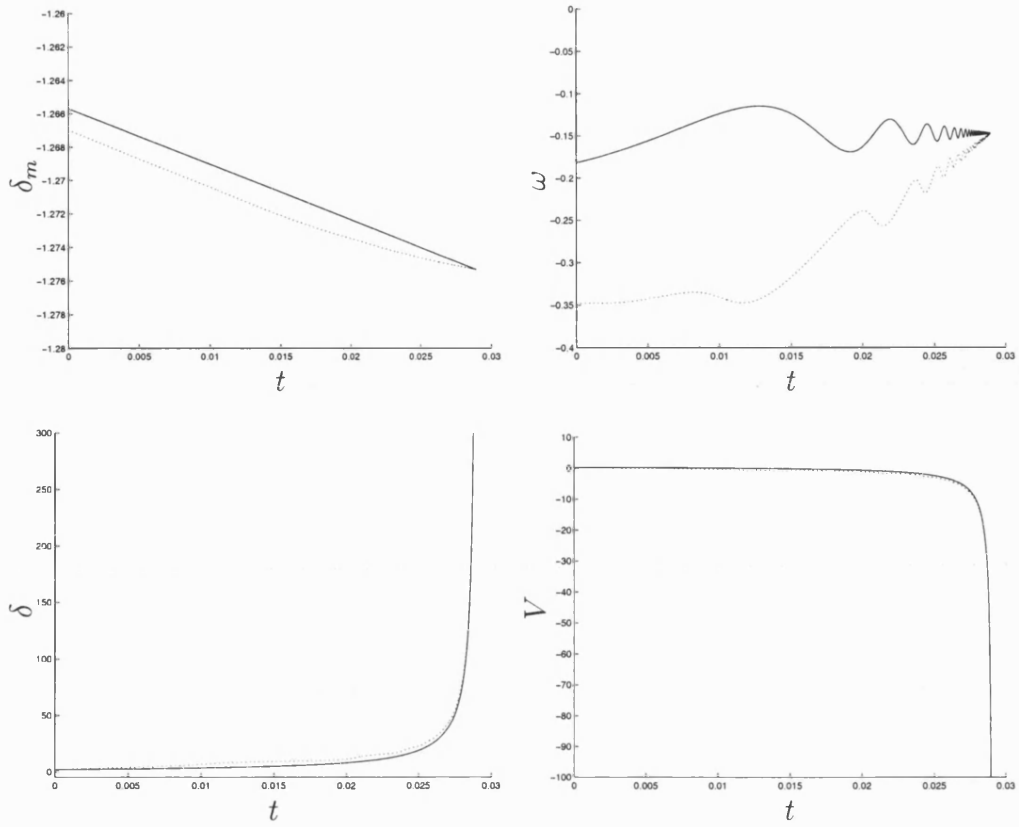

Figure 4.2: Comparison of sample escaping numerical trajectory and asymptotic estimate, $(Q_1, P_1) = (0, 1)$. Full lines are asymptotic estimates, dotted lines are numerically calculated trajectories starting from $(-1.2670, -0.3483, 1.8829, 0.2671)$

order to illustrate that the asymptotic and numerical solutions are in good agreement, we have chosen the same starting values as the numerical trajectories, and determined a value for T_0 by minimising the error between the numerical trajectory and the asymptotic estimate.

The sample plots in Figure 4.2 show both the numerical trajectories and the asymptotic results at the same time-points using the expressions for C, Δ and Ω given above. There is excellent agreement, both qualitative and quantitative, between the numerical and asymptotic results. The asymptotic estimates clearly reproduce the finite time blow-up behaviour at the load. At the generator, the asymptotic results clearly reproduce the bounded oscillatory behaviour present in the variable ω. Note that the frequency of this oscillation increases as the blow-up time is approached. This has a significant effect on the application of numerical methods used to calculate trajectories near collapse.

Also note that the limit $t \to T_0$ would never be observed in practice as other

physical effects (protection devices) rapidly come into play in this limit and our simple model breaks down.

4.4 Numerical methods

4.4.1 Pseudo-arc length continuation

In Chapter 3 we briefly introduced the concept of numerical path following. We now develop this more fully.

Keller's pseudo-Arc length continuation method, as described in [27, 84], can be applied directly to (4.5) to find paths of fixed points with respect to changes in one of the parameters.

In order to make a continuation step of length Δ from a known solution (x_0, λ_0) the method can be formulated as solution of the system

$$F(x,\lambda) = \begin{pmatrix} f(x,\lambda) \\ \tau^T \begin{pmatrix} x - x_0 \\ \lambda - \lambda_0 \end{pmatrix} - \Delta \end{pmatrix} \tag{4.34}$$

where τ is the normalised tangent to the solution locus, given by $(z_0^T, 1)^T$ where $z_0 = f_x^{-1} f_\lambda$ evaluated at (x_0, λ_0). This system can be solved using a Newton method, convergence of which can be guaranteed subject to non-singularity of f_x at the solution point. The step-size Δ can be adjusted (automatically) in order to control accuracy and efficiency.

The method may be extended to compute the loci of other dynamically interesting solutions such as loci of periodic orbits. See for instance [28, 85].

4.4.2 Detection of Hopf and saddle-node bifurcations

Detection of both saddle-node and Hopf bifurcation points during the continuation method is then performed by monitoring the eigenvalues of the linearisation of the system during the course of the computation. A bifurcation may have occurred if the number of eigenvalues in the right half plane changes at successive continuation points (x^1, λ^1), (x^2, λ^2); one real eigenvalue changing sign indicating a possible saddle-node bifurcation, a pair of complex eigenvalues changing sign in their real parts indicating a possible Hopf bifurcation.

Saddle-node point detection

If a possible saddle-node bifurcation point is detected, it can be located to desired accuracy by finding a solution (x^*, λ^*, ϕ^*) of the system

$$\begin{aligned} 0 &= f(x, \lambda) \\ 0 &= f_x \phi \\ 0 &= \phi^T \phi_0 - 1 \end{aligned} \tag{4.35}$$

where ϕ_0 is some fixed reference vector and ϕ is an approximation to the null-space of the Jacobian matrix f_x at the bifurcation point (x^*, λ^*) [84]. This system can be solved using a Newton method.

An alternative method is to apply a secant or similar method on the interval $[\lambda^1, \lambda^2]$, finding a fixed point x at each and calculate the value of the eigenvalue of the Jacobian at the fixed point at that parameter value that is closest to zero. This may not be as robust as finding roots of (4.35) as there may be more than one eigenvalue close to zero for parameters in $[\lambda^1, \lambda^2]$.

Hopf point detection

A Hopf bifurcation with eigenvalues $\pm\omega_H i$ can be located to desired accuracy by solving the non-linear system

$$\begin{aligned} 0 &= f(x, \lambda) \\ 0 &= \tfrac{T}{2\pi} f_x \xi + \eta \\ 0 &= \tfrac{T}{2\pi} f_x \eta - \xi \\ 0 &= \xi^T \xi + \eta^T \eta - 1 \\ 0 &= \eta_0^T \xi - \xi_0^T \eta \end{aligned} \tag{4.36}$$

where $T = 2\pi\omega_H$ is effectively the period of orbits close to the Hopf bifurcation and ξ, η are two vectors spanning the eigenspace associated with the eigenvalues $\pm\omega_H i$ [86]. This method has the advantage that the values T, ξ, η may be used in order to provide initial estimates for computation of periodic orbits.

A simpler and more computationally efficient approach is to measure the real part of an eigenvector close to the imaginary axis, and apply a secant method until this real part is zero. This method may fail if the initial guesses for the secant method are poor, for instance if the eigenvalue chosen to monitor is not the eigenvalue that crosses the imaginary axis. In practice this method works reasonably well if the initial guesses are chosen from successive steps in a continuation method with a reasonably small step-size. If the secant method fails,

better starting guess can be calculated by restarting the continuation method with an even smaller step-size.

4.4.3 Extended systems for continuation of periodic orbits

Periodic orbit

A periodic orbit satisfies the system

$$\begin{aligned} \dot{x} &= f(x) && x \in \mathbb{R}^n,\ t \in [0,T] \\ g(x) = x(0) - x(T) &= 0 && \text{(boundary conditions)} \\ \phi(x(t)) &= 0 && \text{(phase condition)} \end{aligned} \tag{4.37}$$

where T may be fixed or be an unknown. If we normalise the time variable, taking $t' = t/T$, this system becomes

$$\begin{aligned} \dot{x} &= T\, f(x) && x \in \mathbb{R}^n,\ t' \in [0,1] \\ g(x) = x(0) - x(1) &= 0 && \text{(boundary conditions)} \\ \phi(x(t')) &= 0 && \text{(phase condition)} \end{aligned} \tag{4.38}$$

An approximate solution to this system can be found efficiently by the use of a collocation method [84, 25] which we now briefly describe.

Discretisation

We discretise (4.38) on N intervals each containing k collocation points:

$$\text{Mesh points:} \quad \{1 = t_1 < t_2 < \ldots < t_{N+1} = 1\} \tag{4.39}$$

$$\text{Collocation points:} \quad \{0 \le \rho_1 < \rho_2 < \ldots < \rho_k \le 1\} \tag{4.40}$$

We approximate the solution on each mesh interval $[t_i, t_{i+1}]$ by a k-th order polynomial, defined in terms of the Gauss points $\rho_l, l = 1, \ldots, k$, and Legendre polynomials $L_j(t)$ (defined on $[0,1]$ and mapped to $[t_i, t_{i+1}]$). This defines the constants $\beta_j = \int_0^1 L_j(t)dt$ and $\alpha_{jl} = \int_0^{\rho_j} L_j(t)dt$ where $1 \le i, j \le k$.

Let $h_i = (t_{i+1} - t_i)$ and

$$t_{ij} = t_i + h_i \rho_j \qquad j = 1, \ldots, k \tag{4.41}$$

in each mesh interval $i = 1, \ldots, N$. Then we approximate the solution to (4.38) by

$$x(t_{ij}) \approx x_{ij} = x_i + h_i \sum_{l=1}^{k} \alpha_{jl} f(x_{il}) \qquad x_{ij} \in \mathbb{R}^n,\ j = 1, \ldots, k \tag{4.42}$$

$$x(t_{i+1}) \approx x_{i+1} = x_i + h_i \sum_{l=1}^{k} \beta_l f(x_{il}) \qquad x_i \in \mathbb{R}^n \tag{4.43}$$

with boundary conditions

$$g(x_1, x_{N+1}) = x_1 - x_{N+1} = 0 \tag{4.44}$$

This is equivalent to defining a fully implicit Runge-Kutta scheme (defined by ρ, α, β) on each mesh interval and solving for all variables at all mesh intervals simultaneously. We have $n(N(k+1)+1)$ equations (4.42,4.43,4.44) which we can solve for the $n(N(k+1)+1)$ unknowns $x_1, x_{11}, \ldots, x_{1k}$, $x_2, x_{21}, \ldots, x_{2k}$, $\ldots$, $x_N, x_{N1}, \ldots, x_{Nk}$ and x_{N+1}.

This non-linear system could be solved directly, however this is highly inefficient. For each mesh interval i the variables $x_{i,j}$ are dependent only on each other and on x_i, and are independent of the other $x_{i'}$ for $i' \neq i$. A decomposition method for solution of the system, after [25], is presented in Appendix A.

Phase condition

For a general problem, the phase condition $\phi(x(t))$ will typically be specified in terms of the value of some integral over the whole orbit, or a discrete approximation to this integral. Computation of the condition may require use of all solution points in the approximation of the orbit $x(t)$, which will be n-dimensional.

Power systems models of any size will always contain a second order system of type (2.58,2.59) with $\dot{\delta}_i = \omega_i$ at one or more generator buses, hence we can use a much simplified phase condition

$$\omega_i(0) = 0 \tag{4.45}$$

where i is the index of some generator bus. This is guaranteed to have a local solution, due to the second order nature of the system.

Normally caution must be used when taking this approach, as it can lead to numerical difficulties in the presence of steep fronts [87]. Numerical solutions of the boundary value problem will be more accurate if the mesh and phase

condition are allowed to track these fronts; this works well with integral phase conditions but not when specifying a fixed value of one component at one mesh point. However, this proviso primarily applies to the application of collocation and continuation methods to PDE problems. In power system models, we do get large derivatives in the neighbourhood of homoclinic orbits. However the fixed point x^* on this homoclinic orbit will *always* have $\omega_i^* = 0$ for all generator buses i, so we will not have problems with the numerical solution failing to track moving fronts when using this much simplified phase condition.

4.4.4 Detection of cyclic folds and period doubling bifurcations

In [23] details are presented of a method for the computation of Floquet multipliers for the system. The collocation method approximation w_h to the period solution over m points requires solution of the linear system

$$A_h w_h = \Lambda, \tag{4.46}$$

defined by equation (A.7) or (A.13) in Appendix A. This can be shown to be a generalised eigenvalue problem with at least $(m-1)n$ eigenvalues at infinity and n eigenvalues that approximate the Floquet multipliers. Solution of the system by a direct method requires factorisation of A_h. A partial factorisation of the system allows deflation of $(m-1)n$ eigenvalues at infinity, leaving an n-dimensional generalised eigenvalue problem which can be solved to give the Floquet multiplier approximations.

A Floquet multiplier $\lambda_i = 1$ is present in all periodic solutions; the error in the computation of this value allows assessment of the error in this method.

4.4.5 Branch switching at bifurcation points

Upon detection of a bifurcation point, we often wish to switch branches and perform continuation on a different locus. For example, if we detect a Hopf bifurcation while continuing a fixed point, we may wish to calculate the path of periodic orbits emanating from the Hopf point. This process is typically done via the use of a normal form for the system at the bifurcation point, which allows us to calculate an approximation for a point on the new path. This approximation can then be used as a starting guess for a continuation method as before.

Branch switching at Hopf points

A non-degenerate Hopf bifurcation at (x^*, λ^*) implies the local existence of a path of periodic solutions. In order to perform continuation on this path, we must calculate an approximation to a periodic orbit $x(t)$ at some parameter value $\lambda = \lambda^* + \epsilon$. Using simple linear asymptotic estimates for the periodic orbit and its period, [84] gives the following expression for initialising a method to find an initial periodic orbit

$$u(t) \approx x^* + \Delta s \phi(t) \tag{4.47}$$

where

$$\phi(t) = \sin\left(\frac{2\pi t}{\omega_0}\right) w_s + \cos\left(\frac{2\pi t}{\omega_0}\right) w_c. \tag{4.48}$$

where w_s, w_c span the null-space of the Jacobian f_x and ω_0 is the magnitude of the imaginary eigenvalues at the Hopf point.

4.4.6 Trajectories and Poincaré sections

Methods for trajectory calculation for power systems models

Power systems engineers have generally used explicit methods for calculation of system trajectories, especially in methods to estimate "transient stability" [2, 88]. This is due to the large dimension of such systems and hence the reluctance of power system engineers to use implicit methods.

We have tested a number of schemes to calculate trajectories in the 3-Bus model, including an explicit Runge-Kutta scheme (RK-2(3)) and an implicit RK/BDF scheme (TR-BDF2) both with error estimators and automatic step-size selection. Although the latter requires the solution of a non-linear system at each time-step, the efficiency gained through much larger time-steps makes up for this. In addition, major errors were seen when using the explicit scheme; these occurred during periods of rapid oscillation and when the system was close to the point of collapse. At such points the calculated trajectory was seen to be highly non-smooth.

For the most efficient application of these schemes, we must must decide *a priori* how the algorithm will cope near voltage collapse points. Since we know that finite-time blow-up behaviour is likely, we can decide to halt the algorithm if the state x satisfies certain collapse conditions (e.g. $V < 0$). If we do not do

this then the algorithm will continue to calculate the trajectory approaching the collapse point until the minimum step-size is reached.

Poincaré sections for power system models

The second order property of power system models allows us to use the same simple condition for definition of a Poincaré section as used for the calculation of periodic orbits, namely

$$\omega_i(t^*) = 0 \tag{4.49}$$

for some generator i. This will define a hyper-surface which contains all fixed points of the system, but is intersected at least twice by any periodic orbit. So for a unique definition of a Poincaré section we must add the condition

$$\dot{\omega}_i(t^*) > 0 \tag{4.50}$$

These conditions are easy to efficiently monitor as trajectories are calculated numerically. Care must be taken to have a reasonable number of time steps in each orbit, lest the Poincaré section be crossed and re-crossed without detection.

If the Poincaré section is crossed in the time interval $t \in (t_0, t_1)$ then a variety of methods can be used be used to accurately locate the time $t = t^*$ and state $x = x^*$ of intersection. A simple and effective method is to use a bisection or interpolation method to choose the time-step $\Delta t = t^* - t_0$ which satisfies the condition (4.50) to within a specified tolerance. If accuracy is not too important then one linear interpolation between (x_0, t_0) and (x_1, t_1) will suffice to approximate (x^*, t^*).

4.4.7 Implementation

We have used a number of existing packages and our own code to produce the results that follow. The Fortran package AUTO [89] was used to provide initial 1-parameter continuation results and for some of the 2-parameter results discussed in the next chapter (in particular the continuation of cyclic fold and period doubling points). The rest of the results were produced using our own Matlab code, which implemented algorithms not available in AUTO or not easily adaptable from it. This has proved to be very flexible for implementation of efficient BT-point detection algorithms (see next chapter), 1- and 2-parameter continuation and for numerical calculation of trajectories.

4.5 Numerical results

The analysis and methods developed in Chapter 3 can now be applied to a study of the dynamics of the 3-bus model (4.5). To do this we firstly consider varying separately the two parameters Q_1 and P_1 and determining bifurcation points. In the next chapter we will perform two-parameter results leading to a full understanding of the dynamics of this model.

We should note that the data used to specify the system is only given to a finit number of significant figures. Data collection in distributed real-world systems such as power networks is notoriously hard, and so the number of significant figures that could be relied upon in real-world data could be quite low. The numerical techniques we use typically have various tolerances defined within them. Hence caution must be used when interpreting results in the context of actual power system behaviour if this tolerance is a lot smaller than the precision available in the data defining the system.

4.5.1 Continuation in Q_1

Fixed points

In Chapter 3 we looked at various known voltage collapse incidents. A common feature of these is that increasing reactive power demand is believed to be a factor. For this reason Q_1 will be used here as the primary continuation parameter. The bifurcation diagram of fixed points of the system (4.5) with respect to Q_1 is shown in Figure 4.3, with fixed $P_1 = 0$.

Here the upper branch is stable close to the saddle-node bifurcation at $Q_1^{SN1} = 11.41146$ and the lower branch is unstable.

Figure 4.4 shows a schematic of how trajectories in the system might behave in the presence of both a stable and an unstable fixed point[1]. Trajectories may be attracted to either the stable fixed point (a,d) or to infinity (b,e). Note that this allows a connection from the unstable manifold of the unstable fixed point to the stable fixed point.

In the 2-D case, the stable manifold (c) of the unstable fixed point clearly forms a boundary between the two basins of attraction. Such manifolds define similar boundaries in higher dimensional systems (such as power systems) but

[1]It is important to note that power systems have dimension greater than two. In Figure 4.4 and similar schematics, the trajectories represented are therefore 2-D projections of higher dimensional behaviour. We must be careful not to implicitly apply the Poincaré-Bendixson theorem – our projected trajectories are allowed to cross, although for reasons of clarity they are not shown as doing so.

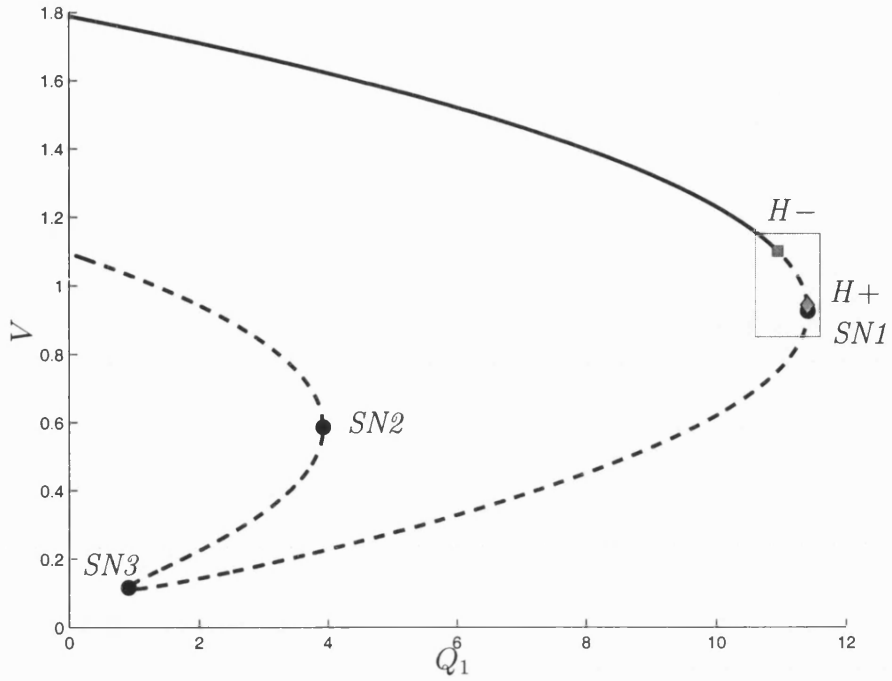

Figure 4.3: Bifurcation diagram in Q_1 for 3-Bus model, $P_1 = 0$

cannot be as easily visualised. Methods do exist [90, 91] to calculate approximations to such manifolds in small dimensions, but they are not suitable for use in very high dimensional systems.

The two saddle-node bifurcations on the unstable branch at $Q_1^{SN2} = 3.92380$ and $Q_1^{SN3} = 0.90944$ have not been previously presented. Previous analysis of power system models has not paid much attention to the unstable branch of fixed points. However, these points are important; in determining the maximum basin of attraction associated with stable fixed points and when they lie on a homoclinic orbit or are associated with boundary crisis events destroying a strange attractor. Any structure in the unstable branch, such as the two bifurcations, is therefore of potential interest and so unstable paths *must* be calculated and considered carefully.

On the branch of stable fixed points exists a pair of Hopf–bifurcation points, at $Q_1^{H-} = 10.94609$ and $Q_1^{H+} = 11.40676$. The first of these two points is a subcritical bifurcation where an unstable periodic orbit coalesces with the fixed point (as we increase Q_1). The second is supercritical giving rise to a stable periodic orbit.

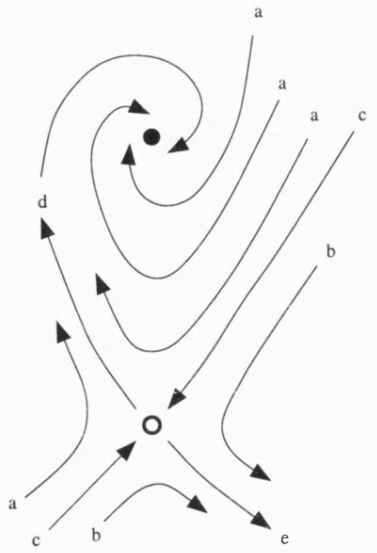

Figure 4.4: Schematic of saddle-node type behaviour

Periodic orbits

Paths of periodic orbits bifurcate from the primary branch at each Hopf point (Figure 4.7). The unstable periodic orbit bifurcating from Q_1^{H-} subsequently coalesces with a stable periodic orbit in a cyclic fold bifurcation at $Q_1^{CF} = 10.81766$. This point has a significant effect on the stability of the electrical system. For $Q_1 < Q_1^{CF}$ the only stable operating point of the 3-bus model is a fixed point, whereas for $Q_1 > Q_1^{CF}$ the fixed point coexists with a stable periodic orbit (bounded but unsatisfactory from an operational viewpoint). As the periodic orbit has a non trivial domain of attraction, it is quite possible that the 3-bus model of the power system may settle into a stable periodic orbit. This may well not be a safe operating condition, although it is bounded and does not result in a voltage collapse.

Figure 4.5 show a schematic of the case where the system has two unstable fixed points and a stable periodic orbit. Trajectories (c) lead to the periodic orbit, trajectories (b) to escape. Again, we should be careful to excessively generalise into higher dimensions the behaviour from this 2-D picture.

Figure 4.6 shows the much more complicated case where there are multiple stable states (one periodic, one fixed). This is to be expected wherever a cyclic fold produces both a stable and unstable periodic orbit. Trajectories can be attracted to either the stable fixed point (b), the stable periodic orbit (a) or escape (d).

We show presently that many cyclic folds are associated with the homoclinic

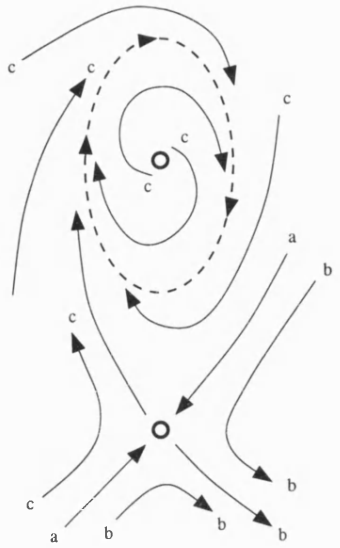

Figure 4.5: Schematic of stable periodic behaviour

orbit which emanates from the BT-point and that they may be computed as parameters vary.

Poincaré maps and chaotic orbits

If Q_1 is increased from Q_1^{CF} then the stable periodic orbit undergoes a sequence of period doubling bifurcations, the first being at $Q_1^{PD1} = 10.87327$, and subsequently evolves into a strange attractor (Figure 4.8). The period doubling cascade in this picture was computed by calculating initial trajectories at each parameter value over a period of 950 seconds, and then computing the Poincaré return map for a further 50 seconds.

The attractor gives an erratic behaviour in the electrical system, but the resulting orbits are all bounded and are indeed not very far from the fixed point.

At the point $Q_1^{BC} = 10.8943$ it was observed in that the strange attractor disappears in a boundary crisis where it collides with the unstable manifold of the neighbouring saddle point [92] (this is also observed in a similar system with different parameters [32]).

If Q_1 is decreased from the value Q_1^{H+} (the super-critical Hopf bifurcation) a similar cascade of period doubling bifurcations can be observed, also leading to chaotic orbits.

For $10.8943 < Q_1 < 11.3766$ there are no bounded attracting states and all initial conditions lead to voltage collapse [43].

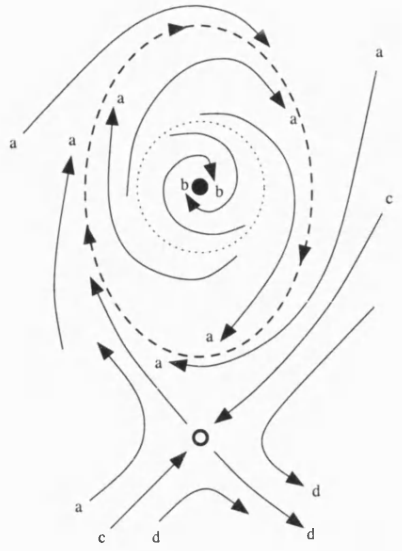

Figure 4.6: Schematic of multiple stable-states

4.5.2 Continuation in P_1

Fixed points

To clarify and unfold the structure observed in the above section we now consider varying the real power demand P_1. Starting from the fixed point at $P_1 = 0$, $Q_1 = 11.25$ we compute the fixed point as a function of P_1, keeping Q_1 fixed. This yields the bifurcation diagram presented in Figure 4.10. This bifurcation diagram has an approximately circular structure, with saddle-node bifurcations at $P_1^{SN1} = 1.44896$ and $P_1^{SN2} = -4.18066$. We observe that whereas the bifurcation at P_1^{SN1} is a coalescence of a stable and an unstable fixed point, that at P_1^{SN2} is a coalescence of two *unstable* fixed points. For this fixed value of Q_1 these two bifurcations give the maximum and minimum real power transfer limits.

As in the previous investigation we observe a super-critical Hopf bifurcation at $P_1^{H+} = 1.28383$ leading to the creation of a stable periodic orbit.

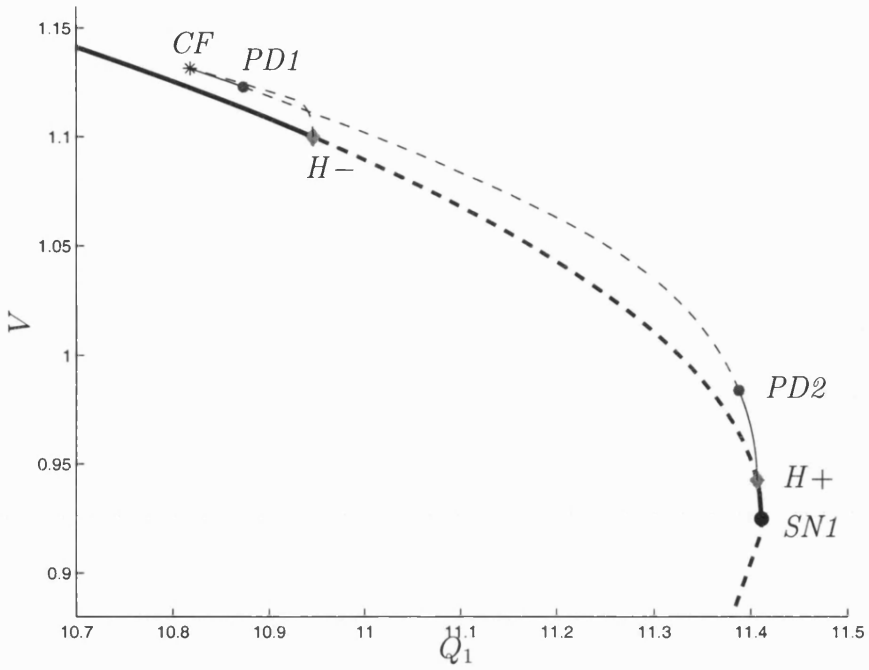

Figure 4.7: Bifurcation diagram in Q_1 for 3-Bus model (detail of periodic orbits)

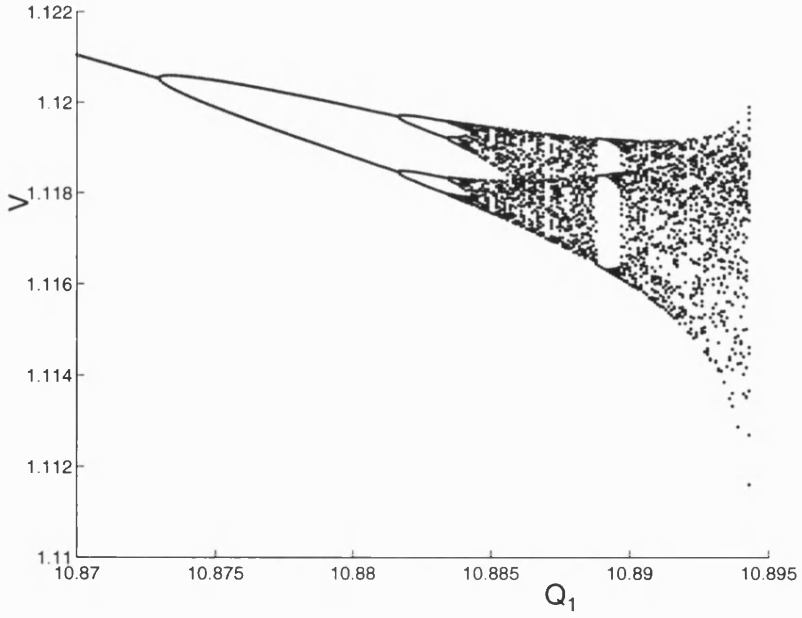

Figure 4.8: Period doubling cascade in 3-Bus model, showing successive period doublings, period-3 behaviour and boundary crisis at $Q_1 \approx 10.8943$

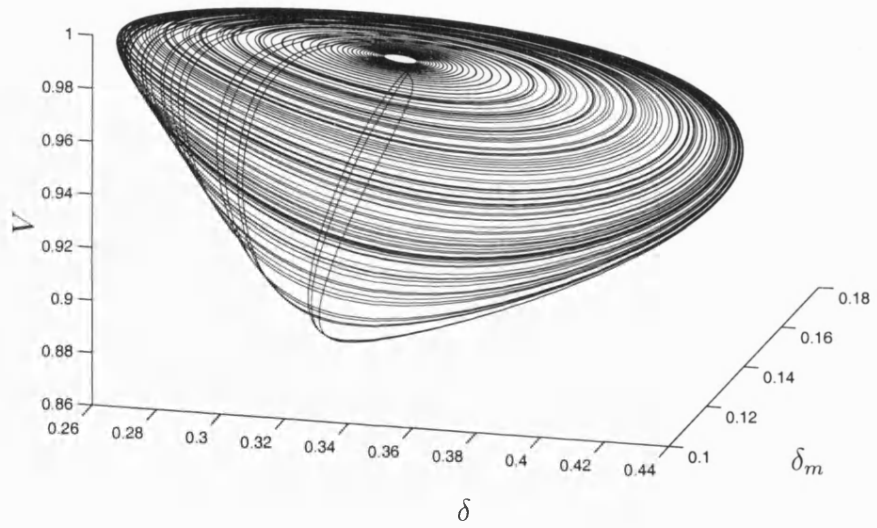

Figure 4.9: Strange attractor in 3-Bus model, $Q_1 = 11.3768$

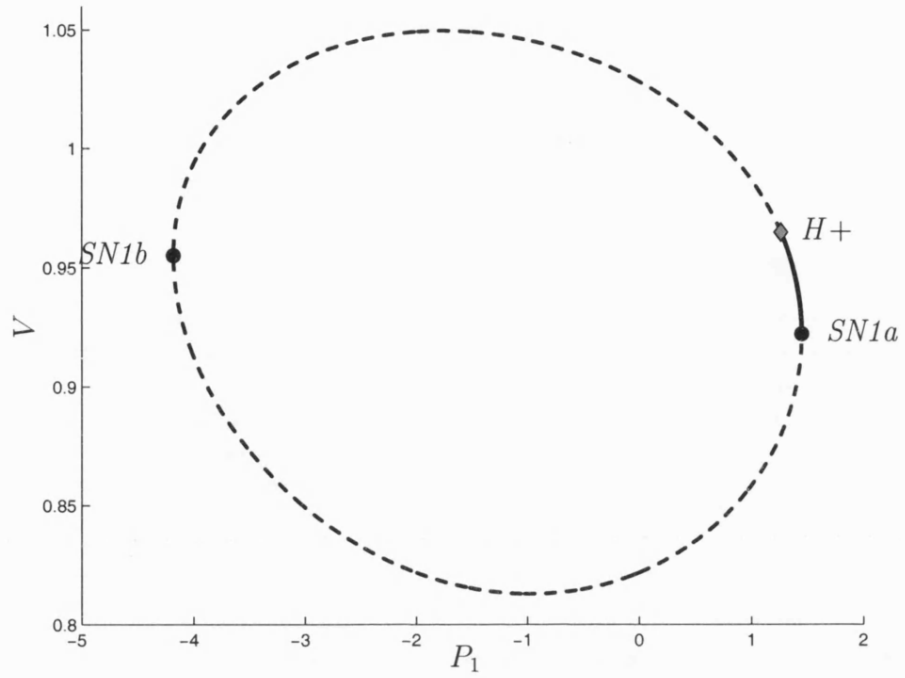

Figure 4.10: Bifurcation diagram in P_1 for 3-Bus model, $Q_1 = 11.25$

Periodic orbits

Again these orbits exhibit cyclic fold and period doubling bifurcations. We will see presently that that further bifurcations from these periodic orbits leads to more complex behaviour.

Šil'nikov homoclinicity

The 3-Bus system contains homoclinic orbits of Šil'nikov type where the homoclinic orbit intersects a fixed point which is a saddle focus (i.e. it has a one dimensional unstable manifold, and its two least stable eigenvectors have complex eigenvalues and span a two-dimensional space). These homoclinic orbits are sometimes referred to as "saddle-focus" homoclinics. Assume the linearisation around the unstable fixed point contained within the homoclinic orbit has one positive real eigenvalue $\nu_1 = \alpha > 0$ and next rightmost eigenvalues are a complex conjugate pair $\nu_{2,3} = -\beta \pm \gamma i$. We can define a useful quantity[2] $\delta = \frac{\beta}{\alpha}$; this can be thought of as the ratio of the speed of rotation and the speed of ejection of orbits near the fixed point [93]. The homoclinic orbit is said to be of Šil'nikov type if $\delta < 1$. In this case the linearisation at the unstable fixed point is dominated by

[2]This ratio is not to be confused with our state variable δ; phase angle at load.

the rightmost, complex, pair of eigenvalues; the stable manifold is then essentially two dimensional, and the homoclinic orbit spirals around the fixed point as it approaches it. In addition there is a characteristic bifurcation diagram for the periodic orbits near this type of homoclinic orbit, and much can also be said about the presence of chaotic orbits [94].

This is well illustrated by considering the 3-Bus model itself. Consider the 1-D bifurcation diagram in P_1 (Figure 4.10) where $Q_1 = 11.25$ and calculate the periodic orbits emanating from the Hopf point P_1^{H+}). A plot of the time period of the orbits on this path (Figure 4.11) show the period increasing with an oscillatory pattern, with orbits of increasing period converging through multiple cyclic folds P_1^{CFn} towards the homoclinic orbit at $P_1^h = -2.30456$. Note that in Figure 4.11 there exist both stable and unstable periodic orbits, but we use a solid line for both types in the interest of clarity. There also exists a period doubling bifurcation associated with each cyclic fold, again these are omitted for clarity. This pattern is characteristic of the behaviour of a (global) Šil'nikov bifurcation, with a sequence of multiple cyclic-fold points also accumulating onto the homoclinic orbit. It is also possible to follow the periodic orbit created in the period doubling bifurcation at $P_1^{PD} = -0.62682$. This orbit also displays an oscillatory structure as it converges towards a double pulse homoclinic orbit at $P_1 = -1.731537$ (Figure 4.12).

If we examine the eigenvalues of the unstable fixed point at $Q_1 = 11.25, P_1^h = -2.30456$, we find that $\delta = 0.01344$ confirming our observations. The value of δ changes along the path of the approximate homoclinic orbits, accounting for the qualitative change in the orbits shown in Figure 5.6.

The main features of a Šil'nikov bifurcation are (i) the creation of an infinite set of cyclic fold points (ii) the creation of an infinite set of period-doubling bifurcations either side of each fold (iii) the existence of complex chaotic behaviour close to the homoclinic orbit. In the latter case it will be very difficult to resolve which part of this region is liable to lead to a voltage collapse. We can however calculate the path of cyclic folds passing through $P_1 = P_1^{CF1}$, $Q_1 = 11.25$ which acts as a boundary for this region in the 2-parameter plane.

This particular form of the dynamics, whilst important, occurs in this example for non-physical values of the real power demand P_1. However, as we shall show in the next chapter, the loci of some of the cyclic fold and period doubling bifurcation points created at this bifurcation can be followed by continuation in P_1 and Q_1 into more physically interesting regions of parameter space.

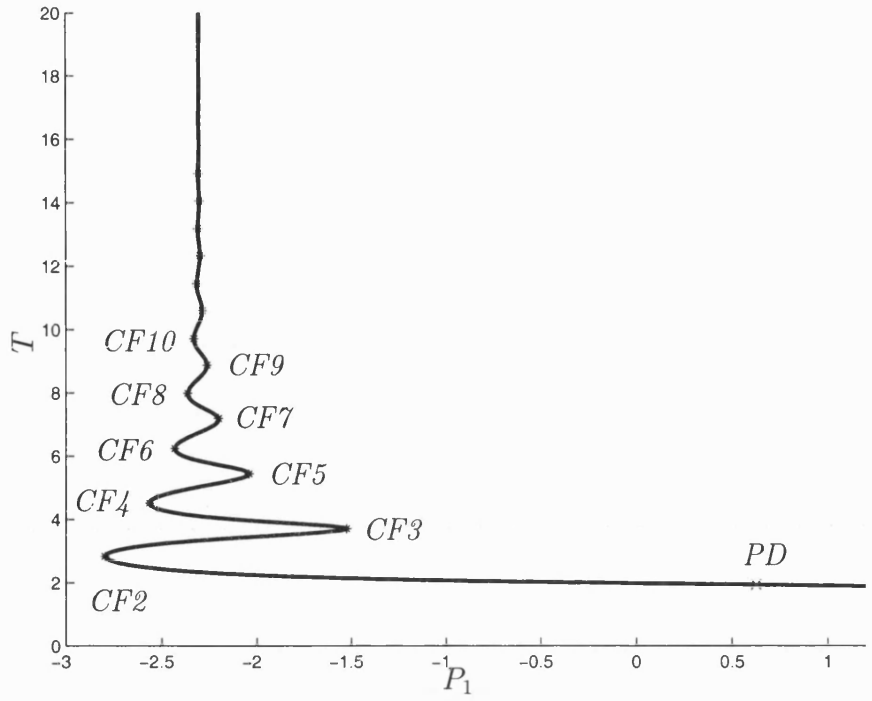

Figure 4.11: Time period of period orbits in 3-Bus model, plotted against parameter P_1. ($Q_1 = 11.25$)

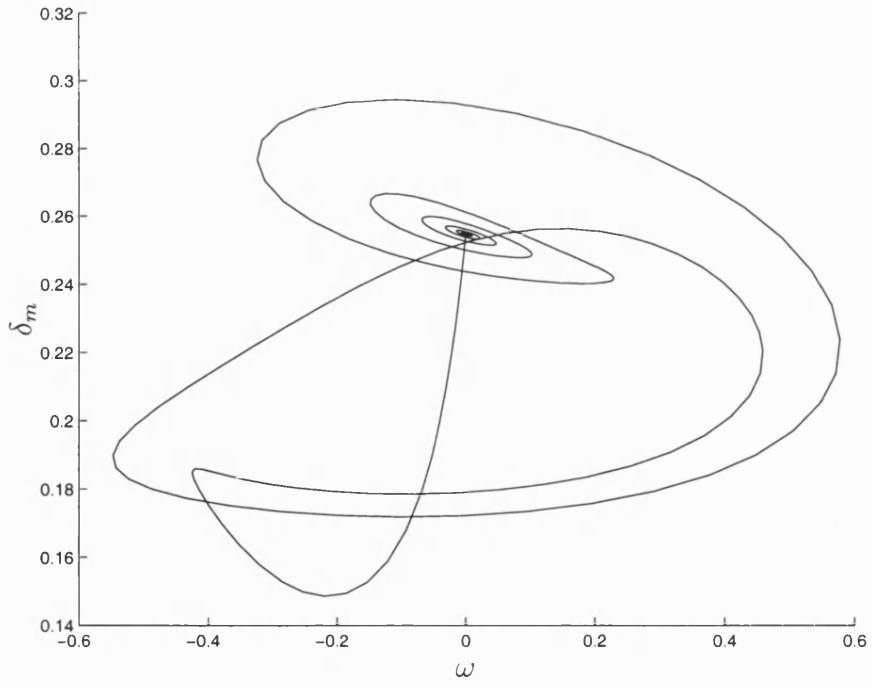

Figure 4.12: Double pulse homoclinic, $(Q_1, P_1) = (11.25, -1.731537)$

4.6 Conclusions and implications

Continuation of fixed points and periodic orbits reveals a wealth of dynamic behaviour in the 3-bus model. At different parameter values, the system may have a wide variety of stable and unstable fixed points, stable and unstable periodic orbits, homoclinic orbits and strange attractors coexisting. These formation of these differing mode of behaviour can be successfully explained in terms of bifurcation points.

These behaviour types all have implications for the study of voltage collapse. Contrary to the previously published work, we feel that it is not possible to say that collapse is the result of one particular type of bifurcation. For instance, coexistence of stable periodic orbits and fixed points can occur prior to a bifurcation related to increasing reactive load. This means that if collapse is related to the loss of a sufficiently large basin of attraction for the desired stable operating point, simple monitoring of bifurcation of fixed points will not be sufficient to identify possible collapse. In the next chapter we will examine the effects of bifurcations and differing modes of behaviour on basins of attraction.

Continuation methods can be successfully and efficiently applied to the 3-Bus model. In particular, a very simple expression can be given for the definition of Poincaré sections and of phase conditions in periodic orbit approximation; this generalises to larger power system models. Implicit methods are recommended for the calculation of trajectories in the system.

Chapter 5

3-Bus Model – 2-Parameter and Basin Erosion Investigation

5.1 Introduction

In this chapter we consider the two-parameter continuation of the saddle-node and Hopf bifurcation points discussed in the previous chapter. We show that loci of saddle-node and Hopf point meet at a co-dimension 2 Bogdanov-Takens point (BT-point) and we link the existence of the BT-point with nearby Šil'nikov-type homoclinic orbits. The BT-point acts as a organising centre[1] in the bifurcation structure of the model and plays a significant role in helping to understand the overall mechanism of voltage collapse through the destabilisation of fixed points and the erosion of basin boundaries.

BT-points will arise naturally in much larger systems as operating parameters change; hence we consider the observed dynamics of the 3-Bus model to be a fairly general explanation for much of the dynamics associated with voltage collapse. Because of the importance of the BT-point we consider in detail techniques for calculating it for both the reduced system and for more complex systems.

This understanding of the bifurcation structure of the 3-Bus model allows us to determine the the number and type of attractors at different parameter values. We then apply a Monte Carlo method to analyse the effect of varying parameters on the basins of attraction of these attractors and draw some conclusions about operating stability of the underlying power system.

The structure of this chapter is as follows. First we discuss the theory and numerical methods used for 2-parameter investigation of bifurcation points, in-

[1]This can loosely be defined as a set of parameter values, within a small neighbourhood of which the system has a variety of qualitatively different behaviours [26]

cluding BT-points (Section 5.2). In Section 5.3 we present the full 2-parameter bifurcation structure of the 3-Bus model. The implications of this structure on the erosion of basin boundaries (and thus the practical stability of the system) are discussed in Section 5.4 along with some interesting numerical results. In Section 5.5 we show how knowledge of both the basin erosion and bifurcation information allows us to predict in detail the behaviour of the the 3-Bus system at different parameter values. Finally, in Section 5.6, we draw some general conclusions from these results.

5.2 Theory and methods

5.2.1 2-parameter continuation of bifurcation points

We have already discussed how a bifurcation point can be defined as the solution to some extended system, such as (4.35). We have also discussed how the implicit function theorem implies the existence of parameter dependent paths of solutions to non-linear equations. We can combine these two facts to produce methods to compute two-parameter paths of bifurcation points.

Continuation of Hopf and saddle-node bifurcation points

The systems (4.35) and (4.36), used for detection of Saddle-node and Hopf bifurcations respectively, can be used within a continuation method to compute 2-parameter paths of these points [85, 95].

Implementation requires the use of a Newton method to solve the extended system at each continuation step. The Jacobian used involves both the first and second derivatives of the dynamical system, f_x, f_{xx}, and can be approximated numerically. However, as we have already noted, the power system distribution network structure leads to a very sparse matrix f_x and an even sparser tensor f_{xx}; moreover this sparsity is known and fixed. Hence it is sensible to use explicitly computed Jacobians in application of the continuation method to 2-parameter continuation of bifurcation points.

5.2.2 BT-points

We briefly introduced the definition of a BT-point in Section 3.2.5. We now present the necessary theory and computational methods in more detail so that we may examine the BT-point in the 3-Bus system.

The algorithm above accurately computes paths of Hopf and saddle-node bifurcations. We wish to identify special values of the second parameter at which these two paths intersect. Such a point is generally referred to as a Bogdanov-Takens point (BT-point). BT-points have been shown to play an important role in 'organising' the dynamics of a variety of physical systems of high dimension, for example [96, 97, 98]. A similar organisation is seen in the 3-Bus model.

A BT-point is a co-dimension 2 bifurcation point; where a fixed point of the system has a Jacobian matrix f_x with a zero eigenvalue of algebraic multiplicity 2 but of geometric multiplicity 1 [16]. An equivalent definition of BT-points is that they are points where the Jordan normal form of the Jacobian f_x has a block of the form

$$\begin{pmatrix} 0 & 1 \\ 0 & 0 \end{pmatrix} \tag{5.1}$$

and no other Jordan block associated with the zero eigenvalue. Subject to satisfaction of transversality conditions and absence of certain symmetries in the system [16] this point occurs when there is a tangential intersection, in the 2-parameter plane, of a path of folds and a path of Hopf-bifurcations.

For parameter values close to that of the BT-point the dynamics of the system can be reduced [16] to that of a much simpler system given by one of the following normal forms:

$$\begin{aligned} \dot{x} &= y \\ \dot{y} &= \nu_1 + \nu_2 x + x^2 \pm xy \end{aligned} \tag{5.2}$$

Considering the $+xy$ case, note that there are fixed points at $(x, y) = (\pm\sqrt{-\mu_1}, 0)$ for $\mu_1 < 0$, no fixed points for $\mu_1 > 0$ and a saddle-node bifurcation at $\mu_1 = 0$, $\forall \mu_2 \in \mathbb{R}$. A Hopf bifurcation exists for $\mu_2 = +\sqrt{-\mu_1}$.

A more detailed analysis [16] of the normal form (5.2) shows that a path of homoclinic orbits also emanates from such a BT-point, at $\mu_1 \approx -\frac{49}{25}\mu_2^2$. This is proved by use of Melnikov's method. A co-ordinate transformation is made to show existence of a Hamiltonian system arbitrarily close to the normal form. A a closed form is given for a homoclinic orbit in this Hamiltonian system and this is then transformed back to the normal form co-ordinates to show existence of a homoclinic in the normal form system.

At the BT-point the homoclinic curve is also tangential to the loci of the saddle-node and Hopf points. As we shall demonstrate, the existence of this homoclinic orbit has a profound effect on the overall stability of the 3-bus system.

Figure 5.1 shows the loci of the bifurcation points near to the BT-point in the normal form (5.2). Note that in the quadrant $\mu_1 < 0, \mu_2 > 0$ there are multiple

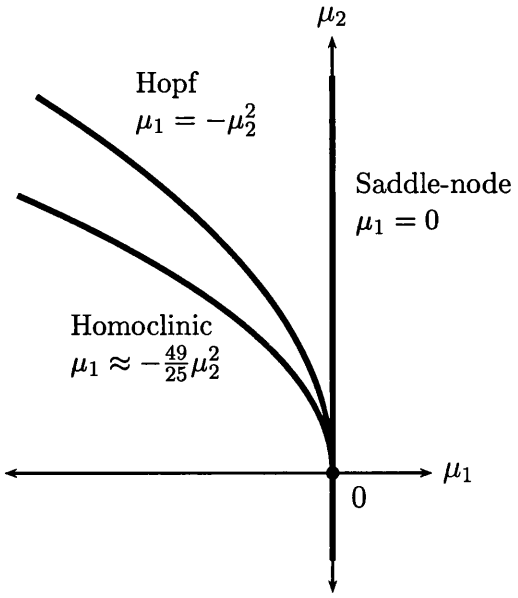

Figure 5.1: Schematic of bifurcation behaviour at a BT-point

fixed points, periodic orbits and homoclinic orbits.

This means that near a BT-point the dynamics of system (3.6) are governed by the solution of (5.2) on a 2-dimensional centre-manifold of the larger system [19]. The dynamics on this manifold, in particular the behaviour of the periodic and homoclinic orbits, completely describes the local behaviour of the original system. This remains true even for systems of much higher dimension than considered here and it is for this reason that we believe that an analysis of the BT-point for the simple 3-bus model is extendable and will give insight into the general behaviour of more complex power system models.

5.2.3 Detection of BT-points

While calculating a path of co-dimension 1 bifurcation points in the two-parameter plane, we may check at each iteration whether we are in the neighbourhood of a BT-point. For instance, while following a path of saddle-node bifurcations we might monitor whether the eigenvalue with the second smallest magnitude changes sign in its real part. Having so detected the possibility of a BT-point we can then apply an algorithm to locate the BT-point to desired accuracy. Once again, this is by the solution of a suitable extended system, roots of which define

a BT-point. Such a system is

$$F(x,\lambda,\mu,v,w) = \begin{bmatrix} f \\ f_x v \\ c_o^T v - 1 \\ f_x w - v \\ c_0^T w \end{bmatrix} = 0 \tag{5.3}$$

Here we are saying that we require a solution to the generalised eigenvalue problem associated with the Jordan block described above (5.1); that is $f_x v = 0$, $f_x w = v$.

In practice this formulation of the BT-point detection problem is highly inefficient. Given that our dynamical system (3.6) has dimension n, the Jacobian matrix for system (5.3) (which must be inverted in a Newton-type solution method) is of dimension $(3n+2)$ by $(3n+2)$. Beyn [99] and Griewank and Reddien [100] developed decomposition methods to solve this problem more efficiently, as now described.

Decomposition

Lemma 1

Define

$$A = \begin{bmatrix} f_x & b_0 \\ c_o^T & 0 \end{bmatrix} \tag{5.4}$$

where $b_0, c_0 \in \mathbb{R}^n$. *Then* A *is non-singular if (for instance)* $b_0 = f_\lambda$ *or* f_μ, *and* $c_0 \notin \mathcal{N}(f_x)$.

Proof: *ABCD-lemma [27].*

Theorem 2 (Griewank and Reddien [100], as presented in Beyn [99])

Let A *be defined as above and let functions* $g, h : (\Omega \times \mathbb{R}^2) \to \mathbb{R}$ *and vectors* $v, w \in \mathbb{R}^n$ *be defined by the solutions to*

$$A \begin{bmatrix} v \\ g \end{bmatrix} = \begin{bmatrix} 0 \\ 1 \end{bmatrix} \quad \text{and} \quad A \begin{bmatrix} w \\ h \end{bmatrix} = \begin{bmatrix} v \\ 0 \end{bmatrix}. \tag{5.5}$$

Then roots x^0, λ^0, μ^0 *of the system*

$$S(x,\lambda,\mu) = \begin{bmatrix} f(x,\lambda,\mu) \\ g(x,\lambda,\mu) \\ h(x,\lambda,\mu) \end{bmatrix} = 0 \tag{5.6}$$

also satisfy the generalised right eigenvalue problem given in (5.3)*, and so define BT-points.*

In addition, if we define $\bar{g}, \bar{h} : (\Omega \times \mathbb{R}^2) \to \mathbb{R}$ *and vectors* $\psi, \zeta \in \mathbb{R}^n$ *by*

$$[\psi^T, \bar{g}]A = [0, 1] \quad \textit{and} \quad [\zeta^T, \bar{h}]A = [\psi, 0]. \tag{5.7}$$

then

$$\begin{aligned} g &= \bar{g} = -\psi^T f_x v, \\ h &= \bar{h} = \psi^T v, \\ g_z &= -\psi^T f_{xz} v, \\ h_z &= -\psi^T f_{xz} w - \zeta^T f_{xz} v, \end{aligned} \tag{5.8}$$

where z *can be either* x, λ *or* μ*; the roots of* (5.6) *and solutions of* (5.7) *give*

$$\begin{aligned} \psi^T f_x &= 0, \quad \psi^T b_0 = 1, \\ \zeta^T f_x &= \psi, \quad \zeta^T b_0 = 0; \end{aligned} \tag{5.9}$$

that is to say the generalised left eigenvalue problem for f_x*.*

Proof: *See [100].*

Newton's method

Newton–type methods to solve (5.6) require us to solve the four $(n+1)$–dimensional linear systems in (5.5) and (5.7) (involving inversion of A and A^T) and then solve the $(n+2)$–dimensional system

$$\begin{bmatrix} f_x & f_\lambda & f_\mu \\ g_x & g_\lambda & g_\mu \\ h_x & h_\lambda & h_\mu \end{bmatrix} \begin{bmatrix} \delta x \\ \delta\lambda \\ \delta\mu \end{bmatrix} = - \begin{bmatrix} f \\ g \\ h \end{bmatrix} \tag{5.10}$$

where we use (5.8) to give the derivatives of g and h (f_{xx}, $f_{x\lambda}$, $f_{x\mu}$ can be calculated explicitly or numerically). The following theorem presents an efficient way to solve this system. This was shown in [100], but is presented here in a different form and with a minor correction[2].

Theorem 3

If we find g, h, v, w, ψ *and* ζ *from* (5.5) *and* (5.7) *as above and solve the following*

[2]The terms invovling g in (5.11) were ommited in [100], but do not affect the final answer as $g = 0$ at the BT-point

three linear systems in A

$$\begin{aligned} A\begin{bmatrix} \tilde{f}_\lambda \\ (\psi^T f_\lambda) + (g c_0^T \tilde{f}_\lambda) \end{bmatrix} &= \begin{bmatrix} f_\lambda \\ 0 \end{bmatrix}, \\ A\begin{bmatrix} \tilde{f}_\mu \\ (\psi^T f_\mu) + (g c_0^T \tilde{f}_\mu) \end{bmatrix} &= \begin{bmatrix} f_\mu \\ 0 \end{bmatrix}, \\ A\begin{bmatrix} \tilde{f} \\ (\psi^T f) + (g c_0^T \tilde{f}) \end{bmatrix} &= \begin{bmatrix} f \\ 0 \end{bmatrix}, \end{aligned} \tag{5.11}$$

then the Newton correction $(\delta x, \delta\lambda, \delta\mu)^T$ *in* (5.10) *is given by solution of the* (3×3) *system*

$$\begin{bmatrix} g & \psi^T f_\lambda & \psi^T f_\mu \\ g_x v & g_\lambda - g_x \tilde{f}_\lambda & g_\mu - g_x \tilde{f}_\mu \\ h_x v & h_\lambda - h_x \tilde{f}_\lambda & h_\mu - h_x \tilde{f}_\mu \end{bmatrix} \begin{bmatrix} \delta t \\ \delta\lambda \\ \delta\mu \end{bmatrix} = - \begin{bmatrix} \psi^T f \\ g - g_x \tilde{f} \\ h - h_x \tilde{f} \end{bmatrix} \tag{5.12}$$

and

$$\delta x = (v\delta t) - (\tilde{f}_\lambda \delta\lambda) - (\tilde{f}_\mu \delta\mu) - \tilde{f}. \tag{5.13}$$

Proof:

Add a further two rows and columns to (5.10) *along with two dummy variables* $\delta\phi, \delta t \in \mathbb{R}$ *to get*

$$\begin{bmatrix} f_x & b_0 & 0 & f_\lambda & f_\mu \\ c_o^T & 0 & -1 & 0 & 0 \\ 0 & -1 & 0 & 0 & 0 \\ g_x & 0 & 0 & g_\lambda & g_\mu \\ h_x & 0 & 0 & h_\lambda & h_\mu \end{bmatrix} \begin{bmatrix} \delta x \\ \delta\phi \\ \delta t \\ \delta\lambda \\ \delta\mu \end{bmatrix} = - \begin{bmatrix} f \\ 0 \\ 0 \\ g \\ h \end{bmatrix}. \tag{5.14}$$

(Note that the principal sub-matrix of this expanded matrix is A *and that* $\delta\phi = 0$*). The first two "rows" of* (5.14) *can be rearranged to give*

$$\begin{bmatrix} f_x & b_0 \\ c_o^T & 0 \end{bmatrix} \begin{bmatrix} \delta x \\ \delta\phi \end{bmatrix} = \delta t \begin{bmatrix} 0 \\ 1 \end{bmatrix} - \delta\lambda \begin{bmatrix} f_\lambda \\ 0 \end{bmatrix} - \delta\mu \begin{bmatrix} f_\mu \\ 0 \end{bmatrix} - \begin{bmatrix} f \\ 0 \end{bmatrix}. \tag{5.15}$$

Pre-multiplying this by A^{-1} *we get*

$$\begin{bmatrix} \delta x \\ \delta\phi \end{bmatrix} = \delta t A^{-1} \begin{bmatrix} 0 \\ 1 \end{bmatrix} - \delta\lambda A^{-1} \begin{bmatrix} f_\lambda \\ 0 \end{bmatrix} - \delta\mu A^{-1} \begin{bmatrix} f_\mu \\ 0 \end{bmatrix} - A^{-1} \begin{bmatrix} f \\ 0 \end{bmatrix}. \tag{5.16}$$

We know from (5.5) *that* $A^{-1}\left[\begin{smallmatrix}0\\1\end{smallmatrix}\right] = \left[\begin{smallmatrix}v\\g\end{smallmatrix}\right]$. *The other three terms involving* A^{-1} *are found as follows. Consider systems of the form*

$$A\begin{bmatrix}\alpha\\ \beta\end{bmatrix} = \begin{bmatrix}\gamma\\ 0\end{bmatrix} \tag{5.17}$$

where $\alpha, \gamma \in \mathbb{R}^n$ *and* $\beta \in \mathbb{R}$. *Pre-multiplying this by* $[\psi^T, 0]$, *gives*

$$\psi^T f_x \alpha + \beta(\psi^T b_0) = \psi^T \gamma. \tag{5.18}$$

From (5.7) *we have* $\psi^T f_x + g c_0 = 0$ *and* $\psi^T b_0 = 1$. *Hence* $\beta = \psi^T \gamma + g c_o^T \alpha$. *We can let* γ *be successively* f_λ, f_μ *and* f; *for these three cases let* α *be referred to as* $\tilde{f}_\lambda, \tilde{f}_\mu$ *and* $\tilde{f}$ *respectively, giving the triple linear system* (5.11).

Equation (5.16) *now gives us* (5.13) *and also*

$$0 = \delta\phi = (g\delta t) - (\psi^T f_\lambda \delta\lambda) - (\psi^T f_\mu \delta\mu) - \psi^T f. \tag{5.19}$$

This gives the first row of (5.12); *the second and third rows are given by substituting* (5.13) *into the last two rows of* (5.14).

In summary, this decomposition of the BT-point detection problem gives us a number of smaller systems to solve (when compared with solving (5.3) directly), involving just 2 large matrices (A and A^T) plus a 3×3 system.

5.2.4 Branch switching at BT-points

As we have already stated, the BT-point acts as an organising centre for paths of folds, Hopf bifurcations and homoclinic orbits in the 2-parameter space. We wish to calculate these paths, using continuation methods. However, to do this we will need to calculate an initial point on each of the paths. We can use ψ, ζ and equations (5.8) as part of this calculation as briefly described above. Further details can be found in [99].

Initialising paths of saddle-node points and Hopf points

For the computation of a paths of folds emanating from the BT-point, the initial step in the continuation algorithm will converge provided we do not attempt to step too far from the BT-point.

For a point on the path of Hopf bifurcations, we require the Jacobian at the fixed point to have a pair of eigenvalues of the form $\lambda = \pm\epsilon i$. The BT-point can

be thought of as the point where $\epsilon = 0$; we must choose a suitably small value of ϵ in the first step of our Hopf-point continuation method. However, it is important not to choose a value too small, as the Jacobian of the defining system may be singular [96].

It is interesting to note that in the investigation of the 3-bus system, the converse applied. The continuation algorithm following a path of Hopf-points broke down as the path tangentially approached a path of folds, giving evidence for what later proved to be a BT-point.

Initialising paths of homoclinic orbits

To start the calculation of the path of homoclinic orbits emanating from the BT-point, a usual procedure is to determine an "approximate" homoclinic orbit close to (but not precisely at) the BT-point and to then use this as the first point in a continuation algorithm for homoclinics. Details of this are given in [99]. The numerical procedure for calculating this approximate orbit is analogous to the procedure used to prove the actual existence of the path of homoclinic orbits. By a change of coordinates, the system is transformed to the normal form (5.2), a homoclinic orbit for this normal form is given explicitly at a specified small distance from the BT-point, and the transformation reversed to give an approximation to the homoclinic orbit in the original system (4.5). This method may not give a very precise approximation to a homoclinic orbit, due to the higher order terms neglected in the normal form calculation, but it has been used with success to initialise more sophisticated homoclinic continuation algorithms.

Limitations of branch-switching methods

The system is highly sensitive at the BT-point, due to the close proximity of multiple paths of bifurcation points. This can cause problems when initialising computation of these paths.

If a starting point is selected that is too close to the BT-point, the accuracy needed to distinguish computationally between the different types of behaviour may be larger than is available, since the BT-point is only computed to finite accuracy. Conversely, if a starting point is chosen too far from the BT-point, non-linear terms in the system may become large and so the normal form (5.2) may not give predictions of sufficient accuracy for initialisation of Newton and continuation methods.

We believe that this is a problem when computing a point on the path of homoclinic orbits, which has caused the branch switching algorithm not to behave

as predicted. Of course, as is often the case with numerical implementations, it is also possible that these problems have arisen as a result of a bug in our code.

5.2.5 Summary

This gives us a computational methodology for a more complete detection of the bifurcation structure. First locate a fixed point of the system (e.g. a stable operating point); perform continuation on this fixed point and detect a saddle-node bifurcation. Compute a path of saddle-node bifurcations and detect a BT-point. Finally, compute paths of Hopf and homoclinic bifurcations emanating from the BT-point.

5.3 2-parameter continuation results

We now demonstrate how the theory and methods developed above can be applied to the 3-Bus model, leading to a full understanding of its 2-parameter bifurcation structure and resulting dynamical behaviour.

5.3.1 Full 2-parameter analysis for 3-Bus model

The physical meaning of the parameter values

These curves naturally all continue into the parameter range $P_1 < 0$. This is apparently an unphysical approach as this would correspond to a scenario in which the loads (or at least the constant part of the empirical induction motor load) are providing power to the rest of the network. However our aim is to investigate the qualitative behaviour of a highly reduced system and demonstrate the effectiveness of certain methods, so there is a two-fold justification for considering the $P_1 < 0$ parameter region.

We find that by following paths of certain bifurcation points we consider values of the parameters which are not especially physical. However, by identifying organising centres (such as the BT-point) for the dynamics in these regimes we can infer a lot about the dynamics in the more physically interesting regions of parameter space. So we may step into the region in which the model is possibly invalid in order to find dynamical phenomena which may have effects in the "valid" region; such a procedure is widely used in other investigations of physical systems.

In addition, the position in 2-dimensional parameter space of the structures and phenomena described may be dependent on further parameters. Hence if

these parameters were to change or be adjusted, the phenomena occurring in a "physically unrealistic" region could move to a parameter region where they might be observable.

Concisely – we are not troubled by taking $P_1 < 0$ since it may lead us to find things out for $P_1 > 0$ that we would not have found otherwise.

2-D loci of saddle-node bifurcations

As we have discussed, a saddle-node point is sufficient to give rise to voltage collapse. We now see that a path of such points provides a clear boundary in parameter space for the region of "feasible" operating points.

The paths of the main saddle-node bifurcation and the two subsidiary saddle-node bifurcations on the the unstable branch of fixed points are given in Figure 5.2. The main fold can be thought of as the maximum reactive power Q_1 transfer point over all values of P_1. This is interesting because it clearly shows that there is an interaction between the the real and reactive loads which can be understood through continuation methods and could be used by engineers to provide a more efficient and stable supply of power to users. The 2-D diagram shows that the curve of saddle-node points itself has a maximum value when $Q_1 = 11.45$ occurring when $P_1 = -1.5$. Observe that this is close to the value obtained when $P_1 = 0$. Thus the observed maximum reactive power point given when $P_1 = 0$ is in fact close to the point of maximum reactive power transfer over all values of P_1.

2-D loci of Hopf bifurcations

A similar diagram to that of the locus of saddle-node bifurcation points is plotted for the paths of the sub-critical and super-critical Hopf bifurcation points (Figure 5.3). It can be seen that for $P_1 > 0$ the two Hopf points approach each other and eventually coalesce at $P_1 \approx 1.46$. The periodic orbits and chaotic structure in the region between the Hopf points (as shown in Section 4.5.1) vanishes for $P_1 > 1.5$ leading to relatively simple and predictable dynamics in this region of parameter space. This scenario of the annihilation (or creation) of complex periodic behaviour has been observed in many systems, see for example [101, 102].

For $P_1 < 0$, the sub-critical Hopf bifurcation occurs at consistently lower values of Q_1 as P_1 is decreased. This implies that the system could be more susceptible to destabilising periodic behaviour at these lower real power demand. In contrast, the path of the right-hand, supercritical, Hopf bifurcation approaches the path of the main saddle-node tangentially as we decrease P_1. This can be see

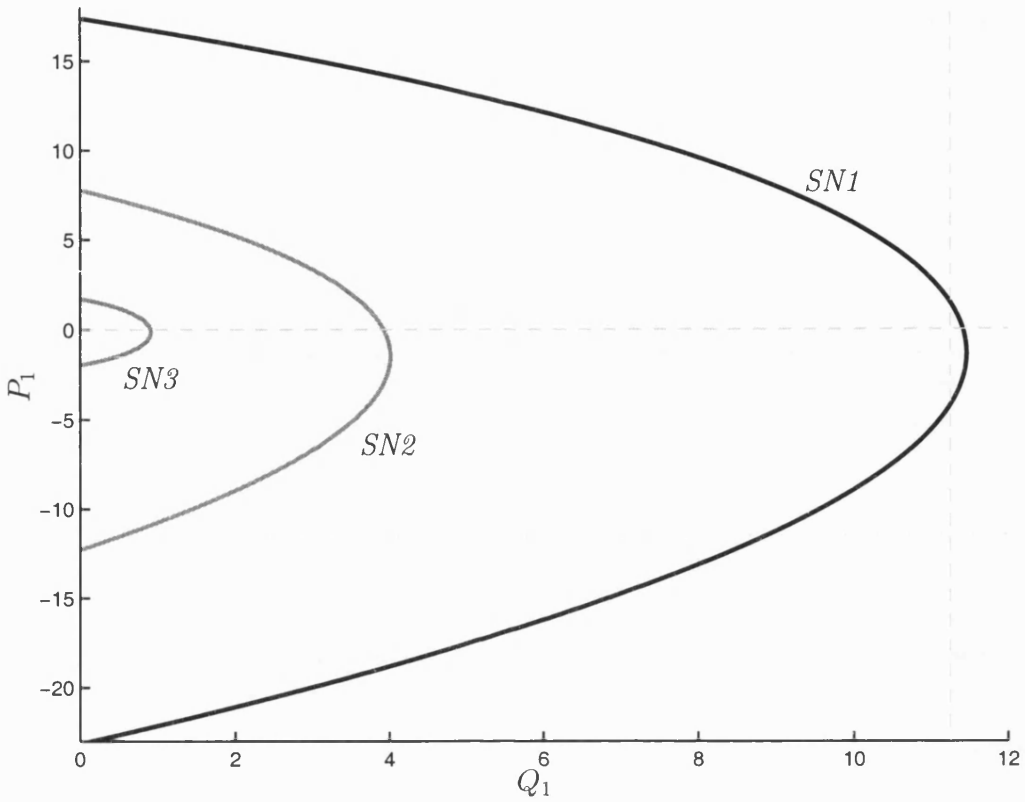

Figure 5.2: Paths of saddle-node bifurcations in 3-Bus model, in P_1–Q_1 parameter plane. Dotted lines denote location of the 1-parameter Figures 4.10,4.3.

more clearly if we plot and enlarge both paths at once, Figure 5.4.

2-D loci of the cyclic fold points

The branch of cyclic fold points which includes the point observed when (Q_1, P_1) $= (10.81766, 0)$ may be followed using the method described above yielding the curve shown in Figure 5.4. Observe that this curve exists for values of Q_1 in general rather less than the value at which Hopf bifurcation occurs, with a consequent reduction in the parameter range in which we see only a stable fixed point. The locus of the cyclic fold point intersects the locus of the Hopf points at $(Q_1, P_1) = (11.14798, 1.31408)$ – below the point of Hopf coalescence. This curve of cyclic folds is not unique; cyclic-folds associated with the Šil'nikov bifurcation are plotted in Figure 5.7.

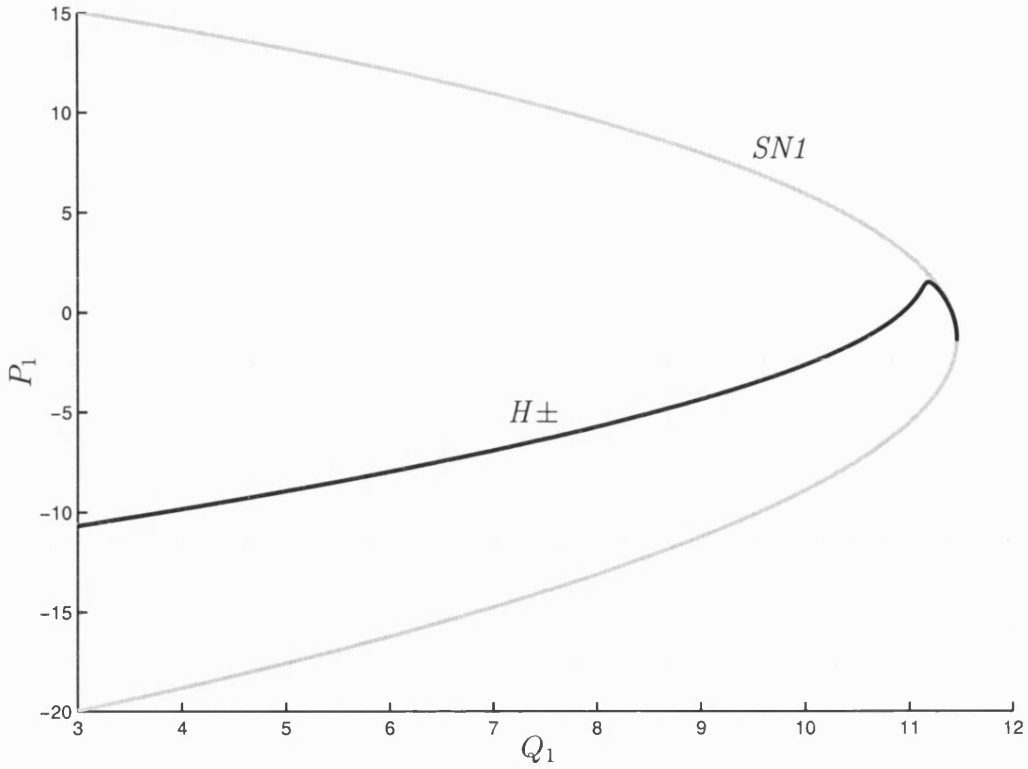

Figure 5.3: Path of Hopf bifurcations in 3-Bus model, in P_1–Q_1 parameter plane

The BT-point in the 3-bus model

The tangential intersection of the paths of saddle-node and Hopf bifurcation points gives strong evidence for the existence of a BT-point as described in the last section. The existence of this point is determined computationally by monitoring the second rightmost eigenvalue of the system Jacobian matrix as we compute the path of saddle-node bifurcations in Figure 5.2. This second eigenvalue must vanish at the BT-point; if it changes sign over two successive continuation steps then the BT-point must lie between them. To further refine the location of this point we apply the algorithm described in section 5.2.3, using one of these two saddle-node bifurcation points as an initial guess.

Applying this method to the 3-Bus system gave a BT-point at

$$(Q_1, P_1) = (11.45907, -1.41946), \tag{5.20}$$

$$(\delta_m, \omega_m, \delta, V)^T = (0.42224, 0, 0.21355, 0.93164)^T. \tag{5.21}$$

The corresponding eigenvalues of the system at this point are $0, 0, -3.059$ and -41.955. Observe that two of these are real and negative and have no effect on the

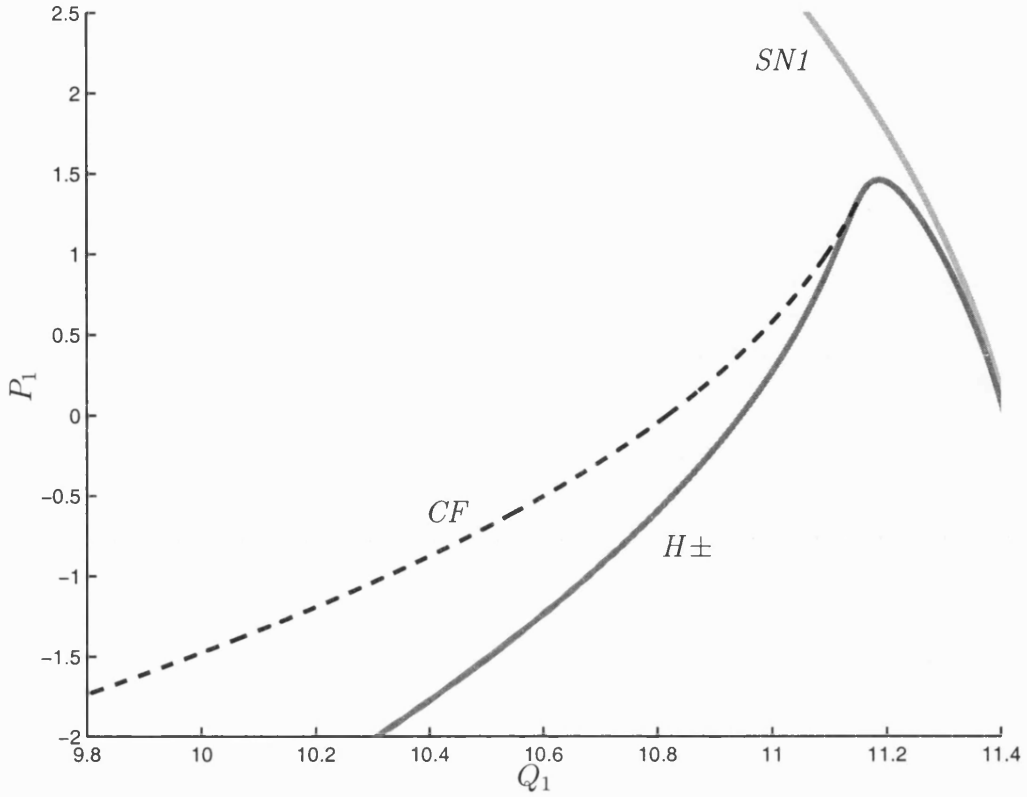

Figure 5.4: Path of cyclic folds in 3-Bus model, in P_1–Q_1 parameter plane

dynamics, merely indicating the rate of convergence onto the centre-manifold of the BT-point. The BT-point now acts as an organising centre for paths of saddle-node bifurcations, Hopf bifurcations, period doubling bifurcations and homoclinic orbits.

5.3.2 Homoclinic orbits

The theory discussed earlier ensures the existence of a path of homoclinic orbits in P_1–Q_1 parameter space starting at the BT-point. Each such homoclinic orbit contains an unstable fixed point.

The method described in Section 5.2.4 was tried for (4.5) but failed in practice. It may be that the initial guess for the homoclinic orbit was not sufficiently precise; this may be due to the linearisation at the BT-point only being valid very close to that point.

An alternative procedure, which did work, was to approximate the path of homoclinic orbits by a path of high period periodic orbits (e.g. period $T^* = 200$). To determine such an orbit, the path of periodic orbits created in a Hopf

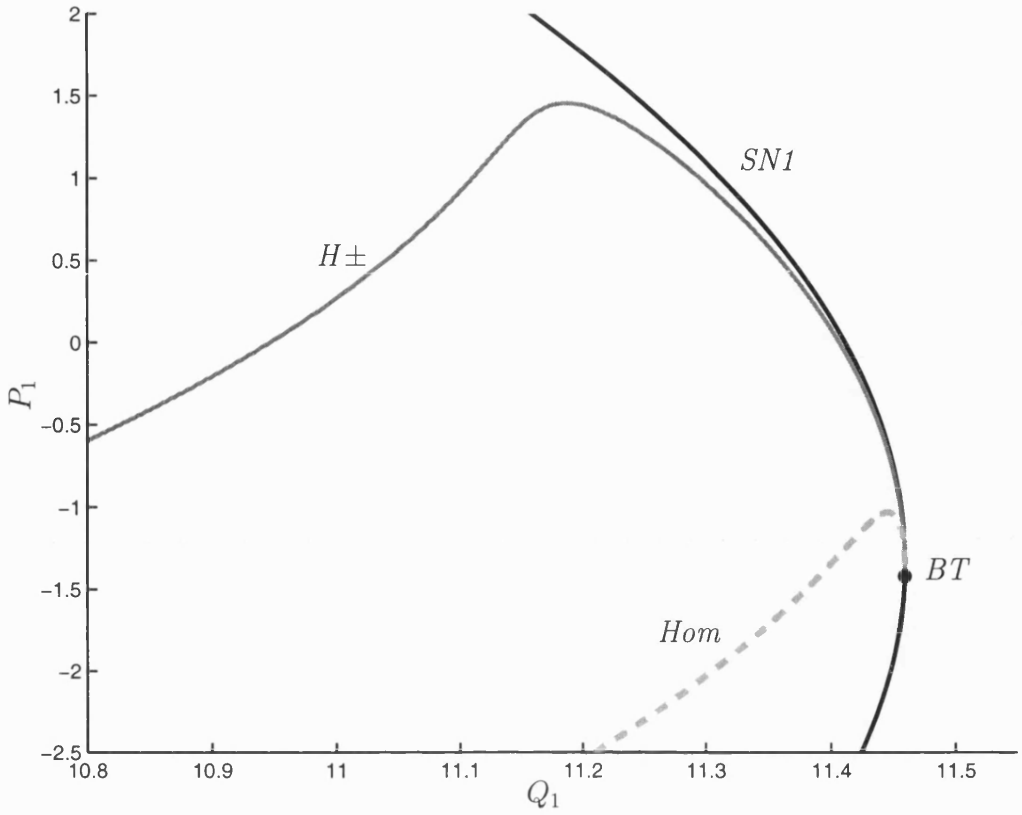

Figure 5.5: 2-D bifurcation diagram for 3-Bus model, in P_1–Q_1 parameter plane, including BT-point.

bifurcation at $P_1 = -1.31329$ and $Q_1 = 11.45918$ was followed as P_1 was varied until the orbit had a period T^*. The locus of the period T^* orbit was then followed as P_1 and Q_1 were varied. The resulting curve in parameter space of these high period points is then shown in Figure 5.5. Note the qualitative similarity between this figure and the Figure 5.1

The resulting computed curve is clearly tangent to the curve of Hopf and Saddle-node points at the BT-point. Furthermore, the curve has a high curvature at this point. This curvature indicates that the normal form will only be an accurate reduction of (4.5) very close to the BT-point and this explains the difficulties with the first procedure for calculating the homoclinic orbits.

We illustrate the above calculation by giving the trajectory of the resulting high period orbit in the two cases of $(Q_1, P_1) = (11.45916, -1.33260)$ which is close to the BT-point and $(Q_1, P_1) = (11.43866, -1.05069)$ which is rather more distant (Figure 5.6). Observe the change in the qualitative form of the orbit in these two cases.

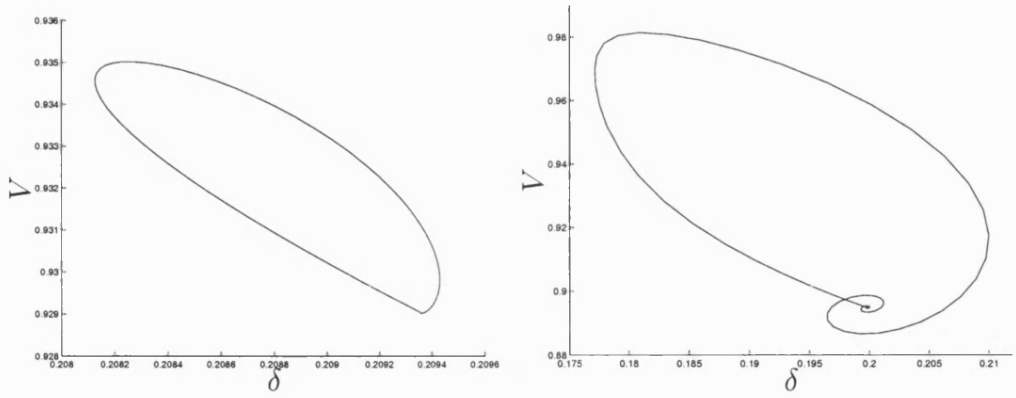

(a) (b)

Figure 5.6: Approximate homoclinic orbits (a) close to, and (b) slightly away from the BT-point

In a comprehensive new figure (Figure 5.7) we plot all these loci. This gives what we believe is a complete picture of the structure of the bifurcations in the two parameter space. This picture is likely to be similar in any related power system models with a BT-point and an associated Šil'nikov bifurcation. Note that the locus of cyclic folds $CF2$ is not the only such locus associated with the Šil'nikov bifurcation. Paths can be plotted of the other cyclic folds shown in Figure 4.11 and these will lie within Regions 5 and 6

5.4 Implications of results of 2-parameter analysis on basin erosion

5.4.1 Basin erosion

When considering the possibility of a systems such as the 3-Bus model (4.5) starting from a *general* initial condition and potentially exhibiting voltage collapse, we are interested in the basins of attraction for the attractors of that system. These are the sets of initial state values for which the corresponding trajectories have the property that they converge to the stable fixed point, or to a stable periodic orbit, or to a chaotic orbit (and are thus bounded). These basins are strongly parameter dependent. It is well known that even for very simple dynamical systems the boundaries of these basins may be highly complicated, even fractal [102]. For calculations of safety margins and for avoiding voltage collapse we must find how these basins change in size and/or form as parameters change,

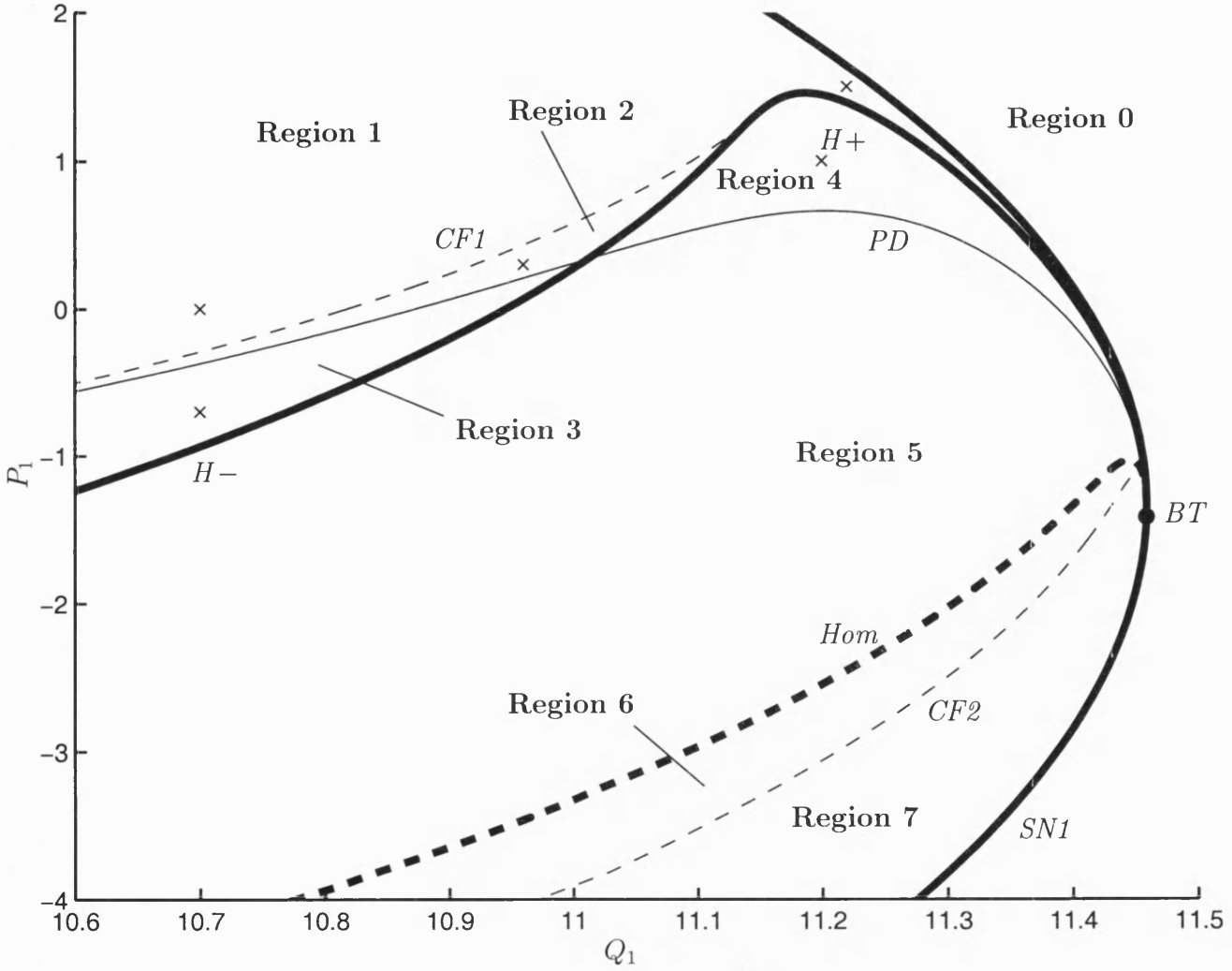

Figure 5.7: Full 2-d bifurcation diagram

particularly as we approach bifurcation points.

From an engineering perspective, the calculation of these basins will give information as to what perturbations away from the stable fixed point are permissible (i.e. the trajectory returns to the desired operating point) and which are not permissible (i.e. convergence to some other attractor, or voltage collapse).

In practice we cannot investigate the whole of phase space, and so we must pick a bounded subset to use as our region of investigation for studies of basins of attraction.

Review of methods – Lyapunov functions, cell mapping and manifold estimation

Various methods exist for estimating basins of attraction. A widely used method (Section 3.4.3) is the construction of a Lyapunov (or "energy") function for the system; trajectories starting from points where this function is concave will converge to the stable point about which the function is constructed. Hence the boundary of the region of concavity of the Lyapunov function is an estimate of the boundary of the basin of attraction.

There are two reasons why this approach has not been followed here. Firstly, although such functions have been constructed successfully for a wide class of power system models [3, 66, 70], it is not clear how to construct a Lyapunov function for the four-dimensional system (4.5) with the dynamical load model of the type we consider necessary for proper understanding of the voltage collapse problem.

Secondly, and more importantly, the Lyapunov function method will only give a subset of the basin of attraction. There may be points outside the region of concavity which have trajectories that converge to the attractor. If the basin boundary is highly structured (e.g. fractal, or if there are multiple attractors) the Lyapunov estimate may be very bad indeed. It is also not known precisely whether the Lyapunov function gives a good indication of the change in the basin as parameters vary.

A second widely used class of methods for calculation of basins of attraction are the cell mapping methods introduced by Hsu [103, 104, 105] and developed by others [106, 107]. These methods avoid the calculation of long time trajectories by dividing the region of investigation into a number of discrete "cells". A short trajectory starting at each cell is calculated to give a discrete mapping from each cell to another. The cell mappings are then combined and analysed in various manners to give a full picture of the long time trajectory behaviour of the system

and hence the basins of attraction. These methods are extremely useful for low dimensional systems. However, the calculation of the mapping from cell to cell does not scale well to dimensions greater than 3; although some initial results using these methods on the 3-Bus system were encouraging, we wished to use a method which is applicable to larger systems.

A third method of investigation of the basins of attraction is the calculation of stable manifolds of the fixed points and periodic orbits of the system. These manifolds will act as boundaries between basins of attraction. A number of efficient and general numerical methods have been proposed for such calculations [90, and references therein]. Although these methods generalise theoretically to high dimensional systems, like the cell mapping methods they are not currently practical for systems with dimension greater than 3 or 4.

Monte Carlo methods

We may randomly select a finite number of starting points within our region of investigation. We can then use a numerical procedure to calculate the trajectories starting from these points, over a suitably long time interval, and examine whether they lead to an attractor or to collapse. This method has been used with success in [108] to determine a wide variety of the possible dynamics in a dynamical system, some of which were not found by path following methods.

This method has several benefits. It is easy to adjust the accuracy of the method by simply changing the number of initial points, the error tolerance of the integration routine and the time-period of the total integration. This allows a preliminary investigation at low tolerance; subsequent calculations can be performed at higher accuracy once regions of interest have been identified. The method is adaptable to systems of higher dimension and of arbitrary structure – we may select an integration routine which most efficiently calculates trajectories for that particular problem. The method is simple to code and to use. Although this is a rather brute force approach to basin calculation, the continuing rapid fall in the cost of computational capacity makes this method viable as an experimental tool and perhaps an industrial one also.

This method can be thought of as the analogy for continuous systems of the iterative methods used to calculate fractal Julia sets.

Some care must be taken in the choice of integration routine used. The computed trajectories are only estimates of those in the real system, but we desire them to have the same qualitative behaviour; that is we wish the numerical schemes, considered as discrete dynamical systems to "shadow" the underlying

continuous system. It has been proved that several commonly used integration methods do not have this property [109]. To guarantee proper qualitative results, for DAE systems and stiff systems such as power system models, we must use methods such as backwards differentiation – even though they may be more computationally expensive.

For the results below, integration was initially performed using the RK-2(3) solver with adaptive step-sizing, which is a default method in Matlab. However, the step-sizes used by this explicit method were too small to be efficient for the long time-period calculations necessary; in addition the step-size selection algorithm created quite obvious errors and discontinuities, probably related to the stiffness of the system (4.5). As an alternative, the implicit second order method TR-BDF2 [110] was used with much greater success.

5.5 The implications of the bifurcation diagram on the system dynamics

The significance of the previous calculations is that we can use bifurcation information to divide up parameter space into different regions where we expect to see contrasting dynamical behaviour. This allows us to estimate which parameter regions are likely to be dangerous from a point of view of voltage collapse and how this might occur.

5.5.1 Interpreting the bifurcation diagram

With respect to problems such as voltage collapse, we may consider the usefulness of the bifurcation diagram in two different ways.

One interpretation is to think of the parameters as real, theoretically measurable values which change over time (but over a time scale much larger than that of individual system trajectories at a particular fixed parameter value). So considering all other parameter values as fixed, we would be interested in what happens as we move continuously through parameter space, especially in the case where we are initially at a stable steady state and then experience a bifurcation as our path through parameter space intersects a path of bifurcation points of this fixed point.

Alternatively we can think of the parameters as being fixed and use the bifurcation diagram to explain the behaviour of the system at those fixed parameter values, in terms of the dynamical objects (e.g. stable and unstable fixed points,

periodic orbits and homoclinic orbits) that the bifurcation diagram tells us may occur at that point. This could be useful if we assume the system at this parameter value to model the behaviour of power system *after* a fault or a disturbance. In this post-fault or post-disturbance case we would not assume that we were at a stable fixed point, but instead we would be interested in what might happen to a general trajectory starting at some point in phase space.

The first interpretation would be useful for real-time monitoring of a system, the second for predicting and analysing the behaviour of a proposed system. The two interpretations are not entirely distinct.

5.5.2 Parameters for trajectory and Monte Carlo computation

The following results were each computed in Matlab using the method described in Section 5.4.1. 8000 initial conditions were used from the range $(\delta_m^0, \omega^0, \delta^0, V^0) \in [-\pi, \pi] \times [-2, 2] \times [-\pi, \pi] \times [0, 2.5]$. The TR-BDF2 method used a relative tolerance of 10^{-3} and an absolute tolerance of 10^{-5}. Trajectories were said to have escaped (voltage collapse) and integration halted if $(\delta_m, \omega, \delta, V)(t) \notin [\delta_m^0 - 2\pi, \delta_m^0 + 2\pi] \times [-2.5, 2.5] \times [\delta^0 - 2\pi, \delta^0 + 2\pi] \times [0, 3.5]$. Here we are not allowing phase changes at load or generator of more than 2π, or allowing negative voltage magnitude – this would be too physically unrealistic. Calculation of trajectories was halted after 100 seconds (or after 50,000 steps), at which time the trajectory was assumed to have converged sufficiently close to an attractor.

These parameters constitute a reasonable trade off between accuracy and speed. More initial points, smaller tolerances, longer integration time and a less naive definition of "attracted" would give more accurate results, but the method would be less useful as an experimental tool. In particular it has been noted [32] that in the presence of periodic and chaotic attractors, the time to collapse may be atypically long. Our observations confirm this and so we suggest use of longer integration time as a way of improving the results rather than more points or better tolerances.

5.5.3 Dynamics for regions in the 2-D bifurcation diagram

We take each region in Figure 5.7 in turn and discuss the likely dynamics and their practical implications. Where applicable we include time series plots of typical trajectories.

Region 0.

Outside the region bounded by 2-parameter path of the primary saddle-node point. There are no known stable (fixed point or periodic) solutions in this region and all trajectories experience voltage collapse.

Region 1.

This region is characterised by reasonably low values of the parameter Q_1, the existence of a stable steady state at a higher (physically realistic) voltage, and an odd number of unstable steady states at a lower (physically unrealistic) voltage.

Some parameter values in this region (i.e. $P_1 < 0$) may be less physically valid than others, but as a whole this parameter region can be thought of as being operationally "safe". The degree of this safety depends on the proximity to the paths of bifurcation points.

For investigation of basins of attraction in this region, we choose four typical parameter values $(Q_1, P_1) = (0, 0)$, $(5, 0)$, $(7.5, 0)$ and $(11.22, 1.5)$; recall that the primary saddle-node bifurcation occurs at $(Q_1, P_1) = (11.41146, 0)$. The results are plotted in Figures 5.8, 5.9, 5.10 and 5.12 respectively. Recall that the only physically realistic attractor in this parameter region is the stable fixed point. All trajectories not leading to this point diverge to ∞ (voltage collapse).

Each shows the randomly chosen initial values $(\delta_m^0, \omega^0, \delta^0, V^0)$ projected onto the planes (δ_m, ω) (plane of generator variables) and (δ, V) (plane of load variables). The values are colour coded depending on whether they lead to the stable fixed point (black) or lead to collapse (yellow). We also plot on each graph the stable (red diamond) and unstable (red square) fixed points for that parameter value.

The first three of these figures show that there is a clear reduction of in the size of the basin of attraction as the reactive power increases towards the value at which Hopf and saddle-node bifurcations occur (but still remains some distance from paths of such points). We may also see that the basin boundary suggested by these computations does not have the hyper-spherical structure as might be suggested by some Lyapunov functions. Instead, there are points inside the basin of attraction (especially in the δ direction) which lie a long way from the stable fixed point.

In Figure 5.11 we plot some typical attracted and collapsing trajectories at these three parameter values.

Figure 5.12 show the basin computations at a point $(Q_1, P_1) = (11.22, 1.5)$

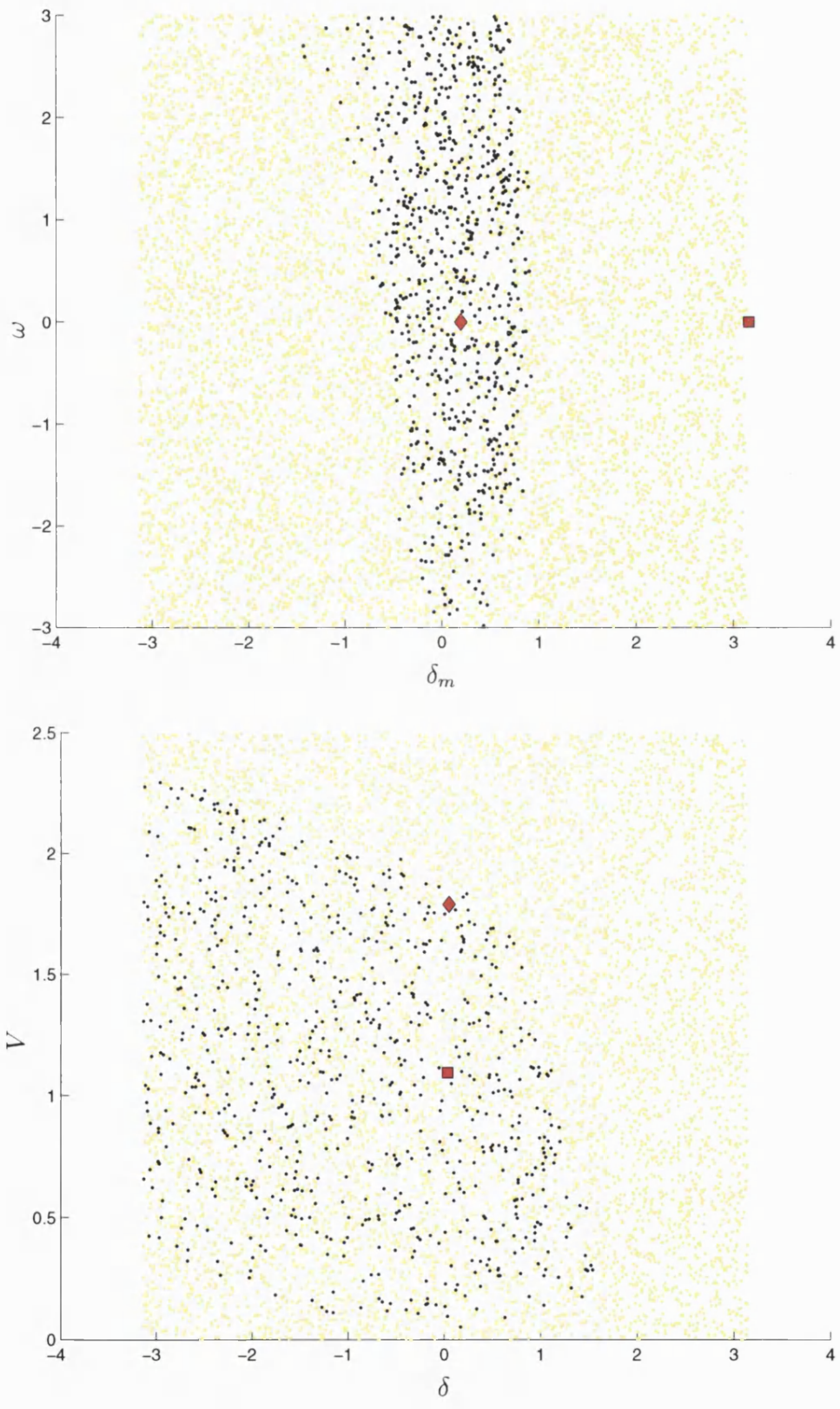

Figure 5.8: Basin investigation results, $(Q_1, P_1) = (0, 0)$

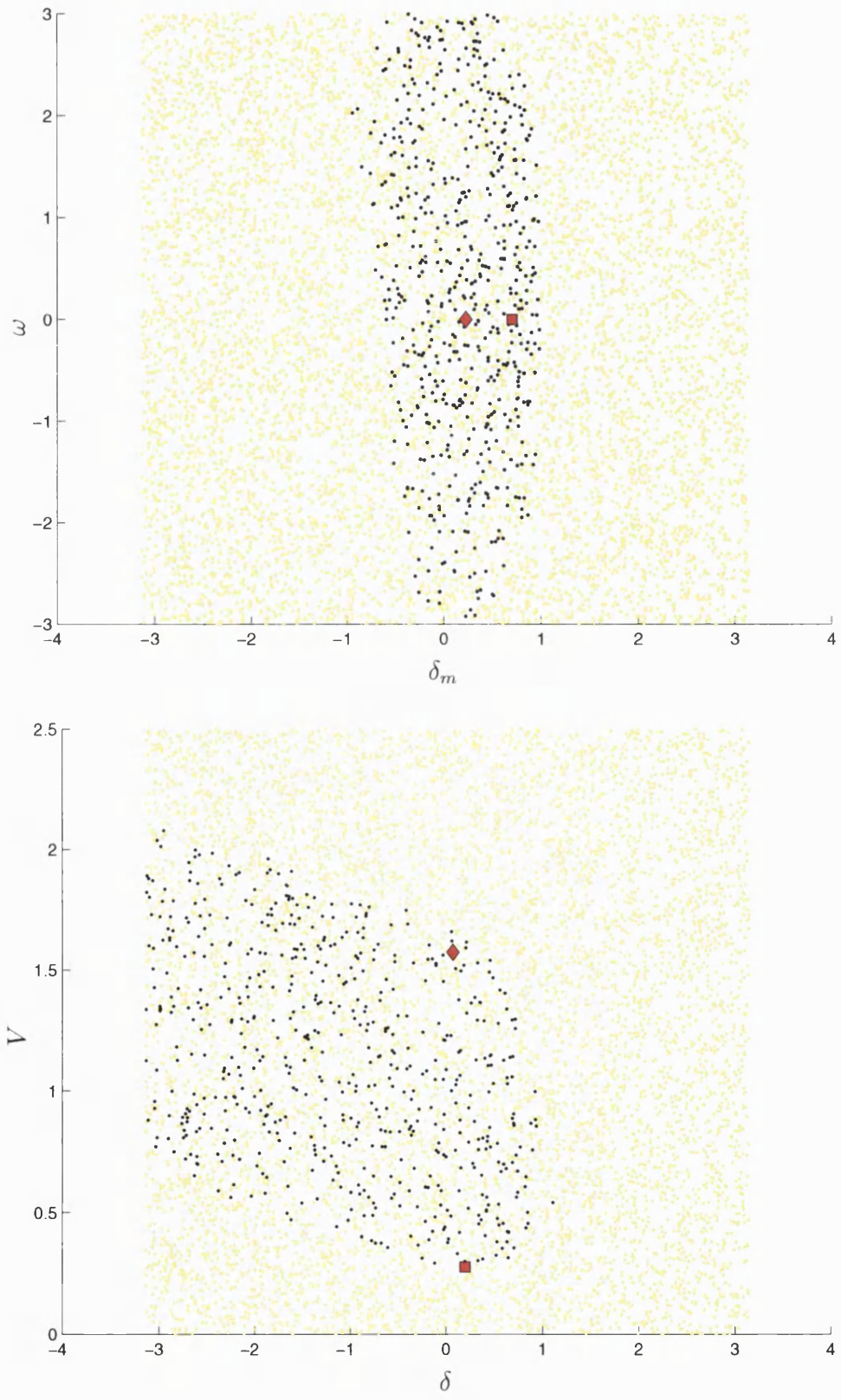

Figure 5.9: Basin investigation results, $(Q_1, P_1) = (5, 0)$

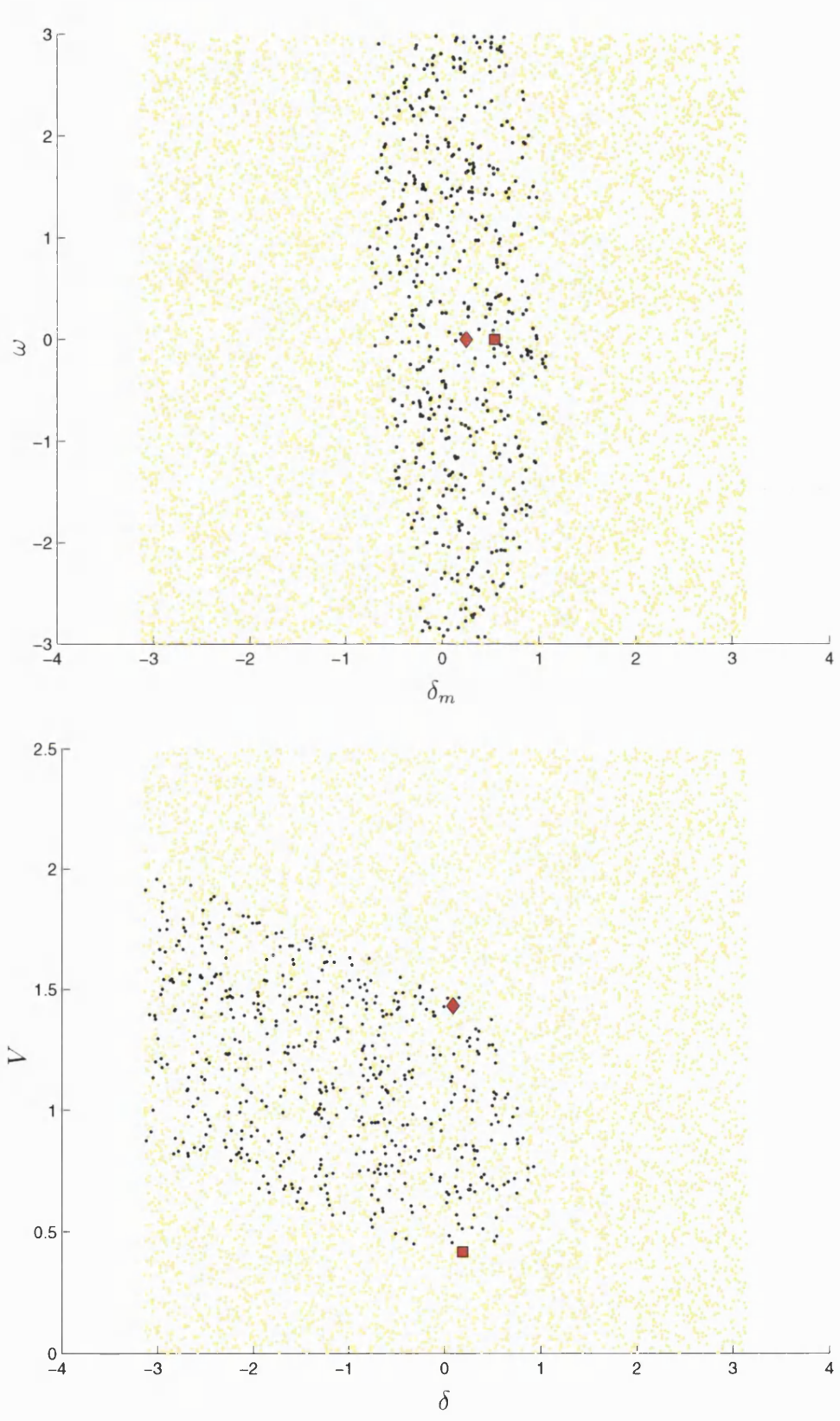

Figure 5.10: Basin investigation results, $(Q_1, P_1) = (7.5, 0)$

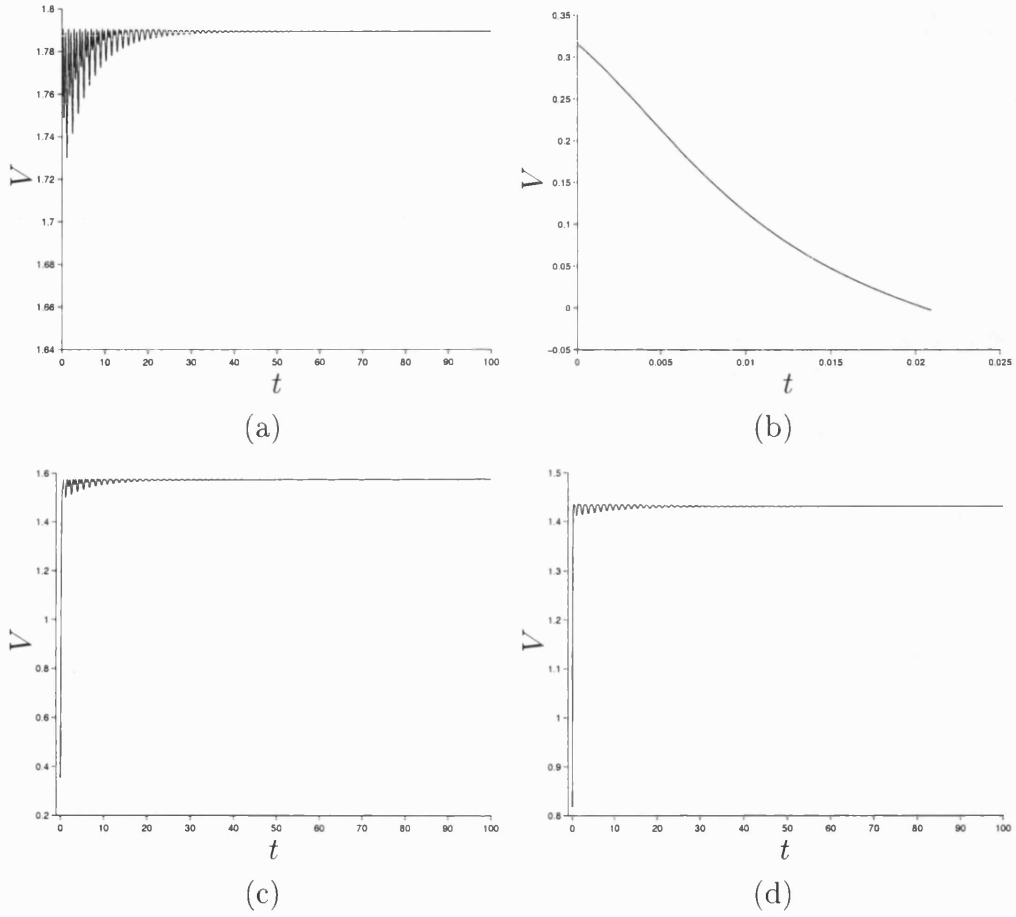

Figure 5.11: Typical trajectories, (a,b) $(Q_1, P_1) = (0, 0)$, (c) $(Q_1, P_1) = (5, 0)$, (d) $(Q_1, P_1) = (7.5, 0)$

close to both the path of Hopf bifurcations and the path of saddle-node points. There are very few points attracted to the stable fixed point. The closeness of this parameter value to the bifurcation points means that the basin of attraction for the operating point has all but disappeared.

Region 2.

The region is bounded by a path of cyclic folds $CF1$ (i.e. limit points on paths of periodic orbits), a path of sub-critical Hopf bifurcations $H-$, and a path of period doublings PD.

In this region there exist multiple stable states – a stable steady state and a stable periodic orbit. There are also unstable periodic orbits and unstable fixed points. If a disturbance were to occur, it would be possible for the trajectory to be attracted to the stable periodic orbit. The resulting oscillatory behaviour may lead to some form of collapse or shutdown.

We plot the basin computation for the parameter value $(Q_1, P_1) = (10.96, 0.3)$ in Figure 5.13. Some sample trajectories at this parameter value, Figure 5.14 clearly show attraction to both the stable fixed point and to the stable periodic orbit, depending on the initial condition.

Region 3.

This region bounded by the path of Hopf bifurcations $H\pm$ and period doublings. PD There are stable periodic orbits and unstable fixed points in this region, but no stable fixed points. The absence of period doublings in this region excludes the possibility of cascades to chaotic behaviour. Basin computations for this region (Figure 5.15) show that the basin of attraction of the periodic orbits is likely to be extremely small.

We plot a typical periodic orbit in Figure 5.16.

Region 4.

A path of sub-critical Hopf bifurcations $H-$ and a path of period doubling bifurcations PD bound the points in this region.

Both stable fixed points and stable (period doubled) periodic orbits are present at some parameter values in this region. (The period doubling path is of period doublings of the stable periodics emanating from the cyclic fold $CF1$, not from the sub-critical Hopf points $H-$). In some parts of this region there may exist further period doublings and cascades of such leading to chaos. There also

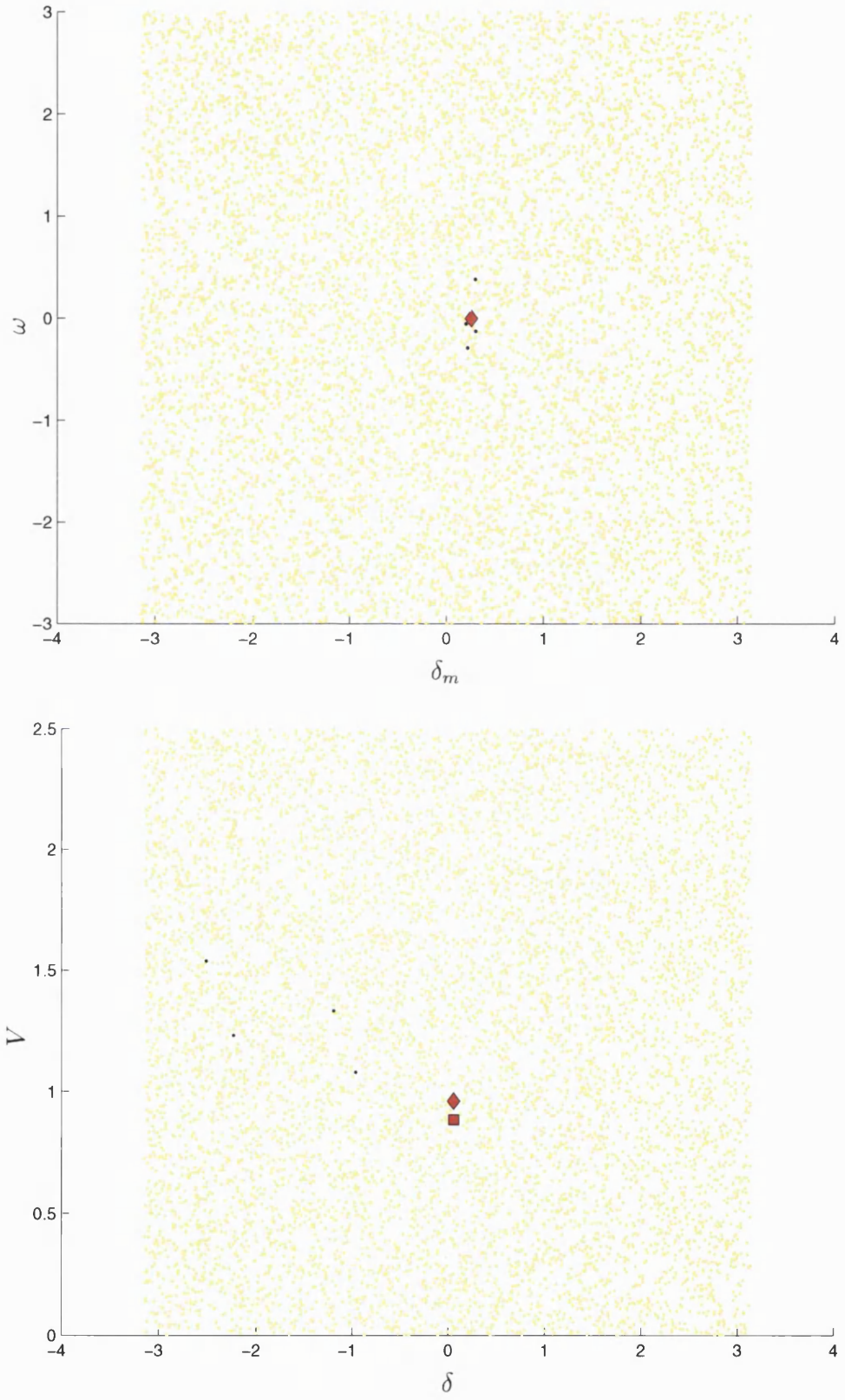

Figure 5.12: Basin investigation results, $(Q_1, P_1) = (11.22, 1.5)$

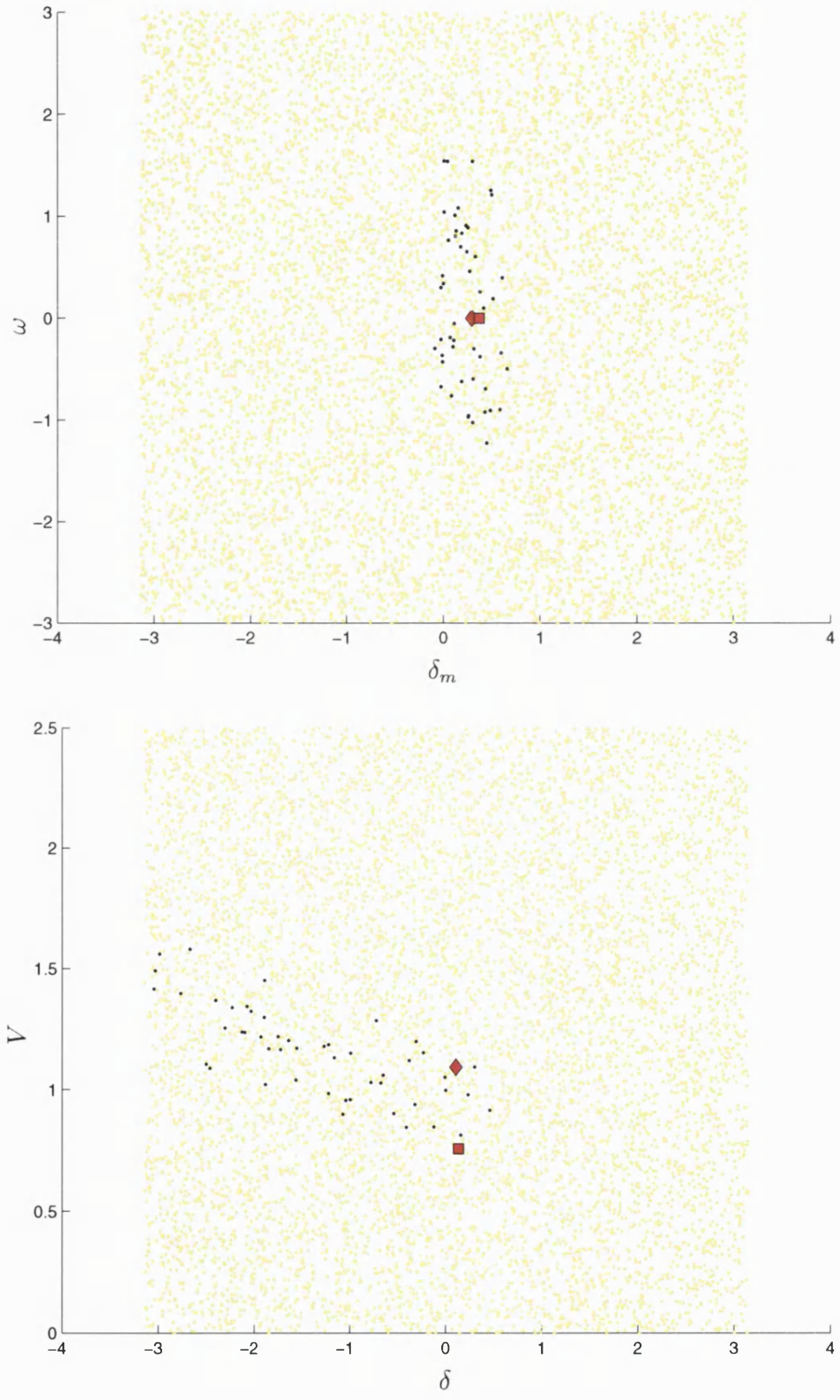

Figure 5.13: Basin investigation results, $(Q_1, P_1) = (10.96, 0.3)$

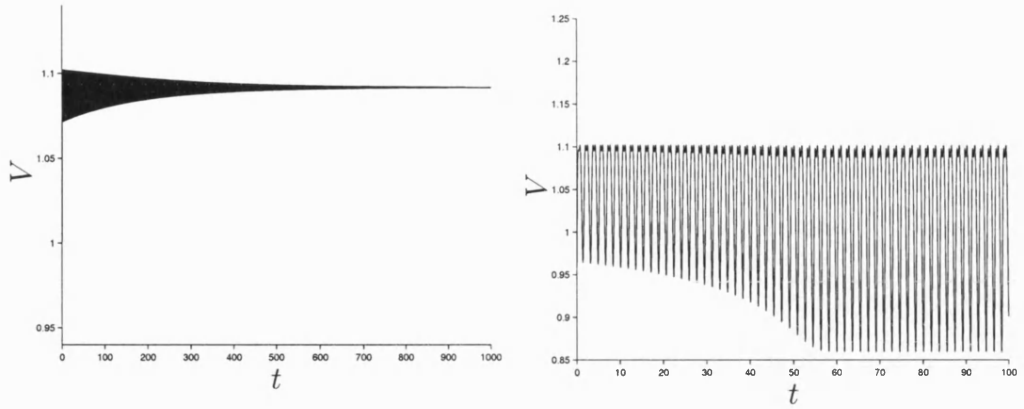

(a) (b)

Figure 5.14: Typical trajectories at $(Q_1, P_1) = (5, 0)$, (a) attracted to fixed point, (b) attracted to periodic orbit.

exist boundary crises of periodic orbits, also leading to loss of stability.

Region 5.

No stable fixed points exist in this region, since we have greater values of Q_1 than at the path $H-$ of sub-critical Hopf points.

This region will contain all manner of periodic orbits (stable and unstable), chaotic orbits, possible boundary crises and double pulse homoclinic orbits, as shown in Figures 4.9 and 4.12. We would expect voltage collapse to be the dominant behaviour in this parameter region.

Since much of this region lies well into the "physically realistic" $P_1 > 0$ region, we would want to avoid it as an operating region.

Region 6.

This region lies between the path of homoclinic orbits *Hom* emanating from the BT-point and the path of the first cyclic folds $CF2$ relating to the Šil'nikov behaviour. It contains an infinite number of periodic orbits and no stable fixed points. Any initial conditions will be attracted either to a periodic orbit or strange attractor, or to infinity (voltage collapse) and so this would not be a sensible parameter range in which to operate the system.

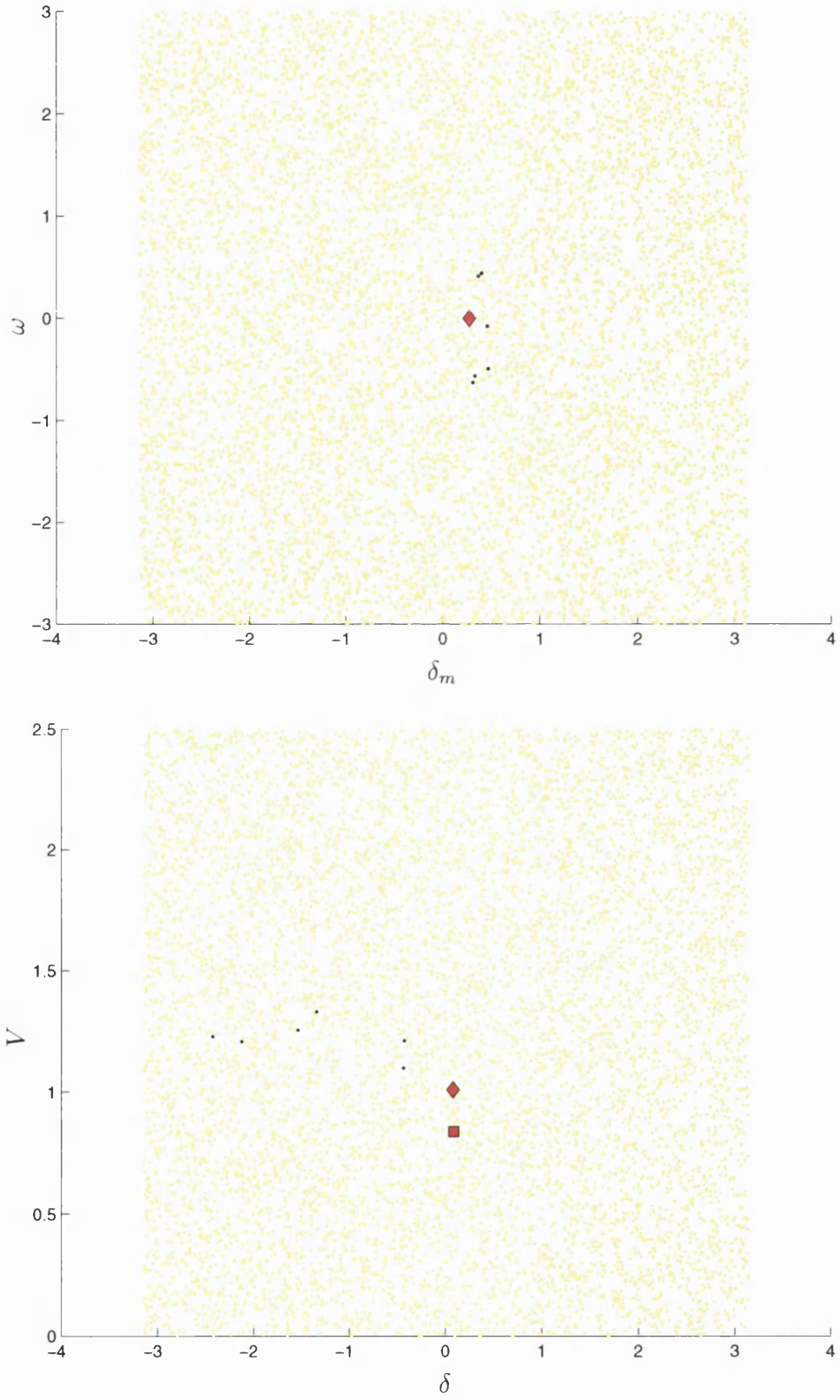

Figure 5.15: Basin investigation results, $(Q_1, P_1) = (11.2, 1.0)$

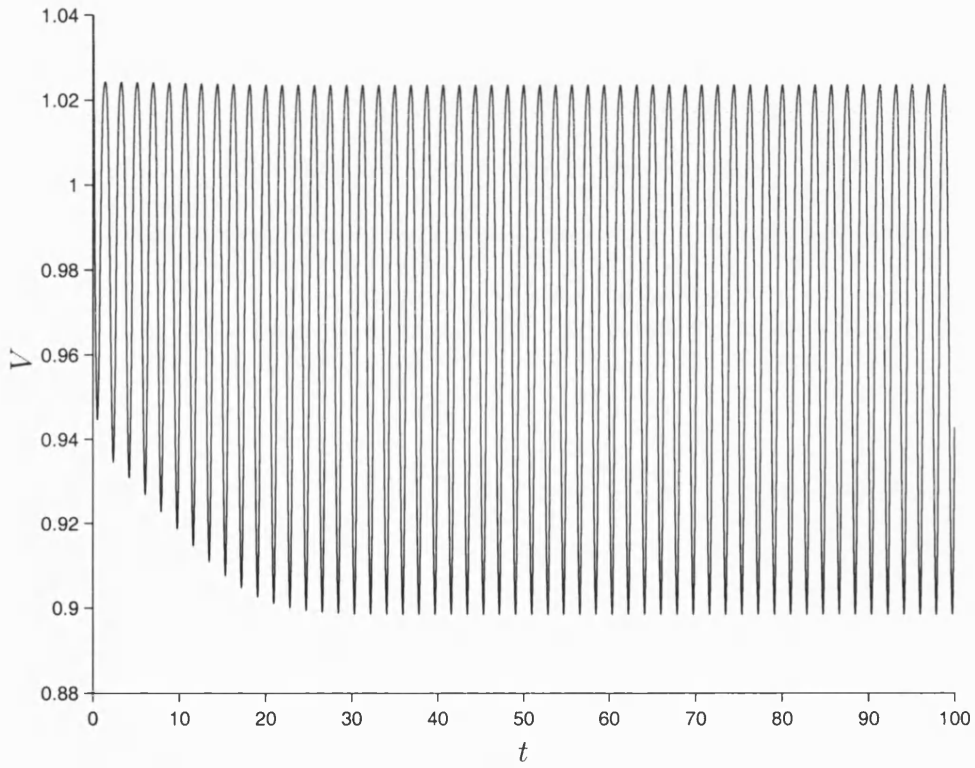

Figure 5.16: Periodic Orbit, $(Q_1, P_1) = (11.2, 1.0)$

Region 7.

There is no known stable behaviour or any periodic behaviour (unstable or homoclinic) in this region.

5.6 Conclusions

5.6.1 General

We have demonstrated that the dynamics of a simple power system model (4.5) may be investigated with reference to a co-dimension 2 Bogdanov-Takens point. This acts as an organising centre for the 2-parameter paths of saddle-node, Hopf and homoclinic bifurcations. The homoclinic orbits can be of Šil'nikov type, leading to multiple periodic and chaotic orbits.

This bifurcation information can then be used to guide an fuller investigation of the 2-parameter dynamics of the model; allowing us to predict the dynamics occurring in different regions. We have shown that significant reductions in the size of basins of attractions of stable fixed points may occur well before actual bifurcation takes place.

We have discussed the numerical methods used for this analysis, allowing for its application to larger problems. The power system models clearly have a rich dynamical structure; investigation of this is of interest to both mathematician and power engineer. In the next chapter we make further investigation, along similar lines, of a larger (hence more physically realistic) system. This will demonstrate that the methods used are practical for bigger systems and that the results for those systems are also highly useful.

5.6.2 Monte-Carlo method

There is scope for refinement of the Monte-Carlo method used to investigate the basins of attraction of the 3-Bus model. One might define hypersheres of varying sizes centered around the attractors and analyse the proportion of initial conditions in each sphere that are attracted. In this way some statistical information about the shrinkage of the basin boundaries might be determined without explicit calculation of the boundaries themselves. In addition, the range from which initial conditions are chosen could be adapted according to the estimated size of the basin, in order to give better representation of the basin as it shrinks. These refinements could be carried out using the 3-Bus model, or some other dynamical

system with better known properties.

Chapter 6

The M4B6 Model

6.1 Introduction

In this chapter we introduce and investigate another power system model, the M4B6 model. This consists of 6 buses, 4 of which are "machines" (generators), with the remaining two buses being loads. This model is similar in concept to the 3-Bus model discussed in previous chapters, but is of increased complexity. We present a full derivation of the model, with reference to our earlier discussion of power system modelling. Some consideration is given to the implementation of the model, and the ways in which this generalises to larger complex power systems. We apply the same methods to the model as used in previous chapters and present some results. In particular we also identify a BT-point in this model.

6.2 The model

6.2.1 Motivation

We will firstly describe a general model and then proceed to describe a particular configuration motivated by real-world data. This is to demonstrate that the model is not dependent on any particular network configuration or set of parameters, and to allow easy implementation by others and extension to even higher dimensional models. As for the 3-Bus model, we can divide the general system into load, network and generation, and the models we use for each are directly motivated by the component models in the 3-Bus system.

The data used for the implementation of the M4B6 system is a simplified representation of the power network in North Wales with connections to the rest of the England & Wales network and to the Scottish network.

North Wales is of particular economic and practical importance to the operation of the UK grid, due to the location there of the two large pumped storage facilities at Dinorwig and Ffestiniog. These hydro-electric facilities use surplus power at off-peak times to pump water into a high level reservoir. At times of high demand this water can be released and used to generate power. These generators are exceptional in that they can achieve full generating capacity in less than 16 seconds [111], a fact which can be crucial in using the power available from pumped storage to help remedy problems elsewhere in the network. They can also be started without needing a supply of power from elsewhere in the network, a fact which could be crucial after a widespread voltage collapse incident.

The data used for the M4B6 model has been used for testing and development of computational analysis techniques by a number of authors [88, 112], and so seemed a sensible choice to further test the methods presented above.

6.2.2 Equations and reduction to ODE

We first consider a general network with $M+1$ generator buses and N load buses. We will then present the network configuration and the parameters that constitute the M4B6 model. This allows us to make some interesting points about the implementation of models of this type and to demonstrate the applicability of the methods to a class of models – not just to one or two special cases.

In implementing this model, careful attention must be paid to the numbering of variables and parameters. Because the of the division of the model into load, generator and network, we need separate but related indices that number each load bus, each generator bus and each dynamical variable. We will use superscripted indices to indicate numbering of variables and parameters at each load bus or at each generator bus, and subscripts to denote indexing of vectors (e.g. for vectors of dynamical variables).

First define the state vector

$$\mathbf{x} = \Big(\underbrace{\delta_m^1, \ldots, \delta_m^M}_{(a)}, \underbrace{\omega^1, \ldots, \omega^M}_{(b)}, \underbrace{\delta^1, \ldots, \delta^N}_{(c)}, \underbrace{V^1, \ldots, V^N}_{(d)} \Big)^T \tag{6.1}$$

composed of (a) the generator phase angles, (b) the generator relative frequencies, (c) the load phase angles and (d) the load voltages.

Generators

We need to choose one generator to measure the other angles against, so without loss of generality we set $\delta_0 = 0$. This generator then becomes a "slack bus" representing the "rest of the network" in a geographically reduced model.

We model the other generators, $i = 1, \ldots, M$, using the "swing" equation (see Chapter 2, Section 2.3). Assuming constant mechanical power input and constant voltage output, at each generator bus i we have

$$M^i \dot{\omega}^i = P_m^i - P_e^i - d_m^i \omega^i \tag{6.2}$$

$$\dot{\delta}_m^i = \omega^i \tag{6.3}$$

Loads

Loads are modelled at each load bus $i = 1, \ldots, N$ using the empirical induction motor load of [8] in parallel with a constant P-Q load (see Chapter 2, Section 2.5). This is

$$P_l^i = P_0^i + P_1^i + K_{p\omega}^i \dot{\delta}^i + K_{pV}^i (V^i + T^i \dot{V}^i) \tag{6.4}$$

$$Q_l^i = Q_0^i + Q_1^i + K_{q\omega}^i \dot{\delta}^i + K_{qV}^i V^i + K_{qV2}^i V^{i2} \tag{6.5}$$

Network

Lines are modelled using the standard π representation (see [36] and Chapter 2, Section 2.4). At each bus the real and reactive powers from generation, load and network injection must balance, giving us two constraint equations for each bus.

For ease of definition of the network power injections, it helps to define vectors of voltages and phase angles at *every* bus. These are

$$\hat{\mathbf{V}} = \Big(\underbrace{V_m^1, \ldots, V_m^M}_{(e)}, \underbrace{V^1, \ldots, V^N}_{(f)}, \underbrace{V_m^0}_{(g)} \Big)^T \tag{6.6}$$

composed of (e) the voltage output parameters for each generator, (f) the voltage variables at each load, (g) the voltage parameter at the slack bus; and

$$\hat{\boldsymbol{\delta}} = \Big(\underbrace{\delta_m^1, \ldots, \delta_m^M}_{(h)}, \underbrace{\delta^1, \ldots, \delta^N}_{(i)}, \underbrace{\delta_m^0}_{(j)} \Big)^T \tag{6.7}$$

composed of (h) the phase variables at each generator, (i) the phase variables at each load and (j) the phase parameter at the slack bus.

Note that these vectors consist of a mixture of dynamical variables and parameters.

Let $c(i)$ be the set of buses connected directly to bus i, for $i = 1, \ldots, (N+M+1)$. A bus is not considered to be connected to itself, so $i \notin c(i)$ or equivalently $G_{ii} = B_{ii} = B_{Sii} = 0$.

Now we may define the real and reactive power injections from the network into each bus i for $i = 1, \ldots, (M+N+1)$, i.e. every bus, including the slack bus,

$$P_{net}(\mathbf{x})_i = \begin{pmatrix} (\hat{V}_i)^2 \sum_{k \in c(i)} G_{ik} \\ -\hat{V}_i \sum_{k \in c(i)} \hat{V}_k \left(G_{ik} \cos(\hat{\delta}_i - \hat{\delta}_k) + B_{ik} \sin(\hat{\delta}_i - \hat{\delta}_k) \right) \end{pmatrix} \tag{6.8}$$

$$Q_{net}(\mathbf{x})_i = \begin{pmatrix} -\hat{V}_i^2 \left(B_{S,i} + \sum_{k \in c(i)} (B_{S,ik} + B_{ik}) \right) \\ -\hat{V}_i \sum_{k \in c(i)} \hat{V}_k \left(G_{ik} \sin(\hat{\delta}_i - \hat{\delta}_k) - B_{ik} \cos(\hat{\delta}_i - \hat{\delta}_k) \right) \end{pmatrix} \tag{6.9}$$

Then we may write

$$P_e(\mathbf{x})^n = +P_{net}(\mathbf{x})_n \qquad n = 1, \ldots, M \tag{6.10}$$

$$Q_l(\mathbf{x})^n = -Q_{net}(\mathbf{x})_{(n+M)} \qquad n = 1, \ldots, N \tag{6.11}$$

$$P_l(\mathbf{x})^n = -P_{net}(\mathbf{x})_{(n+M)} \qquad n = 1, \ldots, N \tag{6.12}$$

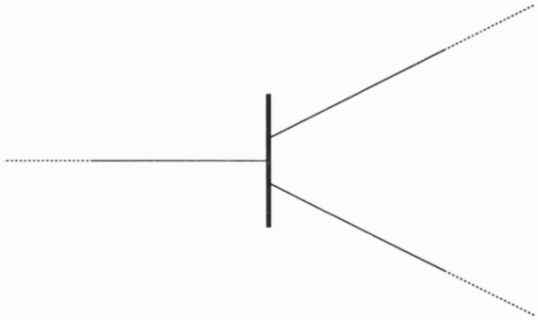

Figure 6.1: A trivial example of a bus acting as a junction (no load or generator)

Vector field

These definitions may now be combined to give the vector field $\dot{\mathbf{x}} = \mathbf{f}(\mathbf{x})$, where

$$f_i(\mathbf{x}) = \begin{cases} \omega^n, & \begin{array}{r} \text{for } i = 1, \ldots, M \\ \text{where } n = i \end{array} \\ \frac{1}{M^n}\left(P_m^n - P_e(\mathbf{x})^n - d_m^n \omega^n\right), & \begin{array}{r} \text{for } i = (M+1), \ldots, 2M \\ \text{where } n = i - M = 1, \ldots, M \end{array} \\ \frac{1}{K_{q\omega}^n}\left(Q_l(\mathbf{x})^n - Q_0^n - Q_1^n - K_{qv}^n V^n - K_{qv2}^n (V^n)^2\right), & \begin{array}{r} \text{for } i = (2M+1), \ldots, (2M+N) \\ \text{where } n = i - 2M = 1, \ldots, N \end{array} \\ \frac{1}{T^n K_{pV}^n}\left(P_l(\mathbf{x})^n - P_0^n - P_1^n - K_{pv}^n V^n - K_{p\omega}^n f_{i-N}(\mathbf{x})\right), & \begin{array}{r} \text{for } i = (2M+N+1), \ldots, 2M+2N \\ \text{where } n = i - (2M+N) = 1, \ldots, N \end{array} \end{cases} \tag{6.13}$$

for $i = 1, \ldots, 2(M+N)$.

Reduction of the DAE to an ODE

In a general power system model we cannot assume that all buses are either generator or load buses. There may be buses of a third type which are merely junctions within the network (Figure 6.1).

At each of these buses we must apply Kirchoff's law (6.8,6.9), leading to a constraint on the system. If we have P such junctions, we must consider the algebraic variables

$$\mathbf{y} = \left(\delta^1, \ldots, \delta^P, V^1, \ldots, V^P\right)^T \tag{6.14}$$

at these buses. If $\hat{\mathbf{V}}$ and $\hat{\boldsymbol{\delta}}$ are suitably extended to include the variables in $\mathbf{y}$ we can then make obvious extensions $\tilde{P}_{net}(\mathbf{x},\mathbf{y})$, $\tilde{Q}_{net}(\mathbf{x},\mathbf{y})$ and $\tilde{\mathbf{f}}(\mathbf{x},\mathbf{y})$ from (6.8,6.9,6.13). We can then write the system as an DAE

$$\begin{aligned} \dot{\mathbf{x}} &= \tilde{\mathbf{f}}(\mathbf{x},\mathbf{y}) \\ 0 &= \mathbf{g}(\mathbf{x},\mathbf{y}) \end{aligned} \tag{6.15}$$

where $\mathbf{g}(\mathbf{x},\mathbf{y})$ is defined by

$$g_i(\mathbf{x}) = \begin{cases} P_{net}(\mathbf{x})_n, & \text{for } i = 1,\ldots,P \\ & \text{where } n = i + (2M+2N+1) = \\ & (2M+2N+2),\ldots,(2M+2N+1+P) \\ Q_{net}(\mathbf{x})_n. & \text{for } i = (P+1),\ldots,2P \\ & \text{where } n = i + (2M+2N+1) - P = \\ & (2M+2N+2),\ldots,(2M+2N+1+P) \end{cases} \tag{6.16}$$

As we have mentioned above (Section 3.4.2) this DAE form in general defines a dynamical system, but leads to a substantial increase in the complexity of both the theory and the computational algorithms needed to analyse the system.

This leads us to a conclusion which is somewhat counter-intuitive from the viewpoint of an engineer. If we allow in our system buses which are simple junctions, or indeed buses which have very simple load models (such as constant loads or some other model depending on only the algebraic variables $\mathbf{y}$) then the system will be a DAE. This will have a consequential impact on the complexity of the techniques needed to analyse the system. If we have no such simple junctions and all load models involve the derivative of some or more of the variables $\mathbf{x}$, then the system will be an ODE and the much simpler investigative techniques discussed in previous chapters may be used. (It is important to note that the resulting ODE may still be stiff). Increasing the complexity of the load models makes the analysis of the entire system *easier*, not harder. This also applies to the consideration of other components such as transformers, which might be considered as a simple junction or by some algebraic form in a simple power system model, but could also be represented by a more complex dynamical model.

In the M4B6 model described below in Section 6.2.3, the physical network is simple enough not to have any junctions of the type shown in Figure 6.1 and so the whole system can be reduced to a system of ODEs.

Derivatives and matrix sparsity

In implementations of models of this type suitable for either continuation or numerical calculation of trajectories, we are likely to want an explicit representation of the Jacobian matrix

$$\mathbf{f_x} = \left\{ \frac{\partial f_i}{\partial x_j} \right\}, \qquad i,j = 1,\ldots,(2M+2N). \tag{6.17}$$

This is given in Table 6.1.

These expressions depend on the following quantities

$$\begin{aligned}
\frac{\partial P_e^n}{\partial \delta_m^{n'}} &= \frac{\partial P_{net}(\mathbf{x})_n}{\partial \hat{\delta}_{n'}}, \\
\frac{\partial P_e^n}{\partial \delta^{n'}} &= \frac{\partial P_{net}(\mathbf{x})_n}{\partial \hat{\delta}_{(n'+M)}}, \\
\frac{\partial P_e^n}{\partial V^{n'}} &= \frac{\partial P_{net}(\mathbf{x})_n}{\partial \hat{V}_{(n'+M)}}, \\
\frac{\partial Q_l^n}{\partial \delta_m^{n'}} &= -\frac{\partial Q_{net}(\mathbf{x})_{(n+M)}}{\partial \hat{\delta}_{n'}}, \\
\frac{\partial Q_l^n}{\partial \delta^{n'}} &= -\frac{\partial Q_{net}(\mathbf{x})_{(n+M)}}{\partial \hat{\delta}_{n'+M}}, \\
\frac{\partial Q_l^n}{\partial V^{n'}} &= -\frac{\partial Q_{net}(\mathbf{x})_{(n+M)}}{\partial \hat{V}_{(n'+M)}}, \\
\frac{\partial P_l^n}{\partial \delta_m^{n'}} &= -\frac{\partial P_{net}(\mathbf{x})_{(n+M)}}{\partial \hat{\delta}_{n'}}, \\
\frac{\partial P_l^n}{\partial \delta^{n'}} &= -\frac{\partial P_{net}(\mathbf{x})_{(n+M)}}{\partial \hat{\delta}_{(n'+M)}}, \\
\frac{\partial P_l^n}{\partial V^{n'}} &= -\frac{\partial P_{net}(\mathbf{x})_{(n+M)}}{\partial \hat{V}_{(n'+M)}}.
\end{aligned} \tag{6.18}$$

Global numbering (i,j)	Local numbering (n,n')	$\frac{\partial f_i}{\partial x_j}$
i=1,...,M	n=i=1,...,M	
j=1,...,(2M+2N) $j\neq i+M$		0
j=i+M		1
i=(M+1),...,2M	n=$i-M$=1,...,M	
j=1,...,M	n'=j=1,...,M	$-\frac{1}{M^n}\frac{\partial P_e^n}{\partial \delta_m^{n'}}$
j=(M+1),...,2M $j\neq i$	n'=$j-M$=1,...,M $n'\neq n$	0
j=$i-M$	n'=$j-M$=n	$-\frac{d_m^n}{M^n}$
j=(2M+1),...,(2M+N)	n'=j-2M=1,...,N	$-\frac{1}{M^n}\frac{\partial P_e^n}{\partial \delta^{n'}}$
j=(2M+N+1),...,(2M+2N)	n'=j-(2M+N)=1,...,N	$-\frac{1}{M^n}\frac{\partial P_e^n}{\partial V^{n'}}$
i=(2M+1),...,(2M+N)	n=i-2M=1,...,N	
j=1,...,M	n'=j=1,...,M	$\frac{1}{K_{q\omega}^n}\frac{\partial Q_l^n}{\partial \delta_m^{n'}}$
j=(M+1),...,2M	n'=$j-M$=1,...,M	0
j=(2M+1),...,(2M+N)	n'=j-2M=1,...,N	$\frac{1}{K_{q\omega}^n}\frac{\partial Q_l^n}{\partial \delta^{n'}}$
j=(2M+N+1),...,(2M+2N) $j\neq i+N$	n'=j-(2M+N)=1,...,N $n'\neq n$	$\frac{1}{K_{q\omega}^n}\frac{\partial Q_l^n}{\partial V^{n'}}$
j=i+N	n'=n	$\frac{1}{K_{q\omega}^n}\begin{pmatrix}\frac{\partial Q_l^n}{\partial V^n}-K_{qv}^n\\ -2K_{qv2}^n V^n\end{pmatrix}$
i=(2M+N+1),...,(2M+2N)	n=i-(2M+N)=1,...,N	
j=1,...,M	n'=j=1,...,M	$\frac{1}{T^n K_{PV}^n}\left(\frac{\partial P_l^n}{\partial \delta_m^{n'}}-\frac{K_{p\omega}^n}{K_{q\omega}^n}\frac{\partial Q_l^n}{\partial \delta_m^{n'}}\right)$
j=M+1,...,2M	n'=$j-M$=1,...,M	0
j=2M+1,...,2M+N	n'=j-2M=1,...,N	$\frac{1}{T^n K_{PV}^n}\left(\frac{\partial P_l^n}{\partial \delta^{n'}}-\frac{K_{p\omega}^n}{K_{q\omega}^n}\frac{\partial Q_l^n}{\partial \delta^{n'}}\right)$
j=2M+N+1,...,2M+2N $j\neq i$	n'=j-(2M+N)=1,...,N $n'\neq n$	$\frac{1}{T^n K_{PV}^n}\left(\frac{\partial P_l^n}{\partial V^{n'}}-\frac{K_{p\omega}^n}{K_{q\omega}^n}\frac{\partial Q_l^n}{\partial V^{n'}}\right)$
j=i	n'=n	$\frac{1}{T^n K_{PV}^n}\begin{pmatrix}\frac{\partial P_l^n}{\partial V^n}-K_{pv}^n\\ -\frac{K_{p\omega}^n}{K_{q\omega}^n}\left(\frac{\partial Q_l^n}{\partial V^n}\quad\cdots\right.\\ \left.-2K_{qv2}^n V^n-K_{qv}^n\right)\end{pmatrix}$

Table 6.1: 1st derivatives of M4B6 type model

These are in turn given by the following

$$\frac{\partial P_{net}(\mathbf{x})_i}{\partial \hat{V}_j} = \begin{cases} \left(\begin{array}{l} 2\hat{V}_i \sum\limits_{k \in c(i)} G_{ik} \\ \quad - \sum\limits_{k \in c(i)} \hat{V}_k \left(G_{ik} \cos(\hat{\delta}_i - \hat{\delta}_k) + B_{ik} \sin(\hat{\delta}_i - \hat{\delta}_k) \right) \end{array} \right) & j = i \\ -\hat{V}_i \left(G_{ij} \cos(\hat{\delta}_i - \hat{\delta}_j) + B_{ij} \sin(\hat{\delta}_i - \hat{\delta}_j) \right) & j \in c(i) \\ 0 & j \notin c(i) \end{cases} \tag{6.19}$$

$$\frac{\partial P_{net}(\mathbf{x})_i}{\partial \hat{\delta}_j} = \begin{cases} \hat{V}_i \sum\limits_{k \in c(i)} \hat{V}_k \left(G_{ik} \sin(\hat{\delta}_i - \hat{\delta}_k) - B_{ik} \cos(\hat{\delta}_i - \hat{\delta}_k) \right) & j = i \\ -\hat{V}_i \hat{V}_j \left(G_{ij} \sin(\hat{\delta}_i - \hat{\delta}_j) - B_{ij} \cos(\hat{\delta}_i - \hat{\delta}_j) \right) & j \in c(i) \\ 0 & j \notin c(i) \end{cases} \tag{6.20}$$

$$\frac{\partial Q_{net}(\mathbf{x})_i}{\partial \hat{V}_j} = \begin{cases} \left(\begin{array}{l} -2\hat{V}_i \left(B_{S,i} + \sum\limits_{k \in c(i)} (B_{S,ik} + B_{ik}) \right) \\ \quad - \sum\limits_{k \in c(i)} \hat{V}_k \left(G_{ik} \sin(\hat{\delta}_i - \hat{\delta}_k) - B_{ik} \cos(\hat{\delta}_i - \hat{\delta}_k) \right) \end{array} \right) & j = i \\ -\hat{V}_i \left(G_{ij} \sin(\hat{\delta}_i - \hat{\delta}_j) - B_{ij} \cos(\hat{\delta}_i - \hat{\delta}_j) \right) & j \in c(i) \\ 0 & j \notin c(i) \end{cases} \tag{6.21}$$

$$\frac{\partial Q_{net}(\mathbf{x})_i}{\partial \hat{\delta}_j} = \begin{cases} -\hat{V}_i \sum\limits_{k \in c(i)} \hat{V}_k \left(G_{ik} \cos(\hat{\delta}_i - \hat{\delta}_k) + B_{ik} \sin(\hat{\delta}_i - \hat{\delta}_k) \right) & j = i \\ \hat{V}_i \hat{V}_j \left(G_{ij} \cos(\hat{\delta}_i - \hat{\delta}_j) + B_{ij} \sin(\hat{\delta}_i - \hat{\delta}_j) \right) & j \in c(i) \\ 0 & j \notin c(i) \end{cases} \tag{6.22}$$

Note that many elements of $\mathbf{f_x}$ are zero. In fact this matrix is even sparser

than might first appear from Table 6.1 since there exists a sparsity in the Jacobian of the physical network upon which it depends – for example $\partial P_{net}(\mathbf{x})_i/\partial\hat{\delta}_j = 0$ if $j \notin c(i)$.

We can quantify the number of non-zero elements in $\mathbf{f_x}$ in terms of N, M and the size of the sets $c(i)$. $\mathbf{f_x}$ has $4M^2 + 8MN + 4N^2$ entries. Table 6.1 shows that $M^2 + 2M + 4MN + 4N^2$ of these are potentially non-zero and so the matrix would appear to be fairly full if M and N are large. However, all but M of these entries depend on network terms, and thus on the sparsity of the network Jacobians (6.19-6.22).

The sparsity of the network matrices can be examined as follows. Suppose each bus i is connected to an average of p other buses. Each network Jacobian has $(M+N+1)^2$ entries, $(p+1)^2$ of which are non-zero. The value of p is dependent on the number of buses geographically close to each bus and is typically much smaller than M and N (the total number of buses of each type). Without actually proving the independence of p from M and N, it is clear that the average number of buses adjacent to any given bus does not increase appreciably as we add extra buses to the system (at least not until an finite area approaches physical saturation with buses!). Hence the number of non-zero entries in each network Jacobian (and hence in $\mathbf{f_x}$) is small, and remains fairly constant with respect to increases in M and N. This holds independently of the particular dynamical models used for the loads and generators, the variables for which are truly local to that component.

Note that we know the sparsity of $\mathbf{f_x}$ *a priori*. We know the network configuration, as represented in the sets $c(i)$; this governs the coupling in the system. So in the assembly of Jacobian matrices we only have to set up the constant values (zero or non-zero) once. We know in advance which values are not constant (with respect to state variables or continuation parameters) and we can calculate these each time the matrix is assembled.

Contrast this with the large sparse matrices typically appearing in the numerical solutions of physical problems from mechanics or from fluid dynamics. The sparsity structure of these matrices depends crucially on the specific discretisation used. For example, in the case of finite element discretisation using simple basis functions with compact support, matrix entry (i, j) will be non-zero if element i is adjacent to element j. Either we must check all (i, j) pairs for adjacency of elements at each assembly of the Jacobian, or we must store and keep track of information about which elements are adjacent. In practical implementations this is non-trivial, especially if we are using such techniques as automatic grid generation, adaptive meshing or multi-grid schemes.

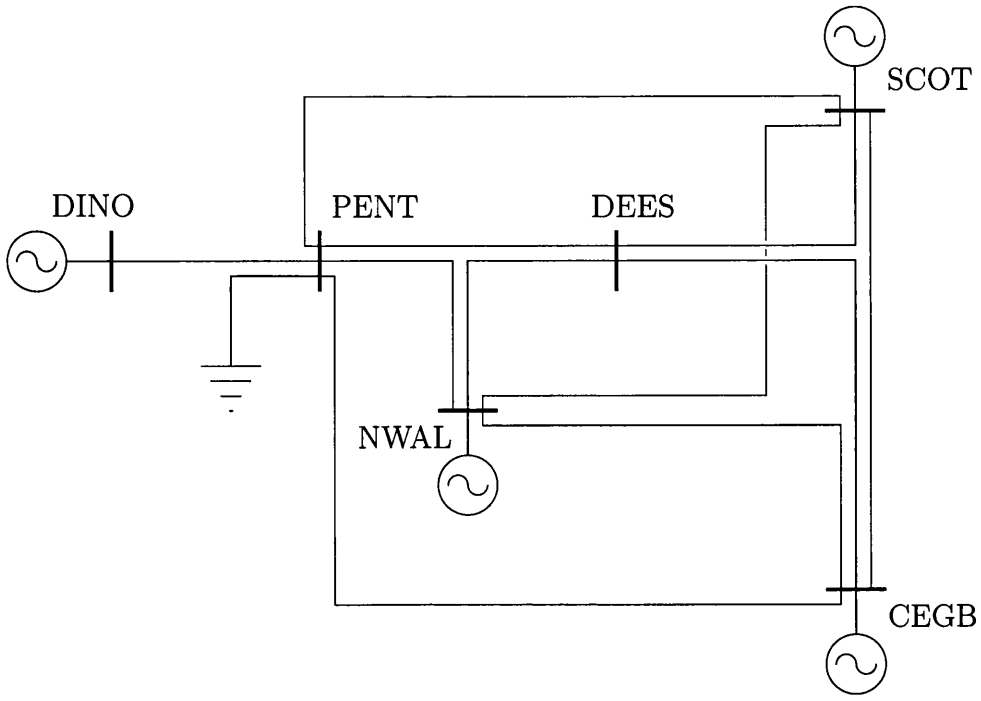

Figure 6.2: Network diagram for the M4B6 model

The second derivatives of $\mathbf{f}$ are needed for computations relating to bifurcation points. They are computed similarly and are given for completeness in Appendix B.

6.2.3 M4B6 model specification

A circuit diagram for the M4B6 network is given in Figure 6.2.

This model consists of two types of bus-bar – 4 generator buses and two load buses. The parameters for this model are given in Appendix B.

6.3 1-parameter results

As with the 3-Bus model, we choose real and reactive load parameters to use as continuation parameters. Since the M4B6 model has two loads, we define

$$P_1^i = P_{1,0}^i + \lambda_P \Delta_i \tag{6.23}$$

$$Q_1^i = Q_{1,0}^i + \lambda_Q \Delta_i \tag{6.24}$$

where λ_P and λ_Q are the values used as continuation parameters. The normalised weighting vector Δ has elements proportional to the total load at each bus, at a

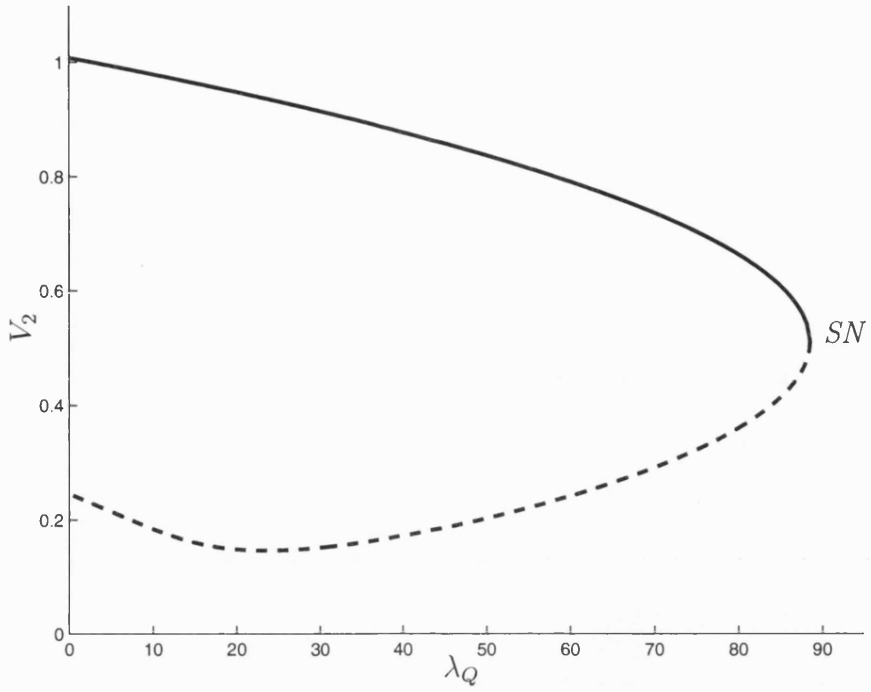

Figure 6.3: Fixed points in M4B6 model, continuation in λ_Q. ($\lambda_P = 0$)

steady state and at rated voltage $V^i = 1$; so that

$$\Delta_i = \frac{\epsilon_i}{||\epsilon||}, \text{ where } \epsilon_i = P_0^i + K_{pV}^i + Q_0^i + K_{qV}^i + K_{qV2}^i. \tag{6.25}$$

6.3.1 λ_Q continuation

Increasing the total reactive load has the effect we expect from studies from the simpler model, namely the creation of a saddle-node point at the maximum power transfer point ($\lambda_Q = 88.4826621$). This is shown in Figure 6.3. Note that at this value of active load ($\lambda_P = 0$) there are no Hopf bifurcation points.

6.3.2 λ_P continuation

Increasing the total active load also has the effect we expect. A circular path of steady states can be calculated (Figure 6.4). The stability of these operating points is lost at a saddle-node bifurcation point ($\lambda_P = 90.5182604$) and at a Hopf bifurcation point ($\lambda_P = -90.9139139$).

Similar calculations can be performed at other values of λ_Q, with similar results.

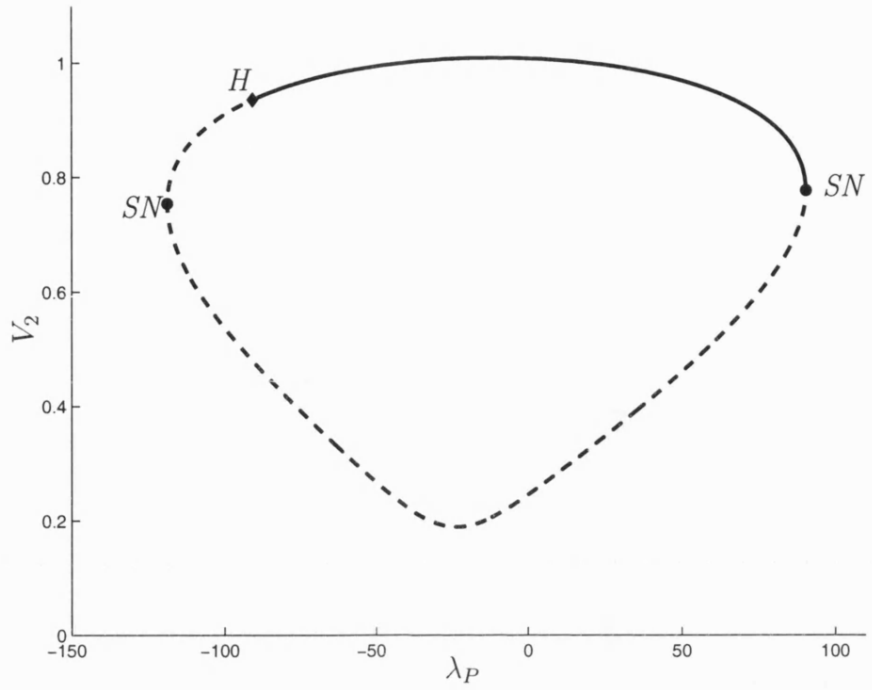

Figure 6.4: Fixed points in M4B6 model, continuation in λ_P. ($\lambda_Q = 0$)

6.4 2-parameter results

Continuation of the saddle-node points discovered in the preceeding 1-parameter investigation give results as shown in Figure 6.5.

As with the 3-Bus model, this path defines a region in parameter space outside which there are no operating states of the system (called the feasibility region by some engineers Venkatasubramanian et al. [59]). To determine which states inside this region are stable and furthermore "safe" from voltage collapse, we must perform some further analysis. Using the methods described in Chapters 4 & 5, we confirm the existence of a BT-point in the M4B6 model, occurring at

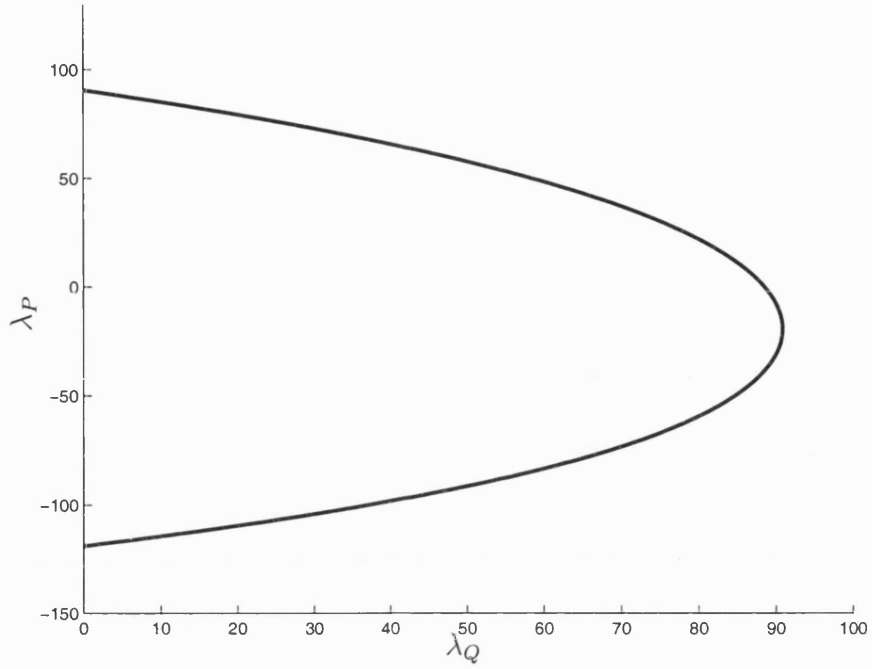

Figure 6.5: The locus of the saddle-node points in M4B6 model, 2-parameter continuation in (λ_P, λ_Q)

the following state and parameter values:

$$\begin{aligned} \lambda_Q &= 90.8667758, \\ \lambda_P &= -18.3734675, \end{aligned} \qquad \mathbf{x} = \begin{pmatrix} -0.231600447 \\ -0.050849513 \\ -0.257625742 \\ 0 \\ 0 \\ 0 \\ -0.261855035 \\ -0.310886531 \\ 0.940186181 \\ 0.497798997 \end{pmatrix}. \tag{6.26}$$

We can also perform 2-parameter continuation of Hopf bifurcations, starting from the point detected in Figure 6.4. This is shown in Figure 6.6.

Contrast these diagrams with those in Section 5.3. The paths of bifurcation points tell us that in the M4B6 model there is a much larger area of parameter space where the system is likely to be "safe" from voltage collapse.

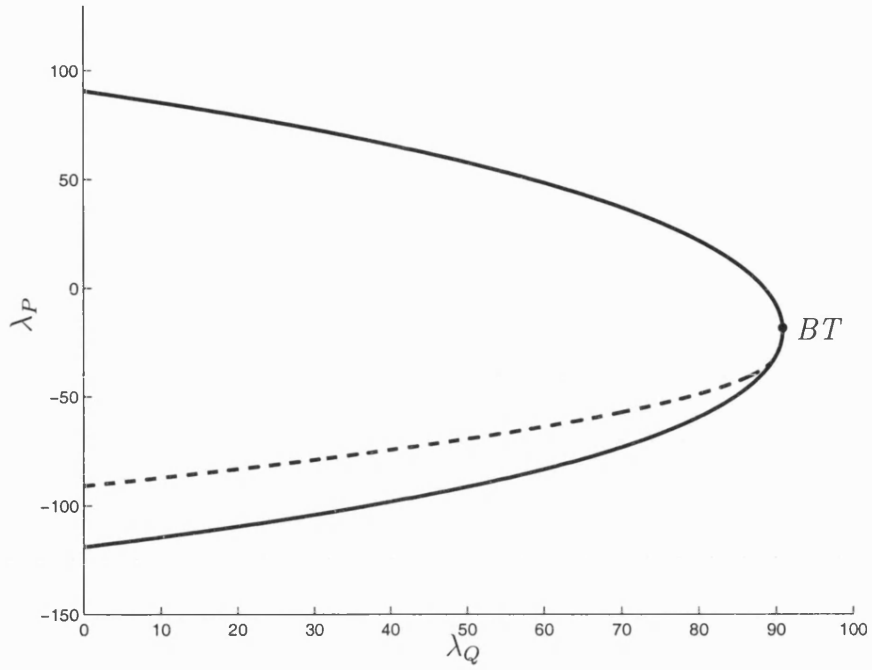

Figure 6.6: The locus of Hopf bifurcation points (dashed) in M4B6 model, 2-parameter continuation in (λ_P, λ_Q)

6.5 Basin results

As for the 3-Bus model, we can use a Monte Carlo method to investigate the effect of changing parameters on the basin of attraction of the operating point.

The following plots show the randomly chosen initial values projected onto the planes $(\delta_{m1}, \omega_1), (\delta_{m2}, \omega_2)$ (planes of generator variables) and $(\delta_1, V_1), (\delta_2, V_2)$ (planes of load variables). The values are colour coded depending on whether they lead to the stable fixed point (black) or lead to collapse (yellow). We also plot on each graph the stable fixed point for that parameter value (red diamond).

Due to the higher dimension of the M4B6 system any effect on the basin is not as easy to show graphically as for the 3-Bus model. However, as expected there is a clear decrease in the number of starting points attracted to the operating point as we move closer to the saddle-node bifurcations (Figures 6.7, 6.8, 6.9) and closer to the Hopf bifurcations (Figure 6.10).

6.6 Qualitative dynamics

The qualitative behaviour of the M4B6 system at collapse is very similar to that of the 3-Bus model.

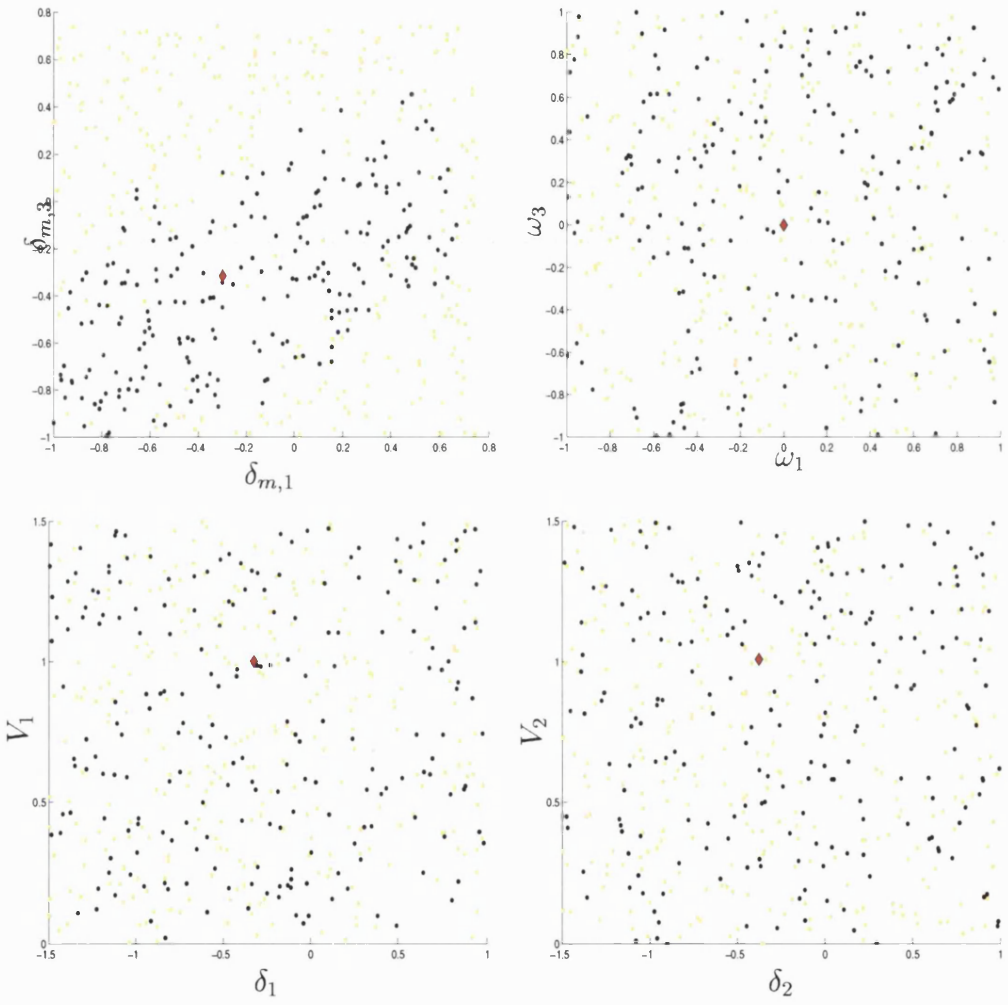

Figure 6.7: Basin investigation results, $(\lambda_P, \lambda_Q) = (0, 0)$

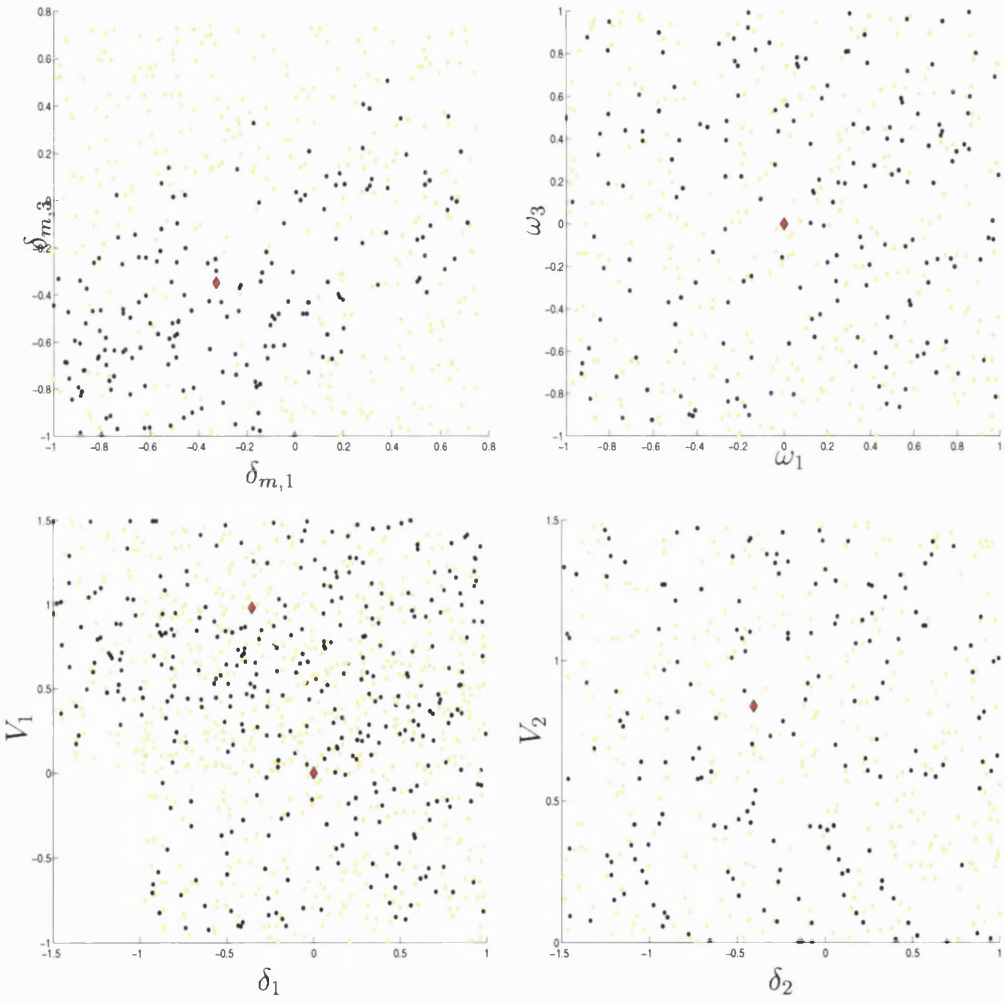

Figure 6.8: Basin investigation results, $(\lambda_P, \lambda_Q) = (0, 50.132958)$

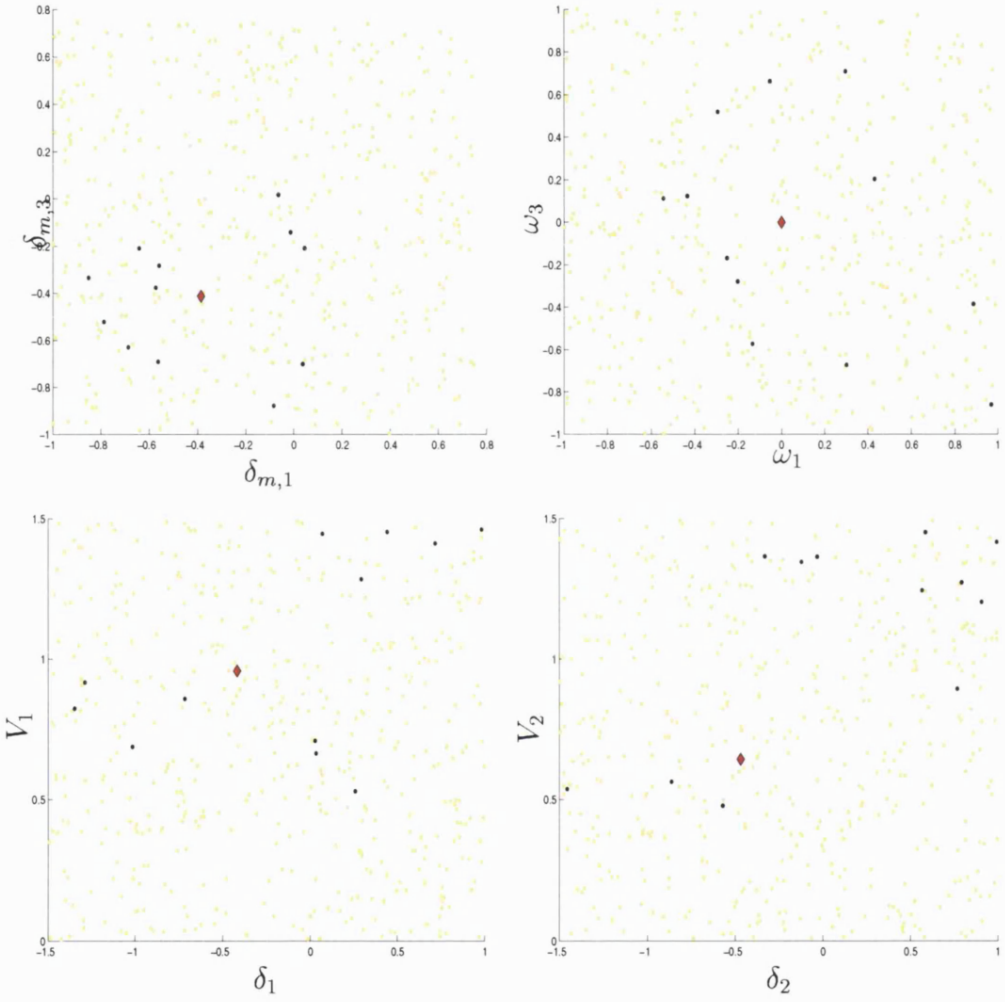

Figure 6.9: Basin investigation results, $(\lambda_P, \lambda_Q) = (0, 82.132038)$

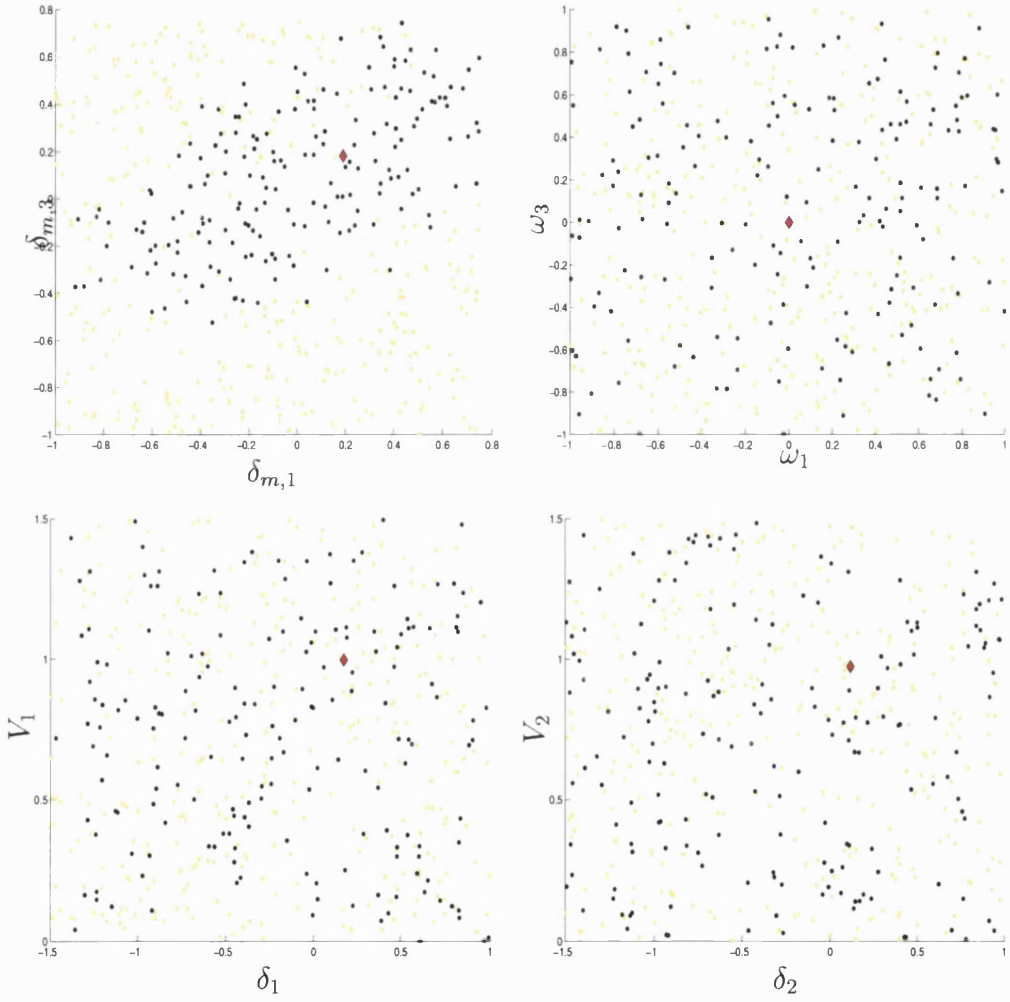

Figure 6.10: Basin investigation results, $(\lambda_P, \lambda_Q) = (-70.614982, 0)$

Figure 6.11 shows part of a typical trajectory of the system while undergoing collapse. The behaviour at the generator side is bounded and oscillatory, while the load voltage demonstrates classic finite-time blow-up behaviour. This is extremely similar to the dynamics shown in Figure 4.2.

6.7 Conclusions

The M4B6 model shares much of its dynamical behaviour with the 3-Bus model, in particular paths of saddle-node and Hopf bifurcations and a BT-point. This has the expected effect on the basins of attraction of the system, with proximity to bifurcation causing a reduction in the basin size and hence making the system more prone to collapse. As with the 3-Bus model this collapse could be triggered either by a slow change of parameters causing the operating state (fixed point) to become unstable, or by a fault causing the system state to move outside the basin of attraction of the operating state.

Further dynamical investigation of this model would be possible. However, it would be equally important to consider other models of this type, with different physical networks, generators and loads.

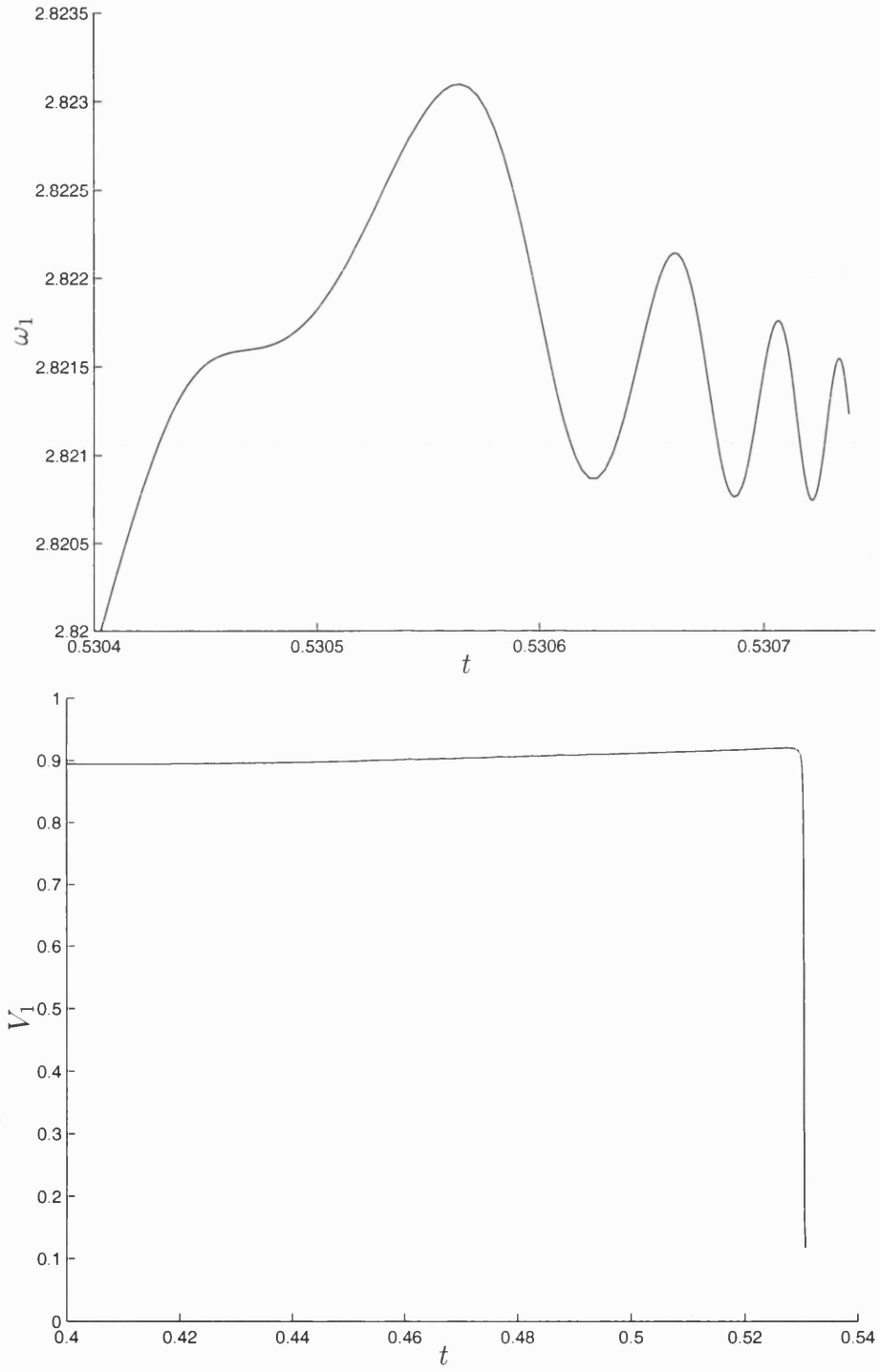

Figure 6.11: Sample collapsing trajectory (detail) $(\lambda_Q, \lambda_P) = (50.133, 0)$

Chapter 7

Conclusions

7.1 General conclusions

In this thesis we have demonstrated the applicability of a dynamical systems approach to the study of power systems models.

7.1.1 Modelling

We have considered a reduced power system model. This has proved to have a rich dynamical structure. However it is far from being what could be called a physically representative model. There exist far more detailed representations of both generator and network components. The dynamic load model used is more complex than some used by engineers for the study of the whole network, but we have shown that this can result in a simpler ODE representation of the power system, as opposed to the DAE representation used in large power system models.

7.1.2 Dynamical behaviour

The models we have examined show a wealth of dynamical behaviour. The bifurcation structure with respect to increasing system loads has been shown to be governed by a Bogdanov-Takens bifurcation point. This point can be found systematically by location and continuation of saddle-node and Hopf bifurcation points. From the BT-point we can determine a wealth of other dynamical information, both in terms of the bifurcation structure of the model and subsequently about the effect of bifurcation on the basins of attraction.

7.1.3 Algorithms

A standard pseudo-arc length continuation algorithm has been used for investigation of the steady state, periodic and bifurcation structure of the power system models. This has been broadly successful. Switching from BT-points to paths of homoclinic orbits was problematic, but alternative methods for location of the homoclinic orbits were successful once the existence of the homoclinics was determined as a consequence of the BT-point.

For calculation of trajectories in the power system models, it is clear that explicit error controlled Runge-Kutta methods do not give good results for these models, as a consequence of stiffness. Excellent results were however obtained using an implicit BDF method, the extra computational expense needed to solve the implicit system was balanced by the much increased step-sizes available.

It has been feasible to use explicitly stated functions for the derivatives of the system, with the Jacobian matrices being highly sparse. Importantly, this sparsity follows from the physical configuration of the power network and so is known *a priori*.

7.1.4 Prediction of voltage collapse

Information about the location of bifurcations and the parameter dependent behaviour of basins of attraction has allowed us to make predictions of possible mechanisms for causing voltage collapse. Collapse can not be said to be the result of one particular bifurcation or other dynamical event, but can be explained in terms of the whole dynamical structure of the model.

We have presented an asymptotic solution of a simple power system model undergoing collapse which agrees excellently with numerical results. The asymptotic solution shows voltage collapse to be a form of finite time blow-up behaviour. This blow-up only occurs in the load variables – the generator demonstrates bounded but rapid oscillatory behaviour. The identification of voltage collapse as a finite-time blow-up phenomenon has implications for the choice and implementation of numerical methods used to investigate the system. We would expect much of the asymptotic analysis to generalise to larger and more complex power system models.

7.2 Implications for power engineers

7.2.1 Modelling

We have shown that incorporation of a dynamic load model can actually make solution of the power system easier, not harder, through reduction of the general power system model from a DAE model to an ODE model (or for larger networks, at least to a DAE with lower dimensional constraints). It is often impractical in an practical engineering context to make a clear distinction between modelling and solution methods – both are just tools used as part of the engineers job of "getting an answer". However, we believe we have shown that a clear exposition of the modelling process can be practically useful, as well as being necessary when formulating the power system theoretically as a dynamical system.

7.2.2 Results

The bifurcation structure of the systems we have investigated has proven to be mathematically rich. For a variety of reasons it is unlikely that all the mathematical modes of behaviour (such as homoclinic orbits) will be directly observable in real systems.

This does not mean that the bifurcation and dynamical systems approach should be dismissed. We have shown that knowledge of the bifurcation structure of a power system gives important and useful information about its behaviour, in terms of the stability of operating points and of the size of the basins of attraction of these points (transient stability). The generation of these bifurcation diagrams is both methodologically feasible (through the location of a BT-point) and computationally feasible.

7.3 Areas for possible future research

Interesting and most likely fruitful further mathematical research could be carried out into many areas of power systems.

7.3.1 Extended models

It is clear that the models used in this thesis only go a small way to representing the behaviour of power systems in the "real-world". The basic framework we have presented could be made more accurate in two ways. Firstly the complexity with which the individual components of the system are modelled could be increased

– we have discussed some of these component models. This could include inclusion in the model of control devices, switches, transformers and even better load models. All of these models would need to be formulated rigorously and their parameters chosen to accurately reproduce observed system behaviour. Secondly, the total number of components in the system could be increased substantially.

7.3.2 Algorithm development

The algorithms used in this thesis could be developed further with application to power system models. In particular more research could be performed into the methods used to solve non-linear systems of equations arising from the study of power systems as dynamical systems. There is some existing research into the solution of such systems arising from numerical integration methods applied to power systems – for instance iterative methods for matrix inversion, or methods that use a physical decomposition of the network to perform a decomposition of the mathematical problem. These could be adapted and applied to the continuation problems studied here. Or a different approach could be taken using, for instance, a recursive projection method.

7.3.3 Expert system

We have shown that a number of features of the behaviour of power system models can be understood in terms of a number of different types of bifurcation points interacting with each other. One could imagine that similar investigations could be performed algorithmically and automatically by an expert system, applied to a large but well defined class of models. This would require further development of numerical algorithms, along with an exhaustive investigation of exactly which bifurcations occur in more realistic systems and their effects on system behaviour such as voltage collapse. This could provide an valuable tool for power systems research.

Appendix A

Collocation Method Decomposition

A.1 Fixed period

Let

$$X = \begin{pmatrix} \mathbf{x}_1 \\ \mathbf{f}_{11} \\ \vdots \\ \mathbf{f}_{1k} \\ \mathbf{x}_2 \\ \mathbf{f}_{21} \\ \vdots \\ \mathbf{f}_{2k} \\ \vdots \\ \vdots \\ \mathbf{x}_N \\ \mathbf{f}_{N1} \\ \vdots \\ \mathbf{f}_{Nk} \\ \mathbf{x}_{N+1} \end{pmatrix}, \qquad F(X) = \begin{pmatrix} \mathbf{r}_1 \\ \mathbf{q}_{11} \\ \vdots \\ \mathbf{q}_{1k} \\ \mathbf{r}_2 \\ \mathbf{q}_{21} \\ \vdots \\ \mathbf{q}_{2k} \\ \vdots \\ \vdots \\ \mathbf{r}_N \\ \mathbf{q}_{N1} \\ \vdots \\ \mathbf{q}_{Nk} \\ \mathbf{g}(\mathbf{x}_1, \mathbf{x}_{N+1}) \end{pmatrix}, \qquad \text{(A.1)}$$

where

$$\mathbf{r}_i = \mathbf{x}_{i+1} - \left(\mathbf{x}_i + h_i \sum_{l=1}^{k} \beta_l \, f_{i,l} \right), \tag{A.2}$$

$$\mathbf{q}_{ij} = \mathbf{f}_{i,j} - f(\mathbf{x}_{ij}), \tag{A.3}$$

with

$$x_{i,j} = x_i + h_i \sum_{l=1}^{k} \alpha_{j,l} \, \mathbf{f}_{il}. \tag{A.4}$$

It can easily be shown [25] that solving the system (4.43,4.42,4.44) is equivalent to solving $F(X) = 0$. Consider a Newton method to solve such a system for the unknowns X. Define matrices

$$D = (\beta_1 I_n, \beta_2 I_n, \ldots, \beta_k I_n), \qquad A_{ij} = f_x(\mathbf{x}_{ij}),$$

$$V_i = \begin{pmatrix} A_{i1} \\ A_{i2} \\ \vdots \\ A_{ik} \end{pmatrix}, \qquad Q_i = \begin{pmatrix} \mathbf{q}_{i1} \\ \vdots \\ \mathbf{q}_{i2} \end{pmatrix}, \tag{A.5}$$

$$W_i = I_{nk} - h_i \begin{pmatrix} \alpha_{11}A_{i1} & \alpha_{12}A_{i1} & \cdots & \alpha_{1k}A_{i1} \\ \alpha_{21}A_{i2} & \alpha_{22}A_{i2} & \cdots & \alpha_{2k}A_{i2} \\ \vdots & \vdots & \ddots & \vdots \\ \alpha_{k1}A_{ik} & \alpha_{k2}A_{ik} & \cdots & \alpha_{kk}A_{ik}, \end{pmatrix},$$

where I_m is the m-dimensional identity matrix. Then it is easy to show that the correction at each Newton iteration is given by the solution to

$$\begin{pmatrix} -I_n & -h_1 D & I_n & & & & & & \\ -V_1 & W_1 & 0 & & & & & & \\ & & -I_n & -h_2 D & I_n & & & & \\ & & -V_2 & W_2 & 0 & & & & \\ & & & & \ddots & \ddots & \ddots & & \\ & & & & & & -I_n & -h_N D & I_n \\ & & & & & & -V_N & W_N & 0 \\ B_1 & & & & & & & & B_2 \end{pmatrix} \begin{pmatrix} \Delta\mathbf{x}_1 \\ \Delta\mathbf{f}_1 \\ \Delta\mathbf{x}_2 \\ \Delta\mathbf{f}_2 \\ \vdots \\ \Delta\mathbf{x}_N \\ \Delta\mathbf{f}_N \\ \Delta\mathbf{x}_{N+1} \end{pmatrix} = - \begin{pmatrix} \mathbf{r}_1 \\ Q_1 \\ \mathbf{r}_2 \\ Q_2 \\ \vdots \\ \mathbf{r}_N \\ Q_N \\ \mathbf{g} \end{pmatrix}, \tag{A.6}$$

where $B_1 = \frac{\partial g}{\partial x_1}$, $B_2 = \frac{\partial g}{\partial x_{N+1}}$.

Now $\Delta\mathbf{f}_i$ only depends on $\mathbf{x}_i$ and $\mathbf{f}_i$, and so a simple rearrangement eliminates

the "local" variables $\mathbf{f}_i$ to give

$$\begin{pmatrix} -\Gamma_1 & I_n & & & \\ & -\Gamma_2 & I_n & & \\ & & \ddots & \ddots & \\ & & & -\Gamma_N & I_n \\ B_1 & & & & B_2 \end{pmatrix} \begin{pmatrix} \Delta\mathbf{x}_1 \\ \Delta\mathbf{x}_2 \\ \vdots \\ \Delta\mathbf{x}_N \\ \Delta\mathbf{x}_{N+1} \end{pmatrix} = - \begin{pmatrix} \mathbf{r}_1 + h_1 D W_1^{-1} Q_1 \\ \mathbf{r}_2 + h_2 D W_2^{-1} Q_2 \\ \vdots \\ \mathbf{r}_N + h_N D W_N^{-1} Q_N \\ \mathbf{g} \end{pmatrix}, \tag{A.7}$$

where

$$\Gamma_i = I + h_i D W_i^{-1} V_i. \tag{A.8}$$

Once this reduced system has been solved for the Newton corrections $\Delta\mathbf{x}_i$, we can update the local variables using

$$\Delta\mathbf{f}_i = W_i^{-1}(-\mathbf{r}_i + V_i \Delta\mathbf{x}_i) \tag{A.9}$$

A.2 Variable period

If we have problem defined on an interval $[0, T]$ with T unknown and with phase condition $\phi = 0$, we can define

$$X' = \begin{pmatrix} X \\ T \end{pmatrix}, \qquad F'(X') = \begin{pmatrix} F(X') \\ \phi(X') \end{pmatrix}, \tag{A.10}$$

and

$$\mathbf{q}'_{ij} = \mathbf{f}_{i,j} - T f(\mathbf{x}_{ij}), \qquad A'_{ij} = T f_x(\mathbf{x}_{ij}), \qquad s_i = \begin{pmatrix} f(\mathbf{x}_{i1}) \\ \vdots \\ f(\mathbf{x}_{ik}) \end{pmatrix}. \tag{A.11}$$

In a Newton method we will need to solve the system

$$\left(\begin{array}{ccccccccc|c} -I & -h_1 D & I & & & & & & & 0 \\ -V_1 & W_1 & 0 & & & & & & & -s_1 \\ & & -I & -h_2 D & I & & & & & 0 \\ & & -V_2 & W_2 & 0 & & & & & -s_2 \\ & & & & \ddots & \ddots & \ddots & & & \vdots \\ & & & & & & -I & -h_N D & I & 0 \\ & & & & & & -V_N & W_N & 0 & -s_N \\ B_1 & & & & & & & & B_2 & 0 \\ \hline \frac{\partial\phi}{\partial\mathbf{x}_1} & 0 & \frac{\partial\phi}{\partial\mathbf{x}_2} & 0 & \cdots & \cdots & \frac{\partial\phi}{\partial\mathbf{x}_N} & 0 & \frac{\partial\phi}{\partial\mathbf{x}_{N+1}} & \frac{\partial\phi}{\partial T} \end{array}\right) \left(\begin{array}{c} \Delta\mathbf{x}_1 \\ \Delta\mathbf{f}_1 \\ \Delta\mathbf{x}_2 \\ \Delta\mathbf{f}_2 \\ \vdots \\ \Delta\mathbf{x}_N \\ \Delta\mathbf{f}_N \\ \Delta\mathbf{x}_{N+1} \\ \hline \Delta T \end{array}\right) = - \left(\begin{array}{c} \mathbf{r}_1 \\ Q_1 \\ \mathbf{r}_2 \\ Q_2 \\ \vdots \\ \mathbf{r}_N \\ Q_N \\ \mathbf{g} \\ \hline \phi \end{array}\right), \tag{A.12}$$

with W_i, V_i and Q_i defined as above but in terms of the T-scaled variables f' and A'.

Then by an analogous process to before, we can eliminate the local dependence on $\mathbf{f}'_{ij}$ in a Newton step, solve

$$\left(\begin{array}{ccccc|c} -\Gamma_1 & I_n & & & & -h_1 DW_1^{-1} s_1 \\ & -\Gamma_2 & I_n & & & -h_2 DW_2^{-1} s_2 \\ & & \ddots & \ddots & & \vdots \\ & & & -\Gamma_N & I_n & -h_N DW_N^{-1} s_N \\ B_1 & & & & B_2 & 0 \\ \hline \frac{\partial \phi}{\partial \mathbf{x}_1} & \frac{\partial \phi}{\partial \mathbf{x}_2} & \cdots & \frac{\partial \phi}{\partial \mathbf{x}_N} & \frac{\partial \phi}{\partial \mathbf{x}_{N+1}} & \frac{\partial \phi}{\partial T} \end{array}\right) \left(\begin{array}{c} \Delta \mathbf{x}_1 \\ \Delta \mathbf{x}_2 \\ \vdots \\ \Delta \mathbf{x}_N \\ \Delta \mathbf{x}_{N+1} \\ \hline \Delta T \end{array}\right) = - \left(\begin{array}{c} \mathbf{r}_1 + h_1 DW_1^{-1} Q_1 \\ \mathbf{r}_2 + h_2 DW_2^{-1} Q_2 \\ \vdots \\ \mathbf{r}_N + h_N DW_N^{-1} Q_N \\ \mathbf{g} \\ \hline \phi \end{array}\right), \tag{A.13}$$

and update the local variables with

$$\Delta \mathbf{f}_i = W_i^{-1}(-\mathbf{r}_i + V_i \Delta \mathbf{x}_i + s_i \Delta T). \tag{A.14}$$

Appendix B

M4B6 and Other Models. Parameters and Implementation details

B.1 M4B6 parameters

We use the following parameters in the M4B6 model, derived from [88].

We have three explicitly modelled generator buses ($N = 3$), two load buses ($M = 2$) and one slack bus. With reference to Figure 6.2 we number them as follows

Bus number	Local number	Name	Type
1	1	$NWAL$	*generator*
2	2	$SCOT$	*generator*
3	3	$DINO$	*generator*
4	1	$PENT$	*load*
5	2	$DEES$	*load*
6	–	$CEGB$	*slack*

(B.1)

Vectors of machine parameters are

$$M = \begin{pmatrix} 0.48710802447650 \\ 1.05816519407804 \\ 0.37815214478634 \end{pmatrix}, \qquad d_m = \begin{pmatrix} 0.05 \\ 0.05 \\ 0.05 \end{pmatrix},$$

$$P_m = \begin{pmatrix} 2.245 \\ 5.636 \\ 12.000 \end{pmatrix}, \qquad V_m = \begin{pmatrix} 0.9932 \\ 1.0047 \\ 0.9998 \end{pmatrix}. \tag{B.2}$$

Load parameters are

$$P_0 = \begin{pmatrix} 2.079419811 \\ 29.591118656 \end{pmatrix}, \qquad Q_0 = \begin{pmatrix} -0.389580189 \\ -4.318881344 \end{pmatrix},$$

$$K_{p\omega} = \begin{pmatrix} 0.4000 \\ 0.4000 \end{pmatrix}, \qquad K_{pv} = \begin{pmatrix} 0.3000 \\ 0.3000 \end{pmatrix}, \tag{B.3}$$

$$K_{q\omega} = \begin{pmatrix} -0.0300 \\ -0.0300 \end{pmatrix}, \qquad K_{qv} = \begin{pmatrix} -2.800 \\ -2.800 \end{pmatrix}, \tag{B.4}$$

$$T = \begin{pmatrix} 8.500 \\ 8.500 \end{pmatrix}, \qquad K_{qv^2} = \begin{pmatrix} 2.100 \\ 2.100 \end{pmatrix}.$$

The network is defined by

$$G = \begin{pmatrix} 0 & -0.00098897510859 & 0 & \dots \\ -0.00098897510859 & 0 & 0 & \dots \\ 0 & 0 & 0 & \dots \\ 0.93870852400344 & -0.00068014015837 & 98.45810477588853 & \dots \\ 0.43552022020421 & 0.32870745838899 & 0 & \dots \\ -0.23016775764199 & 1.09497199525948 & 0 & \dots \end{pmatrix}$$

$$\begin{pmatrix} \dots & 0.93870852400344 & 0.43552022020421 & -0.23016775764199 \\ \dots & -0.00068014015837 & 0.32870745838899 & 1.09497199525948 \\ \dots & 98.45810477588853 & 0 & 0 \\ \dots & 0 & 16.73072396763854 & -0.61960512736276 \\ \dots & 16.73072396763854 & 0 & -5.87123201004326 \\ \dots & -0.61960512736276 & -5.87123201004326 & 0 \end{pmatrix}, \tag{B.5}$$

$$B = \begin{pmatrix} 0 & -0.012859197415709 & 0 & \dots \\ -0.012859197415709 & 0 & 0 & \dots \\ 0 & 0 & 0 & \dots \\ -51.9283844700871 & -0.052633573430683 & -1542.16014044404 & \dots \\ -12.0248754416224 & -5.63742219938867 & 0 & \dots \\ -1.22091917367928 & -21.7113523548601 & 0 & \dots \end{pmatrix}$$
$$\begin{pmatrix} \dots & -51.9283844700871 & -12.0248754416224 & -1.22091917367928 \\ \dots & -0.052633573430683 & -5.63742219938867 & -21.7113523548601 \\ \dots & -1542.16014044404 & 0 & 0 \\ \dots & 0 & -206.202530526901 & -5.03279709419067 \\ \dots & -206.202530526901 & 0 & -146.802385662883 \\ \dots & -5.03279709419067 & -146.802385662883 & 0 \end{pmatrix}, \tag{B.6}$$

$$B_s = \begin{pmatrix} 0 & 0 & 0 & 0 & 0 & 0 \\ 0 & 0 & 0 & 0 & 0 & 0 \\ 0 & 0 & 0 & 1.7203 & 0 & 0 \\ 0 & 0 & 1.7203 & 0 & 0.5238 & 0 \\ 0 & 0 & 0 & 0.5238 & 0 & 0 \\ 0 & 0 & 0 & 0 & 0 & 0 \end{pmatrix} \quad \text{and } B_{shunt} = \begin{pmatrix} 0 \\ 0 \\ 0 \\ -2 \\ 0 \\ 0 \end{pmatrix}. \tag{B.7}$$

The slack bus has parameters

$$V_0 = 0.993700 \qquad \delta_0 = -0.26882608336768. \tag{B.8}$$

B.2 2nd partial derivatives for M4B6

Firstly calculate the 2nd partial derivatives of the network terms,

$$\frac{\partial^2 P_{net}(\mathbf{x})_i}{\partial \hat{V}_j \partial \hat{V}_{j'}} =$$

$$\begin{cases} -2 \sum_{k \in c(i)} G_{ik} & i = j = j' \\ -\left(G_{ij'} \cos(\hat{\delta}_i - \hat{\delta}_{j'}) + B_{ij'} \sin(\hat{\delta}_i - \hat{\delta}_{j'}) \right) & i = j \neq j', \quad j, j' \in c(i) \\ 0 & i \neq j = j', \quad j, j' \in c(i) \\ -\left(G_{j'j} \cos(\hat{\delta}_{j'} - \hat{\delta}_j) + B_{j'j} \sin(\hat{\delta}_{j'} - \hat{\delta}_j) \right) & i = j' \neq j, \quad j, j' \in c(i) \\ 0 & \text{otherwise} \end{cases} \tag{B.9}$$

$$\frac{\partial^2 P_{net}(\mathbf{x})_i}{\partial \hat{\delta}_j \partial \hat{V}_{j'}} =$$

$$\begin{cases} \sum_{k \in c(i)} \hat{V}_k \left(G_{ik} \sin(\hat{\delta}_i - \hat{\delta}_k) - B_{ik} \cos(\hat{\delta}_i - \hat{\delta}_k) \right) & i = j = j' \\ \hat{V}_i \left(G_{ij'} \sin(\hat{\delta}_i - \hat{\delta}_{j'}) - B_{ij'} \cos(\hat{\delta}_i - \hat{\delta}_{j'}) \right) & i = j \neq j', \quad j, j' \in c(i) \\ -\hat{V}_i \left(G_{ij'} \sin(\hat{\delta}_i - \hat{\delta}_{j'}) - B_{ij'} \cos(\hat{\delta}_i - \hat{\delta}_{j'}) \right) & i \neq j = j', \quad j, j' \in c(i) \\ -\hat{V}_j \left(G_{j'j} \sin(\hat{\delta}_{j'} - \hat{\delta}_j) + B_{j'j} \cos(\hat{\delta}_{j'} - \hat{\delta}_j) \right) & i = j' \neq j, \quad j, j' \in c(i) \\ 0 & \text{otherwise} \end{cases} \tag{B.10}$$

$$\frac{\partial^2 P_{net}(\mathbf{x})_i}{\partial \hat{\delta}_j \partial \hat{\delta}_{j'}} =$$

$$\begin{cases} 0 & i = j = j' \\ -\hat{V}_i \hat{V}_{j'} \left(G_{ij'} \cos(\hat{\delta}_i - \hat{\delta}_{j'}) + B_{ij'} \sin(\hat{\delta}_i - \hat{\delta}_{j'}) \right) & i = j \neq j', \quad j, j' \in c(i) \\ \hat{V}_i \hat{V}_{j'} \left(G_{ij'} \cos(\hat{\delta}_i - \hat{\delta}_{j'}) + B_{ij'} \sin(\hat{\delta}_i - \hat{\delta}_{j'}) \right) & i \neq j = j', \quad j, j' \in c(i) \\ -\hat{V}_{j'} \hat{V}_j \left(G_{ij} \cos(\hat{\delta}_{j'} - \hat{\delta}_j) + B_{ij} \sin(\hat{\delta}_{j'} - \hat{\delta}_j) \right) & i = j' \neq j, \quad j, j' \in c(i) \\ 0 & \text{otherwise} \end{cases} \tag{B.11}$$

$$\frac{\partial^2 Q_{net}(\mathbf{x})_i}{\partial \hat{V}_j \partial \hat{V}_{j'}} =$$

$$\begin{cases} -2\left(B_{S,i} + \sum_{k\in c(i)} \left(B_{S,ik} + B_{ik}\right)\right) & i = j = j' \\ -\left(G_{ij'} \sin(\hat{\delta}_i - \hat{\delta}_{j'}) - B_{ij'} \cos(\hat{\delta}_i - \hat{\delta}_{j'})\right) & i = j \neq j', \quad j, j' \in c(i) \\ 0 & i \neq j = j', \quad j, j' \in c(i) \\ \left(G_{ij} \sin(\hat{\delta}_i - \hat{\delta}_j) - B_{ij} \cos(\hat{\delta}_i - \hat{\delta}_j)\right) & i = j' \neq j, \quad j, j' \in c(i) \\ 0 & \text{otherwise} \end{cases} \tag{B.12}$$

$$\frac{\partial^2 Q_{net}(\mathbf{x})_i}{\partial \hat{\delta}_j \partial \hat{V}_{j'}} =$$

$$\begin{cases} -\sum_{k\in c(i)} \hat{V}_k \left(G_{ik} \cos(\hat{\delta}_i - \hat{\delta}_k) + B_{ik} \sin(\hat{\delta}_i - \hat{\delta}_k)\right) & i = j = j' \\ -\hat{V}_i \left(G_{ij'} \cos(\hat{\delta}_i - \hat{\delta}_{j'}) + B_{ij'} \sin(\hat{\delta}_i - \hat{\delta}_{j'})\right) & i = j \neq j', \quad j, j' \in c(i) \\ \hat{V}_i \left(G_{ij} \cos(\hat{\delta}_i - \hat{\delta}_j) + B_{ij} \sin(\hat{\delta}_i - \hat{\delta}_j)\right) & i \neq j = j', \quad j, j' \in c(i) \\ \hat{V}_j \left(G_{ij} \cos(\hat{\delta}_i - \hat{\delta}_j) + B_{ij} \sin(\hat{\delta}_i - \hat{\delta}_j)\right) & i = j' \neq j, \quad j, j' \in c(i) \\ 0 & \text{otherwise} \end{cases} \tag{B.13}$$

$$\frac{\partial^2 Q_{net}(\mathbf{x})_i}{\partial \hat{\delta}_j \partial \hat{\delta}_{j'}} =$$

$$\begin{cases} 0 & i = j = j' \\ -\hat{V}_i \hat{V}_{j'} \left(G_{ij'} \sin(\hat{\delta}_i - \hat{\delta}_{j'}) - B_{ij'} \cos(\hat{\delta}_i - \hat{\delta}_{j'})\right) & i = j \neq j' \quad , j' \in c(i) \\ \hat{V}_i \hat{V}_{j'} \left(G_{ij'} \sin(\hat{\delta}_i - \hat{\delta}_{j'}) - B_{ij'} \cos(\hat{\delta}_i - \hat{\delta}_{j'})\right) & i \neq j = j', \quad j, j' \in c(i) \\ -\hat{V}_{j'} \hat{V}_j \left(G_{j'j} \sin(\hat{\delta}_{j'} - \hat{\delta}_j) - B_{j'j} \cos(\hat{\delta}_{j'} - \hat{\delta}_j)\right) & i = j' \neq j, \quad j, j' \in c(i) \\ 0 & \text{otherwise} \end{cases} \tag{B.14}$$

Now we can calculate the 2nd partial derivatives of the global system, given in Table B.1.

Table B.1: 2nd derivatives of M4B6 type model

Global numbering (i,j,k)	Local numbering (n,n',n'')	$\dfrac{\partial^2 f_i}{\partial x_j \partial x_k}$
i=1,...,M	n=i=1,...,M	
j=1,...,(2M+2N) k=1,...,(2M+2N)		0
i=M+1,...,2M	n=i−M=1,...,M	
j=1,...,M k=1,...,M	n'=j=1,...,M n''=k=1,...,M	$-\frac{1}{M^n}\frac{\partial P_e^n}{\delta_m^{n'}\delta_m^{n''}}$
j=1,...,M k=(2M+1),...,(2M+N)	n'=j=1,...,M n''=k−2M=1,...,N	$-\frac{1}{M^n}\frac{\partial P_e^n}{\delta_m^{n'}\delta^{n''}}$
j=1,...,M k=(2M+N+1),...,2(M+N)	n'=j=1,...,M n''=k−(2M+N)=1,...,N	$-\frac{1}{M^n}\frac{\partial P_e^n}{\delta_m^{n'}V^{n''}}$
j=(2M+1),...,(2M+N) k=1,...,M	n'=j−2M=1,...,N n''=k=1,...,M	$-\frac{1}{M^n}\frac{\partial P_e^n}{\delta^{n'}\delta_m^{n''}}$
j=(2M+1),...,(2M+N) k=(2M+1),...,(2M+N)	n'=j−2M=1,...,N n''=k−2M=1,...,N	$-\frac{1}{M^n}\frac{\partial P_e^n}{\delta^{n'}\delta^{n''}}$
j=(2M+1),...,(2M+N) k=(2M+N+1),...,2(M+N)	n'=j−2M=1,...,N n''=k−(2M+N)=1,...,N	$-\frac{1}{M^n}\frac{\partial P_e^n}{\delta^{n'}V^{n''}}$
j=(2M+N+1),...,2(M+N) k=1,...,M	n'=j−(2M+N)=1,...,N n''=k=1,...,M	$-\frac{1}{M^n}\frac{\partial P_e^n}{V^{n'}\delta_m^{n''}}$
j=(2M+N+1),...,2(M+N) k=(2M+1),...,(2M+N)	n'=j−(2M+N)=1,...,N n''=k−2M=1,...,N	$-\frac{1}{M^n}\frac{\partial P_e^n}{V^{n'}\delta^{n''}}$
j=(2M+N+1),...,2(M+N) k=(2M+N+1),...,2(M+N)	n'=j−(2M+N)=1,...,N n''=k−(2M+N)=1,...,N	$-\frac{1}{M^n}\frac{\partial P_e^n}{V^{n'}V^{n''}}$
i=2M+1,...,2M+N	n=i−2M=1,...,N	
j=1,...,M k=1,...,M	n'=j=1,...,M n''=k=1,...,M	$\frac{1}{K_{q\omega}^n}\frac{\partial Q_l^n}{\delta_m^{n'}\delta_m^{n''}}$
j=1,...,M k=(2M+1),...,(2M+N)	n'=j=1,...,M n''=k−2M=1,...,N	$\frac{1}{K_{q\omega}^n}\frac{\partial Q_l^n}{\delta_m^{n'}\delta^{n''}}$
j=1,...,M k=(2M+N+1),...,2(M+N)	n'=j=1,...,M n''=k−(2M+N)=1,...,N	$\frac{1}{K_{q\omega}^n}\frac{\partial Q_l^n}{\delta_m^{n'}V^{n''}}$
j=(2M+1),...,(2M+N) k=1,...,M	n'=j−2M=1,...,N n''=k=1,...,M	$\frac{1}{K_{q\omega}^n}\frac{\partial Q_l^n}{\delta^{n'}\delta_m^{n''}}$
j=(2M+1),...,(2M+N) k=(2M+1),...,(2M+N)	n'=j−2M=1,...,N n''=k−2M=1,...,N	$\frac{1}{K_{q\omega}^n}\frac{\partial Q_l^n}{\delta^{n'}\delta^{n''}}$
j=(2M+1),...,(2M+N) k=(2M+N+1),...,2(M+N)	n'=j−2M=1,...,N n''=k−(2M+N)=1,...,N	$\frac{1}{K_{q\omega}^n}\frac{\partial Q_l^n}{\delta^{n'}V^{n''}}$

$j=(2M+N+1),...,2(M+N)$ $k=1,...,M$	$n'=j-(2M+N)=1,...,N$ $n''=k=1,...,M$	$\frac{1}{K^n_{q\omega}}\frac{\partial Q^n_l}{V^{n'}\delta^{n''}_m}$
$j=(2M+N+1),...,2(M+N)$ $k=(2M+1),...,(2M+N)$	$n'=j-(2M+N)=1,...,N$ $n''=k-2M=1,...,N$	$\frac{1}{K^n_{q\omega}}\frac{\partial Q^n_l}{V^{n'}\delta^{n''}}$
$j=(2M+N+1),...,2(M+N)$ $k=(2M+N+1),...,2(M+N)$ $j\neq i+N,\ k\neq i+N$	$n'=j-(2M+N)=1,...,N$ $n''=k-(2M+N)=1,...,N$ $n\neq n',\ n\neq n''$	$\frac{1}{K^n_{q\omega}}\frac{\partial Q^n_l}{V^{n'}V^{n''}}$
$j=i+N$ $k=i+N$	$n'=n$ $n''=n$	$\frac{1}{K^n_{q\omega}}\left(\frac{\partial Q^n_l}{V^nV^n}-2K^n_{qv2}\right)$
$i=2M+N+1,...,2(M+N)$	$n=i-(2M+N)=1,...,N$	
$j=1,...,M$ $k=1,...,M$	$n'=j=1,...,M$ $n''=k=1,...,M$	$\frac{1}{K^n_{pV}T^n}\left(\frac{\partial P^n_l}{\delta^{n'}_m\delta^{n''}_m}-K^n_{p\omega}\frac{\partial f_{i-N}}{\partial x_j\partial x_k}\right)$
$j=1,...,M$ $k=(2M+1),...,(2M+N)$	$n'=j=1,...,M$ $n''=k-2M=1,...,N$	$\frac{1}{K^n_{pV}T^n}\left(\frac{\partial P^n_l}{\delta^{n'}_m\delta^{n''}}-K^n_{p\omega}\frac{\partial f_{i-N}}{\partial x_j\partial x_k}\right)$
$j=1,...,M$ $k=(2M+N+1),...,2(M+N)$	$n'=j=1,...,M$ $n''=k-(2M+N)=1,...,N$	$\frac{1}{K^n_{pV}T^n}\left(\frac{\partial P^n_l}{\delta^{n'}_mV^{n''}}-K^n_{p\omega}\frac{\partial f_{i-N}}{\partial x_j\partial x_k}\right)$
$j=(2M+1),...,(2M+N)$ $k=1,...,M$	$n'=j-2M=1,...,N$ $n''=k=1,...,M$	$\frac{1}{K^n_{pV}T^n}\left(\frac{\partial P^n_l}{\delta^{n'}\delta^{n''}_m}-K^n_{p\omega}\frac{\partial f_{i-N}}{\partial x_j\partial x_k}\right)$
$j=(2M+1),...,(2M+N)$ $k=(2M+1),...,(2M+N)$	$n'=j-2M=1,...,N$ $n''=k-2M=1,...,N$	$\frac{1}{K^n_{pV}T^n}\left(\frac{\partial P^n_l}{\delta^{n'}\delta^{n''}}-K^n_{p\omega}\frac{\partial f_{i-N}}{\partial x_j\partial x_k}\right)$
$j=(2M+1),...,(2M+N)$ $k=(2M+N+1),...,2(M+N)$	$n'=j-2M=1,...,N$ $n''=k-(2M+N)=1,...,N$	$\frac{1}{K^n_{pV}T^n}\left(\frac{\partial P^n_l}{\delta^{n'}V^{n''}}-K^n_{p\omega}\frac{\partial f_{i-N}}{\partial x_j\partial x_k}\right)$
$j=(2M+N+1),...,2(M+N)$ $k=1,...,M$	$n'=j-(2M+N)=1,...,N$ $n''=k=1,...,M$	$\frac{1}{K^n_{pV}T^n}\left(\frac{\partial P^n_l}{V^{n'}\delta^{n''}_m}-K^n_{p\omega}\frac{\partial f_{i-N}}{\partial x_j\partial x_k}\right)$
$j=(2M+N+1),...,2(M+N)$ $k=(2M+1),...,(2M+N)$	$n'=j-(2M+N)=1,...,N$ $n''=k-2M=1,...,N$	$\frac{1}{K^n_{pV}T^n}\left(\frac{\partial P^n_l}{V^{n'}\delta^{n''}}-K^n_{p\omega}\frac{\partial f_{i-N}}{\partial x_j\partial x_k}\right)$
$j=(2M+N+1),...,2(M+N)$ $k=(2M+N+1),...,2(M+N)$	$n'=j-(2M+N)=1,...,N$ $n''=k-(2M+N)=1,...,N$	$\frac{1}{K^n_{pV}T^n}\left(\frac{\partial P^n_l}{V^{n'}V^{n''}}-K^n_{p\omega}\frac{\partial f_{i-N}}{\partial x_j\partial x_k}\right)$

References

[1] E. Hughes. *Electrical Technology.* Longman Scientific & Technical, 7th edition, 1995. revised by I. McKenzie Smith.

[2] P.M. Anderson and A.A. Fouad. *Power system control and stability.* Iowa State University Press, 1977.

[3] Y.J. Cao, Q.H. Wu, and S.J. Cheng. An improved Lyapunov function for power system stability. *International. J. Control*, 65(5):791–802, 1997.

[4] E. O'Neill-Carrillo, G.T. Heydt, E.J. Kostelich, S.S. Venkata, and A. Sundaram. Nonlinear deterministic modeling of highly varying loads. *IEEE Trans. Power Delivery*, 14(2):537–542, April 1999.

[5] J.A. Momoh and M.E. El-Hawary. *Electric systems, dynamics, and stability with artificial intelligence applications.* Dekker, 2000.

[6] P. Kundur. *Power system stability and control.* McGraw–Hill, 1984.

[7] B.C. Lesieutre, P.W. Sauer, and M.A. Pai. Development and comparative study of induction machine based dynamic P,Q load models. *IEEE Trans. Power Systems*, 10(1):182–191, 1995.

[8] K. Walve. Modelling of power system components at severe disturbances. In *International Conference on Large High Voltage Electric Systems*, Aug 1986. CIGRÉ paper 38-18.

[9] H. D. Chiang, I. Dobson, R. J. Thomas, J. S. Thorp, and L. Fekih-Ahmed. On voltage collapse in electric-power systems. *IEEE Trans. Power Systems*, 5(2):601–611, 1990.

[10] M. Di Bernardo, C. Budd, and A. Champneys. Grazing, skipping and sliding: analysis of the non-smooth dynamics of the DC/DC buck converter. *Nonlinearity*, 11:859–890, 1998.

[11] H. Lamba, S. McKee, and R. Simpson. The effect of circuit parameters on ferroresonant solutions in an LCR circuit. *J. Phys. A - Mathematical General*, 31:7065–7076, 1998.

[12] I. Dobson, H. Glavitsch, C. C. Liu, Y. Tamura, and K. Vu. Voltage collapse in power systems. *IEEE Circuits & Devices Magazine*, pages 40–45, May 1992.

[13] K. T. Vu and C. C. Liu. Shrinking stability regions and voltage collapse in power- systems. *IEEE Trans. Circuits & Systems - I Fundamental Theory & Applications*, 39(4):271–289, 1992.

[14] F. Bourgin, G. Testud, B. Heilbronn, and J. Verseille. Present practices and trends on the French power system to prevent voltage collapse. *IEEE Trans. Power Systems*, 8(3):778–788, Aug 1993.

[15] U.S. Department of Energy. The electric power outages in the western United States, July 2-3, 1996. Report to the President, U.S. Department of Energy, Washington, D.C., Aug 1996.

[16] J. Guckenheimer and P. Holmes. *Nonlinear Oscillations, Dynamical Systems and Bifurcations of Vector Fields.* Number 42 in Applied Mathematical Sciences. Springer–Verlag, 1983.

[17] G. Q. Zhong. Implementation of Chua's circuit with a cubic nonlinearity. *IEEE Trans. Circuits & Systems - I Fundamental Theory & Applications*, 41:934–941, 1994.

[18] P. Glendinning. *Stability, Instability and Chaos.* Cambridge Texts in Applied Mathematics. Cambridge University Press, 1994.

[19] J. Carr. *Applications of Centre Manifold Theory.* Springer–Verlag, 1981.

[20] R. Seydel. *Practical bifurcation and stability analysis : From equilibrium to chaos.* Springer–Verlag, 2nd edition edition, 1994.

[21] P.G. Drazin. *Nonlinear systems.* Cambridge Texts in Applied Mathematics. Cambridge University Press, 1992.

[22] I. Dobson and H. D. Chiang. Towards a theory of voltage collapse in electric-power systems. *Systems & Control Letters*, 13:253–262, 1989.

[23] T.F. Fairgrieve and A.D. Jepson. O.K. Floquet multipliers. *SIAM J. Numerical Analysis*, 28(5):1446–1462, 1991.

[24] R.I. Bogdanov. Versal deformation of a singularity of a vector field on the plane in the case of zero eigenvalues. *Selecta Mathematica Sovietica*, 1 (4):389–421, 1981. Originally published in *Trudy Sem. Petrovsk*, 2 (1976), pp37–65.

[25] U.M. Ascher, R.M.M. Mattheij, and R.D. Russell. *Numerical solution of boundary value problems for ordinary differential equations.* Prentice Hall, 1988.

[26] M. Golubitsky and D.G. Schaeffer. *Singularities and groups in bifurcation theory.* Springer-Verlag, 1985.

[27] H.B. Keller. Numerical solution of bifurcation and nonlinear eigenvalue problems. In P.H. Rabinowitz, editor, *Applications of Bifurcation Theory.* Academic Press, 1977.

[28] A. Jepson and A. Spence. Folds in solutions of two parameter systems and their calculation, part I. *SIAM J. Num. Anal.*, 22(2):347–368, Apr 1985.

[29] I. Dobson, H. D. Chiang, J. S. Thorp, and L. F. Ahmed. A model of voltage collapse in electric power systems. In *Proceedings of the 27th Conference on Decision and Control*, pages 2104–2109. IEEE, Dec 1988.

[30] E.H. Abed, A.M.A. Hamdan, and H.-C. Lee. On bifurcations in power system models and voltage collapse. In *Proceedings of the 29th Conference on Decision and Control*, pages 3014–3015. IEEE, 1990.

[31] H. D. Chiang, C. W. Liu, P. P. Varaiya, F. F. Wu, and M. G. Lauby. Chaos in a simple power system. *IEEE Trans. Power Systems*, 8(4):1407–1417, Nov 1993.

[32] H. O. Wang, E. H. Abed, and A. M. A. Hamdan. Bifurcations, chaos, and crises in voltage collapse of a model power system. *IEEE Trans. Circuits & Systems - I Fundamental Theory & Applications*, 41:294–302, 1994.

[33] V. Ajjarapu and B. Lee. Bibliography on voltage stability. *IEEE Trans. Power Systems*, 13(1):115–125, Feb 1998.

[34] D.N. Kosterev, C.W. Taylor, and W.A. Mittelstadt. Model validation for the august 10, 1996 WSCC system outage. *IEEE Trans. Power Systems*, 14(3):967–974, 1999.

[35] L. Vargas, V.H. Qunitana, and R. Miranda. Voltage collapse scenario in the Chilean interconnected system. *IEEE Trans. Power Systems*, 14(4): 1415–1421, 1999.

[36] A.S. Debs. *Modern power systems control and operation.* Kluwer, 1988.

[37] D.J. Hill. Nonlinear dynamic load models with recovery for voltage stability studies. *IEEE Trans. Power Systems*, 8(1):166–176, 1993.

[38] D. Karlsson and D.J. Hill. Modelling and identification of nonlinear dynamic loads in power systems. *IEEE Trans. Power Systems*, 9(1):157–166, 1994.

[39] H. O. Wang, E. H. Abed, and A. M. A. Hamdan. Is voltage collapse triggered by the boundary crisis of a strange attractor? In *Proceedings of the 1992 American Control Conference*, pages 2084–2088, 1992.

[40] V. Ajjarapu and B. Lee. Bifurcation-theory and its application to nonlinear dynamic phenomena in an electrical-power system. *IEEE Trans. Power Systems*, 7(1):424–431, 1992.

[41] B. Lee and V Ajjarapu. Period doubling route to chaos in and electrical power system. *IEE Proceedings - C*, 140(6):190–496, 1993.

[42] C. W. Tan, M. Varghese, P. Varaiya, and F. Wu. Bifurcation and chaos in power-systems. *Sādhanā - Academy Proceedings in Engineering Sciences*, 18(5):761–786, 1993.

[43] K.L. Lo and Z.Z. Qi. Nonlinear analysis of a model power system. Presented at IEE International Power Engineering Conference, Singapore, May 1997, May 1997.

[44] C. W. Tan, M. Varghese, P. Varaiya, and F. F. Wu. Bifurcation, chaos, and voltage collapse in power-systems. *Proc. IEEE*, 83:1484–1496, 1995.

[45] H.D. Chiang, T.P. Conneen, and A.J. Flueck. Bifurcations and chaos in electric power systems: Numerical studies. *J. Franklin Institute*, 331B(6): 1001–1036, 1994.

[46] A. H. Nayfeh, A. M. Harb, and C. M. Chin. Bifurcations in a power-system model. *International J. Bifurcation & Chaos*, 6:497–512, 1996.

[47] E.H. Abed and P.P. Varaiya. Nonlinear oscillations in power systems. *Electrical Power & Energy Systems*, 6(1):37–43, Jan 1984.

[48] A. H. Nayfeh, A. M. Harb, C. M. Chin, A.M.A. Hamdan, and L. Mili. Application of bifurcation theory to subsynchronous resonance in power systems. *International J. Bifurcation & Chaos*, 8(1):157–172, 1998.

[49] G.H. Golub and C.F. Van Loan. *Matrix Computations.* Johns Hopkins University Press, 3rd edition edition, 1996.

[50] H. G. Kwatny, A. K. Pasrija, and L. Y. Bahar. Static bifurcations in electric power networks: Loss of steady-state stability and voltage collapse. *IEEE Trans. Circuits & Systems - I Fundamental Theory & Applications*, 33(10): 981–991, October 1986.

[51] H. G. Kwatny, R. F. Fischl, and C. O. Nwankpa. Local bifurcation in power systems: Theory, computation and application. *Proceedings of the IEEE*, 83(11), November 1995.

[52] N. Yorino, H. Sasaki, Y. Masuda, Y. Tamura, M. Kitagawa, and A. Oshimo. On voltage stability from the viewpoint of singular perturbation-theory. *Electrical Power & Energy Systems*, 16(6):409–417, 1994.

[53] T. Gou and R.A. Schlueter. Identification of generic bifurcation and stability problems in power system differential-algebraic model. *IEEE Trans. Power Systems*, 9(2):1032–1044, 1994.

[54] B. Lee and V Ajjarapu. A piecewise global small-disturbance voltage-stability analysis of structure-preserving power system models. *IEEE Trans. Power Systems*, 10(4):1963–1971, Nov 1995.

[55] C. D. Vournas. Voltage stability and controllability indexes for multimachine power–systems. *IEEE Trans. Power Systems*, 10:1183–1194, 1995.

[56] C. A. Cañizares. On bifurcations, voltage collapse and load modeling. *IEEE Trans. Power Systems*, 10:512–522, 1995.

[57] V. Venkatasubramanian, H. Schattler, and J. Zaborszky. Voltage dynamics – study of a generator with voltage control, transmission, and matched mw load. *IEEE Trans. Automatic Control*, 37:1717–1733, 1992.

[58] V Venkatasubramanian. Singularity induced bifurcation and the Van der Pol oscillator. *IEEE Trans. Circuits & Systems - I Fundamental Theory & Applications*, 41(11):765–769, Nov 1994.

[59] V. Venkatasubramanian, H. Schattler, and J. Zaborszky. Dynamics of large constrained nonlinear-systems – a taxonomy theory. *Proc. IEEE*, 83(11): 1530–1561, 1995.

[60] V. Venkatasubramanian, H. Schattler, and J. Zaborszky. Fast varying phasor analysis in the balanced three-phase large electric power system. *IEEE Trans. Automatic Control*, 40(11):1975–1982, Nov 1995.

[61] V. Venkatasubramanian, H. Schattler, and J. Zaborszky. Local bifurcations and feasibility regions in differential- algebraic systems. *IEEE Trans. Automatic Control*, 40:1992–2013, 1995.

[62] R.E Beardmore. Stability and bifurcation properties of index-1 DAEs. *Numerical Algorithms*, 19(1–4):45–53, 1998.

[63] J.Y. Astic, A. Bihain, and M. Jerosolimski. The mixed Adams–BDF variable step size algorithm to simulate transient and long term phenomena in power systems. *IEEE Trans. Power Systems*, 9(2):929–935, May 1994.

[64] Tractabel and Electricité de France. *EUROSTAG 2.4*, May 1996.

[65] B. Meyer and M. Stubbe. Eurostag, a single tool for power-system simulation. *Transmission & Distribution International*, Mar 1992.

[66] R.J. Davy and I.A. Hiskens. Lyapunov functions for multimachine power systems with dynamic loads. *IEEE Trans. Circuits & Systems - I Fundamental Theory & Applications*, 44(9):796–812, 1997.

[67] M. Varghese, H. D. Chiang, and J. S. Thorp. Computer algorithms in power-systems – from constructive methods to truncated fractals. *IEEE Trans. Education*, 36:36–41, 1993.

[68] A. Polchai and C. S. Hsu. Domain of stability of synchronous generators by a cell mapping approach. *International J. Control*, 41:1253–1271, 1985.

[69] K.T. Vu, C.-C. Liu, C.W. Taylor, and K.M. Jimma. Voltage instability: Mechanisms and control strategies. *IEEE Trans. Power Systems*, 83(11): 1442–1455, Nov 1995.

[70] D.J. Hill, I.A. Hiskens, and I.M.Y. Mareels. Stability theory of differential/algebraic models of power systems. *Sādhanā - Academy Proceedings in Engineering Sciences*, 18(5):731–747, 1993.

[71] K. Iba, H. Suzuki, M. Egawa, and T. Watanabe. Calculation of critical loading condition with nose curve using homotopy continuation method. *IEEE Trans. Power Systems*, 6:584–593, 1991.

[72] W. Ma and J.S. Thorp. An efficient algorithm to locate all the load flow solutions. *IEEE Trans. Power Systems*, 8(3):1077–1083, Aug 1993.

[73] C. A. Cañizares and F. L. Alvarado. Point of collapse and continuation methods for large AC DC systems. *IEEE Trans. Power Systems*, 8:1–8, 1993.

[74] V. Ajjarapu, P. L. Lau, and S. Battula. An optimal reactive power planning strategy against voltage collapse. *IEEE Trans. Power Systems*, 9:906–917, 1994.

[75] H. D. Chiang, A. J. Flueck, K. S. Shah, and N. Balu. CPFLOW – a practical tool for tracing power-system steady-state stationary behavior due to load and generation variations. *IEEE Trans. Power Systems*, 10:623–630, 1995.

[76] A.J. Flueck and H.-D. Chiang. Solving the nonlinear power flow equations with an inexact newton method using GMRES. *IEEE Trans. Power Systems*, 13(2):267–273, 1998.

[77] B.D. Davidson. *Recursive Projection for Semi-Linear Partial Differential Equations.* PhD thesis, School of Mathematics, University of Bristol, Bristol, UK, 1995.

[78] B. Lee and V Ajjarapu. Invariant subspace parametric subspace sensitivity (isps) of structure-preserving power system models. *IEEE Trans. Power Systems*, 11(2):845–850, May 1996.

[79] S.K. Joshi and S.C. Srivastava. Estimation of closest Hopf bifurcation in electric power system. In *Proceedings of the 12th Power Systems Computation Conference*, pages 195–200, Aug 1996.

[80] F. Alvarado, I. Dobson, and Y. Hu. Computation of closest bifurcations in power systems. *IEEE Trans. Power Systems*, 9(2):918–928, 1994.

[81] S. Greene, I. Dobson, and F. L. Alvarado. Contingency ranking for voltage collapse via sensitivities from a single nose curve. *IEEE Trans. Power Systems*, 14(1):232–238, Feb 1999.

[82] M. Abramowitz and I.A. Stegun. *Handbook of mathematical functions with formulas, graphs and mathematical tables.* Dover, 1964.

[83] W.H. Press, S.A. Teukolsky, Q.T. Vetterling, and B.P. Flannery. *Numerical Recipes in Fortran 77 – The Art of Scientific Computing.* Cambridge, 2nd edition, 1992.

[84] E. Doedel. Lecture notes on numerical analysis of bifurcation problems. 5th Annual Postgraduate Spring School, University of Bristol, Apr 1996.

[85] B. De Dier, D. Roose, and P. Van Rompay. Interaction between fold and hopf curves leads to new bifurcation phenomena. *J. Computational & Applied Mathematics*, 26:171–186, 1989.

[86] W.-J. Beyn. *Numerical Methods for Dynamical Systems*, chapter Advances in Numerical Analysis, Vol I: Non-linear PDE's and Dynamical Systems, ed. W. Light, pages 175–236. Clarendon Press, Oxford, 1991.

[87] E. Doedel. *AUTO: Software for Continuation and Bifurcation Problems in Ordinary Diferential Equations.* California Institute of Technology, 1986.

[88] L.A. Dale. *Real-time Modelling of Multimachine Power Systems.* PhD thesis, University of Bath, 1986.

[89] E.J. Doedel, A.R. Champneys, T.F. Fairgrieve, Y.A. Kuznetsov, B. Sandsted, and X. Wang. *AUTO 97 – Continuation and bifurcation software for ordinary differential equations (with HomCont).* Concordia University, Montreal, Canada, 1997.

[90] B. Krauskopf and H. Osinga. Globalizing two-dimensional unstable manifolds of maps. *International J. Bifurcation & Chaos*, 8(3):483–503, 1998.

[91] M. Dellnitz and O. Junge. An adaptive subdivision technique for the approximation of attractors and invariant measures. Technical report, Universität Bayreuth, 1997.

[92] H. Osinga. Personal communication, 1998.

[93] T. Mullin, editor. *The Nature of Chaos.* Oxford Scientific Publications, 1993.

[94] P. Glendinning and C. Sparrow. Local and global behaviour near homoclinic orbits. *J. Statistical Physics*, 35(5/6):645–696, 1984.

[95] A. Spence, K.A. Cliffe, and A.D. Jepson. A note on the calculation of paths of hopf bifurcations. *J. Computational & Applied Mathematics*, 26:125–131, 1989.

[96] D. Roose and B. De Dier. Numerical determination of an emanating branch of Hopf bifurcation points in a two-parameter problem. *SIAM J. Scientific & Statistical Computing*, 10(4):671–685, July 1989.

[97] E. Freire, A.J. Rodríguez-Luis, E. Gamero, and E. Ponce. A case study for homclinic chaos in an autonomous electronic circuit – a trip from Takens-Bogdanov to Hopf-Šil'nikov. *Physica D*, 62:230–253, 1993.

[98] A. Gragnani, S. Rinaldi, and G. Feichtinger. Cyclic dynamics in romantic relationships. *International J. Bifurcation & Chaos*, 7(11):2611–2619, 1997.

[99] W. J. Beyn. Numerical-analysis of homoclinic orbits emanating from a Takens–Bogdanov point. *IMA J. Numerical Analysis*, 14:381–410, 1994.

[100] A. Griewank and G. W. Reddien. Computation of cusp singularities for operator equations and thier discretisations. *J. Computational & Applied Mathematics*, 26:133–153, 1989.

[101] J.M.T. Thompson and F.A. McRobie. Intermediate bifurcations and the dynamics of driven oscillators. In *Proceedings of the First European Nonlinear Oscillations Conference*, pages 107–128, 1993.

[102] J.M.T. Thompson. *Non-Linear Maths & Applications*, chapter Global Dynamics of Driven Oscillators: Fractal Basins and Indeterminate Bifurcations, ed. P.J. Aston. Cambridge University Press, 1996.

[103] C. S. Hsu. A theory of cell-to-cell mapping dynamical-systems. *J. Applied Mechanics – Trans. ASME*, 47:931–939, 1980.

[104] C. S. Hsu and R. S. Guttalu. An unravelling algorithm for global analysis of dynamical systems – an application of cell-to-cell mappings. *J. Applied Mechanics – Trans. ASME*, 47:940–948, 1980.

[105] C. S. Hsu. A generalized theory of cell-to-cell mapping for non-linear dynamical-systems. *J. Applied Mechanics – Trans. ASME*, 48:634–642, 1981.

[106] B. H. Tongue and K. Gu. Adaptive mesh strategies for interpolated mapping procedures. *International Journal Engineering Science*, 27:1143–1154, 1989.

[107] J. Levitas and T. Weller. Poincare linear interpolated cell mapping – method for global analysis of oscillating-systems. *J. Applied Mechanics – Trans. ASME*, 62:489–495, 1995.

[108] C. J. Budd and A. G. Lee. Double impact orbits of periodically forced impact oscillators. *Proc. Royal Soc. London Series A – Mathematical Phys. Engineering Sciences*, 452:2719–2750, 1996.

[109] A.M. Stuart and A.R. Humphries. *Dynamical Systems and Numerical Analysis*. Cambridge University Press, 1996.

[110] L.F Shampine and M.W. Reichelt. The Matlab ODE suite. *SIAM J. Scientific Computing*, 18(1):1–22, 1997.

[111] First Hydro Company. Web page, 2000. `http://www.fhc.co.uk/`.

[112] T. Berry, L. A. Dale, A. R. Daniels, and R. W. Dunn. Real-time modeling of multimachine power-systems. *IEE Proc. – C Generation Transmission Distribution*, 140:241–248, 1993.